Biodynamics: A novel quasi-first principles theory on the fundamental mechanisms of cellular function/dysfunction and the pharmacological modulation thereof

Gianluca Selvaggio[1*] and Robert A. Pearlstein[1*]

[1]Global Discovery Chemistry, Computer-Aided Drug Discovery, Novartis Institutes for BioMedical Research, 181 Massachusetts Avenue, Cambridge, MA 02139, USA.

[*]Corresponding authors

E-mail: gianluca.selvaggio@gmail.com

E-mail: robert.pearlstein@novartis.com

Key words: dynamic occupancy; non-equilibrium binding; binding kinetics; dynamic counter-balancing; analog computing; cellular function

ABSTRACT

Cellular function depends on heterogeneous dynamic intra-, inter-, and supramolecular structure-function relationships. However, the specific mechanisms by which cellular function is transduced from molecular systems, and by which cellular dysfunction arises from molecular dysfunction are poorly understood. We proposed previously that cellular function manifests as a molecular form of analog computing, in which specific time-dependent state transition fluxes within sets of molecular species ("molecular differential equations" (MDEs)) are sped and slowed in response to specific perturbations (inputs). In this work, we offer a theoretical treatment of the molecular mechanisms underlying cellular analog computing (which we refer to as "biodynamics"), focusing primarily on non-equilibrium (dynamic) intermolecular state transitions that serve as the principal means by which MDE systems are solved (the molecular equivalent of mathematical "integration"). Under these conditions, bound state occupancy is governed by k_{on} and k_{off}, together with the rates of binding partner buildup and decay. Achieving constant fractional occupancy over time depends on: 1) equivalence between k_{on} and the rate of binding site buildup); 2) equivalence between k_{off} and the rate of binding site decay; and 3) free ligand concentration relative to k_{off}/k_{on} ($n \cdot K_d$, where n is the fold increase in binding partner concentration needed to achieve a given fractional occupancy). Failure to satisfy these conditions results in fractional occupancy well below that corresponding to $n \cdot K_d$. The implications of biodynamics for cellular function/dysfunction and drug discovery are discussed.

INTRODUCTION

We proposed in our previous work [1] that time-dependent cellular function is derived from a molecular form of analog computing [2,3], in which sets of coupled ordinary differential equations and their integral solutions are modeled physically by changes in the rates of buildup and decay among the populations of biomolecular species to/from specific intra- and intermolecular states (the hardware and software are one and the same) (Fig 1). We referred to these constructs as "molecular differential equations" (MDEs) [1], the major forms of which include:

Intramolecular:

$$\frac{d\gamma_i(t)}{dt} = k_{in} \cdot [species\ i_{state\ m}](t) - k_{out} \cdot [species\ i_{state\ n}](t) \quad (1a)$$

Non-covalent intermolecular:

$$\frac{d\gamma_{i-j}(t)}{dt} = k_{on} \cdot [free\ species\ i](t) - k_{off} \cdot [free\ species\ j](t) \quad (1b)$$

Enzyme-substrate:

$$\frac{d\gamma_{i-j}(t)}{dt} = k_{on} \cdot [free\ enzyme\ i](t) \cdot [free\ substrate\ j](t) - k_{off} \cdot [enzyme\ i - sul](t) - k_{cat} \cdot [enzyme\ i - substrate\ j](t) \quad (1c)$$

where $d\gamma_k(t)/dt$ represents the rates of non-equilibrium occupancy buildup and decay of state k from one or more predecessor to one or more successor states. State transition rates are governed by adjustable barriers originating from intra- or intermolecular interactions (which we referred to as "intrinsic rates") and time-dependent changes in the concentrations or number densities of the participating species (which we referred to as "extrinsic rates") [1]. Molecular populations "flow"

over time in a transient (Markovian) fashion from one specific structural state to another (Fig 1) in response to production/degradation or translocation-driven changes in the levels of the participating species.

Fig 1. (A) Markovian state transition behavior exemplified for the human cardiac ether-a-go-go related gene (hERG) potassium channel between closed (C1, C2, and C3), open (O) and inactivated states (I) underlying the state probability curves in (B) [4]. The rate constants are labeled with Greek letters. (B) Molecular populations of hERG "flow" from one specific state to another based on intrinsic voltage-dependent rates of entry and exit. Multiple fluxes occur in parallel between specific states, speeding and slowing in response to dynamic perturbations. For example, the open (orange) and inactive (blue) states are fed by the closed state (magenta); the open and closed states are fed by the inactive state; and the inactive and closed states are fed by the open state. The time-dependent output of the overall system (i.e. the membrane potential in this case) is solved in cardiomyocytes via integration of the full complement of sodium, potassium, and calcium ion channel MDEs (which can be simulated using the O'Hara-Rudy model of the human cardiac AP [5]).

MDEs are "solved" by cells in aggregate for the corresponding time-dependent state occupancies of the participating species $\{\gamma_k(t), k = 1, n\}$ (e.g. dynamic ion channel states and currents, dynamic enzyme activation states, etc.), together with higher order (convergent) properties that we refer to as $\Gamma_a(t)$ (Fig 2). $\{\gamma_k(t), k = 1, n\}$ and $\Gamma_a(t)$ manifest as transient stimulus-response-driven "action potential-like" waveforms, in which the intrinsic or extrinsic rates of one or more MDEs are sped or slowed in response to $\Gamma_a(t)$. [1].

Fig 2. Cellular analog computing is based on the transduction of molecular state transitions into cellular function. MDEs $\{d\gamma_k(t)/dt,\ k = 1,\ n\}$ are "solved" in aggregate for the corresponding time-dependent state occupancies of the participating species $\{\gamma_k(t),\ k = 1,\ n\}$ (e.g. dynamic intra- and intermolecular states), together with higher order properties that we refer to as $\Gamma_a(t)$. The underlying MDEs accelerate or decelerate recursively in response to $\Gamma_a(t)$ according to their specific response mechanisms.

Building on our previous work [1] and that of others [2,6–11], we have developed a comprehensive multi-scale (atomistic → molecular systems) first principles theory on the basic mechanisms of cellular function that we refer to as "biodynamics" (Fig 3).

Fig 3. The six branches of biodynamics theory, which span the intra-/peri-cellular (micro-cellular) and macro-cellular levels (see text). Such processes can be simulated using multi-scale modeling approaches, ranging from atomistic molecular dynamics-based [1] to "atom-less" time-dependent ODE-based simulations ("MDE mimetics") [1].

Our theory encompasses the major mechanisms by which:

1) MDEs are generated, powered, solved (integrated), and transduced into function at the micro- and macro-cellular levels.

2) Cellular dysfunction results from molecular dysfunction and alterations in the corresponding MDEs and $\Gamma_a(t)$.

3) Cellular dysfunction can be mitigated by exogenously applied MDEs, consisting of drug-target occupancy.

In our previous work, we described the putative mechanisms by which free energy is transduced into non-equilibrium conditions and kinetic barriers (i.e. which we refer to here as "energy dynamics") [1,4,12–15], and exemplified cellular computing by way of the cardiac AP [4] and a generic MAP kinase-phosphatase system [1]. Here, we focus on binding as a key "integrator" of MDE systems, and in particular, the specific implications of non-equilibrium conditions on occupancy of the bound states of both endogenous molecules and drugs (i.e. the interplay between the "molecular dynamics" and "binding dynamics" branches of our theory).

Biodynamics both promotes and exploits non-equilibrium conditions

Rapid, transient perturbation-induced responses underlying cellular function depend on open systems, in which mass (chemical precursors, degradation products, and other substances) and energy are exchanged to/from the extracellular volume. Such responses are dampened by reversibility in closed systems exhibiting mass and energy conservation, noting that some species may undergo slow rates of buildup and decay when the overall response rate is slow. In the classical equilibrium view, covalent or non-covalent states i and j are populated according to their free energy differences ($\{\Delta G_{ij}\}$), such that the total free energy of the system is minimized. Dynamic state transitions of the participating species necessarily depend on perturbation-re-equilibration under this scenario, which is subject to the following limitations:

1) Perturbation-induced re-equilibration (i.e. equilibrium 1 → equilibrium 2) is time-consuming, and therefore, poorly suited for rapid biological responses.

2) Optimization of complex equilibria is cumbersome and offers extremely limited evolutionary adaptability.

Molecular systems are displaced from equilibrium (analogous to strain) when the participating species are continuously produced and degraded or translocated [16–21] (analogous to stress).

Fig 4. Molecular species and states build and decay transiently (i.e. sources → sinks), thereby generating non-equilibrium conditions. Such conditions promote unidirectional fluxes on which cellular analog computing is based.

The resulting strain energy is proportional to the stress, analogous to that of a spring stretched away from its equilibrium state. Reversibility (e.g. A + B ⇌ AB) is circumvented by "tensioned" operation, in which ΔG is maintained permanently above zero via chemical or physical entry and exit of the species to/from the system over time (sources and sinks) (Fig 4). The potential energy of a system under such conditions (ΔG_{noneq}) is given by:

$$\Delta G_{noneq} = G_{strain} - G_{eq} \quad (2)$$

where G_{strain} is the strain energy, and G_{eq} is the equilibrium free energy. Strained systems relax via mass action upon release of the corresponding stress, wherein $\Delta G_{noneq} \rightarrow 0$, and the participating species transition toward their equilibrium state distributions (i.e. [species $A_{state\ i}$]/[species $A_{state\ j}$] = K_{eq}). Reversibility is conveyed indirectly through concurrent (but out-of-phase) buildup and decay processes (e.g. A + B → AB; AB + C → A + B + C), which we refer to as "dynamic counter-balancing" ("Ying-Yang") (Figs 2 and 5). Examples include kinase- versus phosphatase-mediated phospho-transfer and inward versus outward ion channel currents.

Fig 5(A). Buildup and decay of a Yin (typically an enzyme), together with its substrate, product (and substrates thereof), Yang across their accessible states, as depicted by a plumbing system consisting of pipes, vessels, and valves. A given function-generating system is constituted from an interdependent collection of m such systems. Each system is

maintained at non-equilibrium (analogous to "pressurization") via continuous inputs and outputs of molecular species ("fluxes"). The dynamic fluid levels within the ($n \cdot m$) member vessels of the overall system, which define its instantaneous state, are solved by integration of the m MDE collections ($\{d\gamma_k(t)/dt =$ rate of entry to state k – rate of exit from state $k\}_i$, where $k = 1, 2, 3, ..., n$, and $i = 1, 2, 3, ..., m$). The vessels may be connected in series or parallel. The flow rates to/from each vessel depend on the input and output valve settings (representing both the intrinsic and extrinsic free energy barriers in this simplified example), which are governed by the overall state of the system (constituting a feedback loop). (B) Dynamic counter-balancing prevents runaway exponential growth and decay of molecular species and state levels. The rates of buildup and decay consist of the net difference in Yin and Yang rates over time. The Yin-Yang balance is tipped toward the Yin during the buildup phase (left side of the blue curve) and toward the Yang during the decay phase (right side of the blue curve). The absolute rates of species or state level changes are irrelevant, except in cases where runaway behavior is functionally desirable (e.g. caspase activation). The overall buildup-decay cycle length is denoted as Λ, noting that long lived species or states likely result from slow decay rather than slow buildup (which would otherwise dampen the maximum level). Fast buildup has important implications for bound state occupancy, which are discussed later in the text.

The Yin-Yang architecture serves to:

1) Prevent over- and undershooting desired $\gamma_k(t)$ due to the exponential behavior of molecular processes (noting that the integral solutions of MDEs are exponential functions). Yins and Yangs are necessarily maintained in an out-of-phase relationship by

159 way of "clocking" (e.g. a phosphatase whose activation depends on a species whose
160 buildup lags behind its target kinase).

161 2) Restore the initial conditions of the system.

162 The widespread practice of measuring biochemical (and even cellular and *in vivo*) effects as a
163 function of free ligand concentration, rather than occupancy per se, reflects the extent to which the
164 equilibrium assumption is relied upon throughout the biological sciences. However, our results
165 suggest that time-independent equilibrium metrics of state occupancy are poor approximations to
166 actual occupancy under cellular conditions *in vivo* when the rates of binding partner buildup and
167 decay are fast.

168 **MATERIALS AND METHODS**

169 We derived two complementary analytical expressions capturing the simultaneous exponential
170 buildup and decay of the binding site (molecular dynamics) and bound state (binding dynamics)
171 based on a simplified second order non-competitive interaction scheme:

$$B_{free} + L \underset{\boldsymbol{k_{off}}}{\overset{\boldsymbol{k_{on}}}{\rightleftharpoons}} C \tag{3}$$

172
173 where k_{on} is the association rate constant, k_{off} is the dissociation rate constant, and B_{free}, C, and
174 L are the free binding site, free ligand, and bound state concentrations, respectively. The rate of
175 change of C (the mathematical equivalent of a binding MDE) is given by:

$$\frac{dC(t)}{dt} = k_{on} \cdot B_{free}(t) \cdot L - k_{off} \cdot C(t) \tag{4a}$$

176
177 Solution of this equation is facilitated by the following assumptions:

1) Molecular response is proportional solely to dynamic fractional occupancy, which in some cases, may depend additionally on the binding mode (e.g. agonist, partial agonist, inverse agonist, and antagonist in the case of receptors).

2) The total binding site level ($B_{total}(t)$) is conserved instantaneously, wherein:

$$B_{free}(t) = B_{total}(t) - C(t) \tag{4b}$$

Substituting $B_{free}(t)$ in equation 4a with equation 4b leads to:

$$\frac{dC(t)}{dt} = k_{on} \cdot (B_{total}(t) - C(t)) \cdot L - k_{off} \cdot C(t) \tag{5}$$

3) That cellular systems operate in the transient regime, in which state population levels build and decay cyclically over time (although quasi-equilibrium operation is possible in some cases).

4) Buildup of $B_{total}(t)$ consists of the separate synthesis of the biomolecule (typically a protein) and generation of its binding-competent structural state. We further assume that state transitions occur on a timescale ≥ the rate of synthesis of the binding site-containing species.

5) Both free and ligand-bound binding sites are lost during degradation, whereas, in practice, different rates of degradation of the bound and unbound states are possible.

6) $B_{total}(t)$ builds and decays exponentially via two distinct processes:

    a) Production and degradation of the binding site-containing species, or inter-compartmental transfer to/from the site of action, whichever is slower.

b) Formation and loss of the binding competent structural state.

7) That $B_{total}(t)$ builds to the equilibrium level (B_∞) at t = ∞.

8) That buildup and decay can be treated as separate sequential processes. Although $B_{total}(t)$ builds and decays simultaneously, net buildup occurs prior to B_∞, followed by net decay. Possible forms of the buildup term include exponential growth (equation 6a), positive exponential decay (equation 6b), or logistic growth (equation 6c). Possible forms of the decay term include exponential (equation 6d) or logistic (equation 6e) decay (multiphasic exponential growth and decay behaviors are also conceivable):

Buildup

$$B_{total}(t) = B_\infty \cdot \left(e^{k_i \cdot t} - 1\right);\quad t < \xi \tag{6a}$$

$$B_{total}(t) = B_\infty \cdot \left(1 - e^{-k_i \cdot t}\right);t < \xi \tag{6b}$$

$$B_{total}(t) = \frac{B_\infty}{\left(1 + e^{-k_i \cdot (t - t_{01})}\right)};t < \xi \tag{6c}$$

Decay

$$B_{total}(t) = B_\infty \cdot e^{-k_{-i} \cdot (t - \xi)};t \geq \xi \tag{6d}$$

$$B_{total}(t) = B_\infty \cdot \left(1 - \frac{1}{\left(1 + e^{-k_{-i} \cdot (t - t_{02})}\right)}\right);t \geq \xi \tag{6e}$$

where B_∞ is B_{total} at t = ∞, k_i and k_{-i} are the buildup and decay rate constants, respectively, ξ is a characteristic time at which the function switches from net buildup to net decay, and t_{01} and t_{02} are the times at which the logistic curves reach 50% of their dynamic range during buildup and decay, respectively. We chose to approximate the buildup and decay phases of the binding site-containing species using equations 6b (based on [22]) and 6d,

and the buildup and decay phases of the binding site using equations 6c and 6e, which roughly approximates the state probability curves shown in Figs 1B and 2A.

9) k_{-i} defines the lower limit of k_{off} (i.e. k_{off} is "hijacked" by the rate of binding site decay), necessitating the correction of k_{off} and K_d in cases where $k_{off} < k_{-i}$:

$$k_{off}^{'} = k_{off}\ (where\ k_{off} > k_{-i}) \mid k_{-i}\ (where\ k_{off} \leq k_{-i})$$

$$K_d^{'} = k_{off}^{'}/k_{on}$$

10) L is fixed at a constant concentration (L_o). In practice, L is expected to build and decay dynamically, which serves to further constrain the buildup of the bound state.

Scenario 1: putative production and degradation of binding site-containing species

Substituting equations 6b and 6d into equation 5 leads to:

$$\begin{cases} \dfrac{dC(t)}{dt} = k_{on} \cdot B_{\infty} \cdot L_0 \cdot \left(1 - e^{-k_i \cdot t}\right) - C(t) \cdot (k_{on} \cdot L_0 + k_{off}^{'}) & t < \xi \\ \dfrac{dC(t)}{dt} = k_{on} \cdot B_{\infty} \cdot L_0 \cdot e^{-k_{-i} \cdot (t-\xi)} - C(t) \cdot (k_{on} \cdot L_0 + k_{off}^{'}) & t \geq \xi \end{cases} \quad (7)$$

where ξ is the time required to reach equilibrium binding (conventionally referred to as the "settling time"). The net flux switches from buildup to decay at this time. ξ is defined conventionally as the time to reach $0.95 \cdot B_{\infty}$ (which we refer to as B_{max}), given that B_{∞} is only asymptotically reached over long time periods [22], whereas B_{max} is reached over finite times. Solving for $t_{settling}$ leads to:

$$B_{max} = B_{0.95} = B_{\infty} \cdot (1 - e^{-k_i \cdot t_{settling}}) \quad (8a)$$

$$0.95 = 1 - e^{-k_i \cdot t_{settling}} \rightarrow \xi = t_{settling} = -\ln\frac{(0.05)}{k_i} \cong \frac{3}{k_i} \quad (8b)$$

Equation 7 can be recast in dimensionless form to facilitate parameter-independent occupancy comparison, reduce the dimensionality of the system, and allow grouping of the rate terms:

$$\begin{cases} \dfrac{dc(\tau)}{d\tau} = \alpha \cdot \left(1 - e^{-\tau}\right) - c(\tau) \cdot (\alpha + \beta) & \tau < \bar{\xi} \\ \dfrac{dc(\tau)}{d\tau} = \alpha \cdot e^{-\gamma \cdot (\tau - \bar{\xi})} - c(\tau) \cdot (\alpha + \beta) & \tau \geq \bar{\xi} \end{cases} \tag{9}$$

where $c = \frac{C}{B_{max}}$, $\tau = (k_i \cdot t)$, $\alpha = \frac{k_{on} \cdot L_0}{k_i}$, $\beta = \frac{k_{off}^{'}}{k_{-i}}$, $\gamma = \frac{k_{-i}}{k_i}$, and $\bar{\xi} = 3$. Solving equation 9 for $c(\tau)$ leads to:

$$\begin{cases} c(\tau) = \dfrac{\alpha \cdot e^{\lambda_1 \cdot \tau}}{(\alpha + \beta) \cdot (\alpha + \beta - 1)} - \dfrac{\alpha \cdot e^{\lambda_2 \cdot \tau}}{\alpha + \beta - 1} + \dfrac{\alpha \cdot e^{\lambda_3}}{\alpha + \beta} & \tau < \bar{\xi} \quad \text{(10a)} \\ c(\tau) = \dfrac{0.95 \cdot c_\infty}{\alpha + \beta - 1} \cdot e^{-(\alpha + \beta) \cdot (\tau - \bar{\xi})} \cdot (\alpha \cdot e^{(\alpha + \beta - \gamma) \cdot (\tau - \bar{\xi})} + \beta - \gamma) & \tau \geq \bar{\xi} \quad \text{(10b)} \end{cases}$$

where $\lambda_1 = -(\alpha + \beta)$, $\lambda_2 = -1$, and $\lambda_3 = 0$. The behavior of equation 10a as a function of α and β can be described as follows:

$\alpha + \beta > 0$ (satisfied when $\alpha \geq \beta$) → stable conditions.

$\alpha = \beta$ → $k_{on} \cdot L_0 = k_{off}$ and cancellation of k_i. Under these conditions, equation 10a reduces to:

$$c(\tau) = \frac{e^{-2 \cdot \alpha \cdot \tau}}{2 \cdot (2 \cdot \alpha - 1)} - \frac{\alpha \cdot e^{-\tau}}{2 \cdot \alpha - 1} + \frac{1}{2} \tag{11a}$$

the first term of which undergoes rapid decay at $\alpha \gtrsim 10$ (translating to $k_{onSS} = k_{on} \gtrsim 10 \cdot k_i / L_o$, where $L_0 = n \cdot K_d$'), resulting in:

$$c(\tau) \cong -0.5 \cdot e^{-\tau} + \frac{1}{2} \tag{11b}$$

Constant fractional occupancy exists at all time points of equation 11b, which we define as the steady-state occupancy (SSO) profile. Conversely, variable time-dependent fractional occupancy occurs at $\alpha < 10$, which we define as the non-steady-state occupancy (nSSO) profile. Unlike the equilibrium case, an asymmetric relationship exists between k_{on} and L_0 in governing dynamic occupancy, which follows from the requirement that $\alpha = \beta \gtrsim 10$. The nSSO profile prevails at all non-saturating L_0 in the absence of $\alpha = \beta \gtrsim 10$. For example:

1) $\alpha = \beta = 1$ at $\boldsymbol{L_0} =$ **1x10^{-9} M**, $k_{on} =$ 1x10^{5} M^{-1} s^{-1}, $k_{off} =$ 1x10^{-4} s^{-1}, and $k_i =$ 1x10^{-4} s^{-1} (noting that only $\alpha = \beta$ is satisfied in this case).

2) $\alpha = 10$ and $\beta = 1$ at $\boldsymbol{L_0} =$ **1x10^{-8} M**, $k_{on} =$ 1x10^{5} M^{-1} s^{-1}, $k_{off} =$ 1x10^{-4} s^{-1}, and $k_i =$ 1x10^{-4} s^{-1} (noting that only $\alpha \gtrsim 10$ is satisfied in this case).

$\boldsymbol{\alpha + \beta \gg 1} \rightarrow$ rapid decay of the first term in equation 10a, which at infinite time, reduces to the equilibrium case:

$$c(\tau)_{\tau, \bar{\xi} \to \infty} = c_\infty = \frac{\alpha}{\alpha + \beta} = \frac{k_{on} \cdot L_0}{k_{on} \cdot L_0 + k_{off}} = \frac{\text{on - rate}}{\text{on - rate } + \text{ off - rate}} \tag{12}$$

We assume that species or state population levels $\geq$ 50% of B_{max} make significant contributions to cellular function, translating to a "functional" buildup + decay time window:

$$\Lambda = \left[\frac{3}{k_i} - \left(\frac{\ln(2)}{k_i}\right)\right] + \frac{\ln(2)}{k_{-i}} \tag{13}$$

where k_i and k_{-i} likely range between ms^{-1} (e.g. voltage-gated ion channels) to hr^{-1}.

Fig 6. The buildup and decay phases of $B_{total}(\tau)$ simulated using equations 6b and 6d (scenario 1). The maximum $B_{total}(\tau)$ is normalized to 1.0, and always occurs at the normalized time $\tau = 3$. The curve adopts a canonical "saw-tooth" morphology.

Scenario 2: putative buildup and decay of the binding competent state

Substituting equations 6c and 6e into equation 5 leads to:

$$c(\tau) = \frac{\alpha \cdot e^{-\tau_{01}}}{\alpha+\beta+1} \cdot \left[e^{\tau} \cdot {}_2F_1\left(1,\alpha+\beta+1;\alpha+\beta+2;-e^{\tau-\tau_{01}}\right) - e^{-\tau\cdot(\alpha+\beta)} \cdot {}_2F_1\left(1,\alpha+\beta+1;\alpha+\beta+2;-e^{-\tau_{01}}\right)\right] \quad \tau < \bar{\xi} \tag{14a}$$

$$c(\tau) = \frac{e^{-(\tau-\xi)\cdot(\alpha+\beta)}}{\alpha+\beta} \cdot \left[c_\infty \cdot (\alpha+\beta) + \alpha \cdot e^{(\tau-\xi)\cdot(\alpha+\beta)} \cdot {}_2F_1\left(1,\alpha+\beta;\alpha+\beta+1;-e^{\tau-\tau_{02}-\xi}\right) - \alpha \cdot {}_2F_1\left(1,\alpha+\beta;\alpha+\beta+1;-e^{-\tau_{02}}\right)\right] \quad \tau \geq \bar{\xi} \tag{14b}$$

where ${}_2F_1(a,b;c;x)$ denotes the hypergeometric function. Unlike equation 6b, equation 6c contains a lower asymptote, which approaches zero along the negative time axis. We set $B_{total}(\tau = 0)$ to 5% of its full maximum value, and then calculated τ_{01}, τ_{02}, and $\bar{\xi}$ (the normalized settling time corresponding to $B_{max} = 95\%$ of the final value), as follows:

$$B_{total}(\tau) = \frac{1}{1+e^{-(\tau-\tau_{01})}} \rightarrow 0.05 = \frac{1}{1+e^{\tau_{01}}} \rightarrow \tau_{01} = \ln(19) \approx 2.94 \tag{15}$$

$$\bar{\xi} = 3 + \tau_{01} \approx 5.94 \tag{16}$$

$$\tau_{02} = 3 + \bar{\xi} \approx 8.94 \tag{17}$$

We solved equation 14 both analytically and numerically using Wolfram Alpha (Wolfram Research, Champaign, IL, 2017) and MATLAB (Version 9.2a, The MathWorks, Inc., Natick, MA 2017), respectively. As for scenario 1, we assume that species levels or state populations $\geq$ 50% of B_{max} make significant contributions to cellular function, which leads to the following expression for Λ:

$$\Lambda = 2 \cdot \ln(2)/k_i \tag{18}$$

Fig 7. The buildup and decay phases of $B_{total}(\tau)$ simulated using equations 6c and 6e (scenario 2). The maximum $B_{total}(\tau)$ is normalized to 1.0, and always occurs at $\tau = 6$. The morphology approximately resembles that of the state transition curves in Figs 1B and 2A, keeping in mind that the plot is normalized in all cases to a uniform width of $\tau =$ 12 at all Λ.

Comparison of equilibrium versus non-equilibrium occupancy

Static non-competitive, non-cooperative occupancy (γ) under equilibrium conditions can be described by the following form of the Hill equation [23]:

$$\gamma = L_o/(L_o + K_d) \tag{19}$$

where $L_o = \mathrm{n} \cdot K_d$. Fractional occupancy under the non-equilibrium SSO profile ($c(\tau)$) is constant over time, and is also described by equation 19. However, K_d is non-equivalent under equilibrium versus non-equilibrium conditions:

Equilibrium: $K_d = k_{off}/k_{on}$ → absolute occupancy $= \gamma \cdot B_o$, where B_o is the fixed binding site concentration.

Non-equilibrium SSO: $K_d' = \frac{k_{off}'}{k_{onSS}} = \frac{L_o \cdot k_{off}'}{10 \cdot k_i}$ → absolute occupancy $= \gamma \cdot B_{total}(t)$. Achieving the SSO profile depends on in-step buildup and decay with $B_{total}(t)$, which in turn, depends on $k_{on} \geq k_{onSS}$.

Non-equilibrium nSSO: K_d' = the upper limit of fractional occupancy at B_{max}. nSSO occurs at all $k_{on} < k_{onSS}$, irrespective of k_{off}' and K_d'. The quasi-steady-state occupancy profile is achieved at near saturating L_o levels (referred to hereinafter as qSSO).

We assume the most biologically and pharmacologically desirable profile consists of SSO (i.e. where the intrinsic and extrinsic rates are tuned), which gives rise to constant fractional occupancy ($B_{free}(t)/B_{total}(t)$) over time. However, the other profiles may suffice in cases where cellular function or pharmacological/toxic effects are driven by peak, rather than sustained occupancy (e.g. ion channel blockade vis-à-vis pro-arrhythmia [4]), which necessarily coincides with C_{max}.

Characterization of dynamic binding site occupancy under conditions of time-dependent binding site availability

We used equations 10 and 14 to explore the effect of decreasing Λ (and, in particular, speeding k_i) on achieving the SSO versus nSSO profile as a function of:

Λ: 83,000 hr (equilibrium) to 300 ms (the approximate timescale of ion channel transitions), sampled as noted.

$\boldsymbol{K_d'}$ (for reference): fixed at 1 nM, except where otherwise noted.

$\boldsymbol{k_{on}}$: $1x10^9$ (diffusion limit) to $1x10^3$ M^{-1} s^{-1}, sampled as noted.

$\boldsymbol{k_{off}'}$: $1x10^0$ to $1x10^{-6}$ s^{-1}, sampled as noted.

314 $\boldsymbol{L_0}$: sampled at 1 nM (i.e. 50% occupancy at equilibrium, equating to 0.95 · 50% in our model),
315 19 nM (95% occupancy at equilibrium, equating to 0.95 · 95% in our model), as well as other
316 concentrations (as noted).

317 ***Key limitations of our approach***

318 Our generalized analytical occupancy relationships avoid assumptions about the specific dynamic
319 mechanisms driving binding site availability. However, such simplified relationships are subject
320 to certain limitations compared with Markov-based simulation models tailored to specific cellular
321 systems (e.g. as was used in our previous work [1,4]), including the potential for underestimated
322 sensitivity of dynamic occupancy to decreasing Λ resulting from: 1) the use of fixed free ligand
323 concentration (where ligand and binding site buildup may or may not occur in phase); and 2)
324 neglect of competition with endogenous molecules that may also build and decay over time.

325 **RESULTS**

326 Whereas static occupancy can be quantified using the Hill, Michaelis-Menten, and similar
327 algebraic expressions, quantification of dynamic occupancy necessitates more complex time-
328 dependent differential equation-based models. However, detailed knowledge of the participating
329 species, parameters (e.g. rate constants), and initial conditions (e.g. states and species levels) is
330 needed to fully implement such models. We set about in this work to characterize the relationships
331 between intrinsic and extrinsic rates and SSO versus nSSO profiles using a set of closed form
332 dimensionless relationships that we derived for this purpose (described in MATERIALS AND
333 METHODS).

334 ***Scenario 1***

335 In this scenario, binding site lifetimes are assumed to depend on the rates of production and
336 degradation of binding site-containing species versus formation and decay of the binding-
337 competent state (i.e. transition to the binding competent state fully mirrors the buildup and decay
338 of the species). $k_{off}^{'}/k_{on} = L_0$ was maintained in all cases, except as otherwise noted. We
339 characterized the sensitivity of $c(\tau)$ to k_{on} and k_{off} as a function of decreasing Λ based on the
340 following criteria:

341 1) The non-equilibrium threshold of Λ at which occupancy becomes kinetically- versus K_d-
342 driven (i.e. the equilibrium regime).

343 2) The approximate k_{on} and $k_{off}^{'}$ required to achieve 50% and 95% occupancy under SSO
344 conditions ($L_0 = K_d$' and $19 \cdot K_d$', respectively).

345 3) The fold-increase in L_0 required to approach the qSSO profile.

346 The results are summarized below and in Table 1.

347 *The equilibrium regime*

348 The equilibrium regime extends from $\Lambda > 83{,}333$ hr ($k_i = k_{-i} =$ 1x10^{-8} s^{-1}), at which $c(\tau)$ is fully
349 independent of absolute k_{off} and k_{on} (constrained in our study to $k_{off}/k_{on} = K_d$), converging in
350 all cases to the SSO profile (Fig 8). Under these conditions, the bound fraction is 50% or 95% (L_0
351 $=$ 1 nM or 19 nM, respectively) at all instants of time, and $c(\tau)$ exhibits the signature "saw-tooth"
352 morphology of $B_{total}(\tau)$. The quasi-equilibrium regime resides between $833 < \Lambda < 83{,}333$ hr (Fig
353 9A).

Fig 8. (A) Plot of $B_{total}(\tau)$ (gray), $c(\tau)$ (red), and $B_{free}(\tau)$ (obscured by $c(\tau)$). $k_i = k_{-i} =$ 1x10^{-8} s^{-1}, $\Lambda =$ 83,333 hr, and $L_0 = K_d =$ 1 nM, which yields 50% SSO at all times (denoted by equal lengths of the vertical arrows above and below their respective centroids), irrespective of k_{on} and k_{off} (holding K_d constant at 1 nM). (B) Same as A, except with $L_0 = 19 \cdot K_d$, which yields the expected SSO = 95%.

The non-equilibrium regime

$c(\tau)$ enters the non-equilibrium regime in our model at $\Lambda \cong$ 833 hr ($k_i = k_{-i} =$ 1x10^{-6} s^{-1}), where the SSO profile is achieved at $k_{on} \geq k_{onSS} =$ 1x10^{4} M^{-1} s^{-1} (Fig 9). Suboptimal k_{on} results in the nSSO profile and loss of the signature saw-tooth morphology. $c(\tau)$ lags behind, and decays ahead of $B_{total}(\tau)$, and c_{50} and c_{95} are no longer achieved.

Fig 9. (A) Plot of $B_{total}(\tau)$ (gray), $c(\tau)$ at a fixed $L_0 = K_d =$ 1 nM and $\Lambda =$ 8,333 hr ($k_i = k_{-i} =$ 1x10^{-7} s^{-1}), in which k_{on} was sampled between 1x10^{3} M^{-1} s^{-1} to 1x10^{5} M^{-1} s^{-1} (solid lines color-coded from blue to red as a function of increasing k_{on}), and $B_{free}(\tau)$ (dotted lines color coded the same as $c(\tau)$). $c(\tau)$ diverges slightly from SSO at $k_{on} =$ 1x10^{3} M^{-1} s^{-1}. (B) Same as A, except $\Lambda =$ 1,667 hr ($k_i = k_{-i} =$ 5x10^{-7} s^{-1}, $k_{onSS} =$ 1x10^{3} M^{-1} s^{-1}). (C) Same as A, except $\Lambda =$ 833 hr ($k_i = k_{-i} =$ 1x10^{-6} s^{-1}, $k_{onSS} =$ 1x10^{4} M^{-1} s^{-1}). (D) Same as A, except $\Lambda =$ 167 hr ($k_i = k_{-i} =$ 5x10^{-6} s^{-1}, $k_{onSS} =$ 5x10^{4} M^{-1} s^{-1}). (E) Same as A, except $\Lambda =$ 3 hr ($k_i = k_{-i} =$ 1x10^{-5} s^{-1}, $k_{onSS} =$ 1x10^{5} M^{-1} s^{-1}). (F) Same as A, except $\Lambda =$ 8.3 hr ($k_i = k_{-i} =$ 1x10^{-4} s^{-1}, $k_{onSS} =$ 1x10^{6} M^{-1} s^{-1}). (G) Same as A, except $\Lambda =$ 50 min ($k_i = k_{-i} =$ 1x10^{-3} s^{-1}, $k_{onSS} =$ 1x10^{7} M^{-1} s^{-1}). (H) Same as A, except $\Lambda =$ 5 min (k_i

$= k_{-i} =$ 1x10^{-2} s^{-1}, $k_{onSS} =$ 1x10^{8} M^{-1} s^{-1}). $k_{on} =$ 1x10^{5} M^{-1} s^{-1}, the fastest k_{on} sampled at this k_i (1,000-fold < k_{onSS}), results in nearly zero occupancy.

Higher steady-state occupancies are achieved with decreasing Λ and k_{on} in the range of 1x10^{5} to 1x10^{7} M^{-1} s^{-1} (Fig 10).

Fig 10. (A) Plot of $B_{total}(\tau)$ (gray), $c(\tau)$ at a fixed $L_0 = K_d =$ 1 nM and $\Lambda =$ 8.3 hr ($k_i = k_{-i} =$ 1x10^{-4} s^{-1}, $k_{onSS} =$ 1x10^{6} M^{-1} s^{-1}), in which k_{on} was sampled between 1x10^{5} M^{-1} s^{-1} to 1x10^{7} M^{-1} s^{-1} (solid lines color-coded from blue to red according to increasing k_{on}), and $B_{free}(\tau)$ (dotted lines color coded the same as $c(\tau)$). (B) Same as A, except $\Lambda =$ 50 min ($k_i = k_{-i} =$ 1x10^{-3} s^{-1}). (C) Same as A, except $\Lambda =$ 5 min ($k_i = k_{-i} =$ 1x10^{-2} s^{-1} $k_{onSS} =$ 1x10^{8} M^{-1} s^{-1}). (D) Same as A, except $\Lambda =$ 30 s ($k_i = k_{-i} =$ 1x10^{-1} s^{-1}, $k_{onSS} =$ 1x10^{9} M^{-1} s^{-1}). (E) Same as A, except $\Lambda =$ 3 s ($k_i = k_{-i} =$ 1x10^{0} s^{-1}, $k_{onSS} =$ 1x10^{10} M^{-1} s^{-1}). $k_{on} =$ 1x10^{7} M^{-1} s^{-1}, the fastest k_{on} sampled at this k_i (1,000-fold < k_{onSS}), results in nearly zero occupancy.

Additional simulation results as a function of Λ, k_{on}, and k_{off} are provided in the Supplementary Information (S1-S4 Figs).

Table 1. Approximate k_{onSS} values needed to achieve the SSO profile as a function of k_i, calculated from $10 \cdot k_i/L_0$, where $L_0 = K_d$ and $k_{off} \geq k_{-i}$ (noting that k_{off} is not hijacked under these conditions).

Λ	k_i (s^{-1})	Buildup $t_{1/2}$	k_{-i} (s^{-1})	$K_d = k_{off}/k_{on}$ (nM)	$k_{off} = K_d \cdot k_{on}$ (s^{-1})	$\sim k_{onSS}$ (M^{-1} s^{-1})
83,333 hr	1x10^{-8}	19,254 hr	1x10^{-8}	1	-	-
833 hr	1x10^{-6}	192.5 hr	1x10^{-6}	1	1x10^{-5}	1x10^{4}

83	$1x10^{-5}$	19.25 hr	$1x10^{-5}$	1	$1x10^{-4}$	$1x10^{5}$
8.33 hr	$1x10^{-4}$	1.9 hr	$1x10^{-4}$	1	$1x10^{-3}$	$1x10^{6}$
50 min	$1x10^{-3}$	11.6 min	$1x10^{-3}$	1	$1x10^{-2}$	$1x10^{7}$
5 min	$1x10^{-2}$	1.16 min	$1x10^{-2}$	1	$1x10^{-1}$	$1x10^{8}$
30 s	$1x10^{-1}$	6.9 s	$1x10^{-1}$	1	$1x10^{0}$	$1x10^{9}$§
3 s	$1x10^{0}$	0.69 s	$1x10^{0}$	1	$1x10^{1}$	$1x10^{10}$§
300 ms	$1x10^{1}$	69 ms	$1x10^{1}$	1	$1x10^{2}$	$1x10^{11}$§
199 hr	$1x10^{-4}$	1.9 hr	$1x10^{-6}$	1	$1x10^{-3}$	$1x10^{6}$
20 hr	$8x10^{-4}$	14.4 min	$1x10^{-5}$	1	$1x10^{-2}$	$1x10^{7}$
2.1 hr	$3x10^{-3}$	3.9 min	$1x10^{-4}$	1	$1x10^{-1}$	$1x10^{8}$

§Exceeds the diffusion limit (further gains in $c(\tau)$ are necessarily driven by L_0).

Achieving the SSO profile depends on fast k_{on}, even for long-lived binding sites

We assume that long lifetimes of cognate partners are achieved via fast buildup and slow decay of the binding-competent structural state or species levels, the latter of which may consist of synthesis and degradation or inter-compartmental shuttling (noting that species dilution caused by cell growth is not necessarily well described by our exponential functions). As is apparent from Fig 11, achieving steady-state occupancy remains dependent on $k_{on} \geq k_{onSS}$, even at very slow binding site decay rates. At $k_{on} < k_{onSS}$, $c(\tau)$ may converge to $B_{total}(\tau)$ far beyond the B_{max} time point.

Fig 11. (A) Plot of $B_{total}(\tau)$ (black), $B_{free}(\tau)$ (blue), and $c(\tau)$ (gold) for $\Lambda =$ 199 hr ($k_i =$ $k_{-i} =$ $1x10^{-4}$ s^{-1} $1x10^{-6}$ s^{-1}, $k_{onSS} =$ $1x10^{6}$ M^{-1} s^{-1}), $L_0 = K_d =$ 1 nM, $k_{off} =$ $1x10^{-5}$ s^{-1}, and $k_{on} =$ $1x10^{4}$ M^{-1} s^{-1}. (B) Same as A, except $\Lambda =$ 199 hr ($k_i =$ $1x10^{-4}$ s^{-1}, $k_{-i} =$ $1x10^{-6}$ s^{-1}, $k_{onSS} =$ $1x10^{6}$ M^{-1} s^{-1}), $k_{off} =$ $1x10^{-3}$ s^{-1}, and $k_{on} =$ $1x10^{6}$ M^{-1} s^{-1}. In this example, approximate SSO is achieved at this k_{on}. (C) In this example, k_{on} is too slow to keep up

with $B_{total}(\tau)$, but $c(\tau)$ converges to steady-state during the decay phase. Same as A, except $\Lambda =$ 20 hr ($k_i =$ 8x10^{-4} s^{-1}, $k_{-i} =$ 1x10^{-5} s^{-1}, $k_{onSS} =$ 1x10^{6} M^{-1} s^{-1}), $k_{off} =$ 1x10^{-3} s^{-1}, and $k_{on} =$ 1x10^{6} M^{-1} s^{-1}. (D) Same as A, except $\Lambda =$ 2.1 hr ($k_i =$ 3x10^{-3} s^{-1}, $k_{-i} =$ 1x10^{-4} s^{-1}, $k_{onSS} =$ 1x10^{7} M^{-1} s^{-1}), $k_{off} =$ 1x10^{-3} s^{-1}, and $k_{on} =$ 1x10^{6} M^{-1} s^{-1}. Approximate SSO is achieved at this k_{on}.

Scenario 2

Binding site buildup and decay in this scenario are assumed to depend on fast conformational dynamics relative to the lifetime of the binding site-containing species, which may range case-by-case from ms (e.g. voltage-gated ion channels) to hr. We assume that scenarios 1 and 2 play different roles in biodynamics (i.e. the generation of non-equilibrium conditions and MDEs, respectively). However, our overall conclusions do not depend on this assumption. As for scenario 1, we set about to characterize the effect of decreasing time-dependent binding site availability on $c(\tau)$.

The hypothetical equilibrium regime

As for scenario 1, the SSO profile is achieved in the equilibrium case in a kinetics-agnostic manner ($\Lambda =$ 3,851 hr and $k_i = k_{-i} =$ 1x10^{-7} s^{-1}) (S5 Fig). Under these conditions, the bound fraction is 50% or 95% ($L_0 =$ 1 nM or 19 nM, respectively) at all instants of time, and $c(\tau)$ exhibits the same signature bi-sigmoidal morphology as that of $B_{total}(\tau)$ (S5 Fig).

The non-equilibrium regime

As for scenario 1, faster k_{on} is needed to achieve the SSO profile as k_i becomes progressively faster. The nSSO profile, and loss of the signature bi-sigmoidal $c(\tau)$ morphology, result from

suboptimal k_{on}. In such cases, c_{max} may no longer reach c_{50} or c_{95}, and $c(\tau)$ lags behind, and decays ahead of $B_{total}(\tau)$. $c(\tau)$ enters the non-equilibrium regime at $\Lambda \cong 833$ hr ($k_i = k_{-i} =$ 1x10^{-6} s^{-1}), where a minimum k_{on} of ~1x10^5 M^{-1} s^{-1} is required to fully achieve the SSO profile (Fig 12).

Fig 12. (A) Plot of $B_{total}(\tau)$ (gray), $c(\tau)$ at a fixed $L_0 =$ 1 nM and $\Lambda =$ 3,851 hr ($k_i = k_{-i} =$ 1x10^{-7} s^{-1}), in which k_{on} was sampled between 1x10^3 M^{-1} s^{-1} to 1x10^5 M^{-1} s^{-1} (solid lines color-coded from blue to red according to increasing k_{on}), and $B_{free}(\tau)$ (dotted lines color coded the same as $c(\tau)$). The $c(\tau)$ are beginning to diverge from the steady-state at this Λ. (B) Same as A, except $\Lambda =$ 385 hr ($k_i = k_{-i} =$ 1x10^{-6} s^{-1}). (C) Same as A, except $\Lambda =$ 3.85 hr ($k_i = k_{-i} =$ 1x10^{-4} s^{-1}). (D) Same as A, except $\Lambda =$ 23.1 min ($k_i = k_{-i} =$ 1x10^{-3} s^{-1}). $k_{on} =$ 1x10^5 M^{-1} s^{-1}, the fastest k_{on} sampled at $k_i = k_{-i} =$ 1x10^{-2} s^{-1}, results in nearly zero occupancy (not shown).

Additional simulation results as a function of Λ, L_0, k_{on}, and k_{off} are provided in S6-S7 Figs.

The implications of binding dynamics for known short-lived binding sites

We next assessed the implications of binding dynamics for hERG channel blockade and LDL receptor (LDL-R) binding to wild type (*wt*) versus the disease-causing gain-of-function D374Y mutant form of PCSK9.

PCSK9-LDL receptor

We characterized PCSK9-LDL-R dynamic occupancy based on our scenario 1 model and the pH-dependent binding kinetics data reported in [12] (summarized in Table 2). Rapid buildup of PCSK9 can be inferred from its observed ~5 min half-life [24], which is driven by zymogen activation [25] rather than *de novo* expression (as may be the case for many short Λ species). Negligible

PCSK9-LDL-R occupancy at neutral pH follows from the exceptionally high K_d relative to circulating plasma PCSK9 (which ranges between 30-3,000 ng/ml in humans (~405 pM to 40.5 nM) [26]), suggesting that extracellular binding depends on other factors. Binding and LDL-R degradation have indeed been shown to depend on heparin sulfate proteoglycans present on the extracellular surface of hepatocytes [27]. On the other hand, significant nSSO is achieved at the upper end of the concentration range for both *wt* and mutant forms of PCSK9 at lysosomal pH (Fig 13), suggesting that gain-of-function mutations act either through relatively small increases in dynamic occupancy relative to *wt*, or through some other means (e.g. by slowing PCSK9 degradation).

Table 2. Measured binding kinetics data for *wt* and D374Y mutant PCSK9- LDL-R [12]. Fold differences between k_{on} and k_{off} for D374Y versus *wt* are shown in parenthesis, noting that the $t_{1/2}$ of the bound complex is similar to that of *wt* PCSK9, but considerably longer than that of the D374Y mutant (which is likely subject to k_{off} hijacking). The ratio of k_{onSS}/k_{on} was calculated based on $k_{onSS} =$ 1x10^8 M^{-1} s^{-1}, corresponding to $k_i =$ 1x10^{-2} s^{-1} (predicted from equation 13 under the assumption that $k_i = k_{-i}$).

	wt		**D374Y**	
	pH 7.4	**pH5.3**	**pH 7.4**	**pH5.3**
$\boldsymbol{k_{on}}$ **(M^{-1} s^{-1})**	1.86x10^3	4.73x10^5	4.57x10^3 (+2.5-fold)	6.74x10^5 (+1.4-fold)
$\boldsymbol{k_{onSS}/k_{on}}$	53,763	211	21,881	148
$\boldsymbol{k_{off}}$ **(s^{-1})**	1.17x10^{-3}	1.97x10^{-3}	4.64x10^{-4} (-2.5-fold)	3.64x10^{-4} (-5.4-fold)
$\boldsymbol{k_{off}'}$ **(s^{-1})**	1.17x10^{-3}	1.97x10^{-3}	2.3x10^{-3}§	2.3x10^{-3}§
$\boldsymbol{K_d}$ **(M)**	628x10^{-9}	4.19x10^{-9}	101x10^{-9}	0.54x10^{-9}

K_d' (M)	628x10^{-9}	4.19x10^{-9}	503x10^{-9}	3.4x10^{-9}

[§]Similar clearance rates are assumed for both mutant and *wt* PCSK9.

Fig 13. (A) Plot of the hypothetical $B_{total}(\tau)$ (gray) and $c(\tau)$ for PCSK9 and PCSK9-LDL-R binding at a fixed PCSK9 $L_0 =$ 1 nM, $\Lambda =$ 5 min ($k_i = k_{-i} =$ 1x10^{-2} s^{-1}), and the k_{on} and k_{off} values given in Table 2 (solid lines color-coded as follows: *wt*/pH 7.4 dark blue (not visible); *wt*/pH 5.3 purple; D374Y/pH 7.4 cyan; D374Y/pH5.3 green), and $B_{free}(\tau)$ (dotted lines color coded the same as $c(\tau)$). Simulated occupancy is essentially zero for both *wt* and mutant PCSK9 at neutral pH, whereas negligible nSSO is achieved at low pH. (B) Same as A, except $L_0 =$ 20 nM. Moderate nSSO is achieved at low pH (maximum occupancy = 68% versus 75% for the wt and mutant forms, respectively). (C) Same as A, except $L_0 =$ 40.5 nM. High nSSO is achieved at low pH, where the gap between wt and mutant forms narrows to only a few percent at all time points (maximum occupancy = 82% versus 85% for the wt and mutant forms, respectively).

hERG channel blockade by non-trappable compounds

Certain hERG blockers are trapped within closed channels (which we refer to as "trappable"), whereas others are expelled during channel closing (which we refer to as "non-trappable") [4,28]. Trappable blocker occupancy builds to K_d' (the specific time-dependence of which depends on k_{on}), whereas that by non-trappable blockers builds and decays during each gating cycle. The ultrashort ~350 ms lifetime of the open and inactivated channel states results in k_{off} hijacking, in which $k_{off}^{'} = k_{off} \gtrsim \frac{k_{-i}}{3} (\sim 0.693\ s^{-1})$ and $k_{off} \geq k_{-i}\ (\sim 2\ s^{-1})$ for the trappable and non-trappable cases, respectively [4]. In our previous work, we characterized the dynamic occupancy

of a set of hypothetical non-trappable blockers using an alternate model, consisting of the O'Hara-Rudy action potential (AP) simulator, in which we replaced the Hodgkin-Huxley hERG model with a Markov state model incorporating blocker binding [4]. Here, we used the predicted pro-arrhythmic $n \cdot K_d'$ versus $n \cdot K_d$ as a function of k_{on}, k_{off}, and $k_{off}^{'}$ as a metric of dynamic occupancy, and qualitatively compared the results with our binding dynamics models (Fig 14 versus S6(E) Fig and Table 3 versus Table 1).

Fig 14. (A) Plot of dynamic fractional hERG occupancy in mid-myocardial (M) cells by a hypothetical non-trappable blocker exhibiting $k_{on} =$ 1x10^5 M^{-1} s^{-1} and $k_{off} =$ 5x10^{-1} s^{-1} ($K_d =$ 5 μM and $K_d^{'} =$ 20 μM) sampled at 10 and 25 μM (green solid and dashed curves, respectively). The total dynamic binding site level consists of the sum of the open/conducting and inactivated channel populations (gray dotted, solid, and dashed curves corresponding to 0, 10, and 25 μM blocker concentrations, respectively). The overall shape of the channel state population curves qualitatively resembles our logistic model (in which k_i is very fast), noting that recovery from inactivation (the decay region of the curves) is slowed by blockade due to the smaller contribution of the hERG current to the membrane potential, which in turn, alters the response of the channel population (consistent with the recursive effect depicted in Fig 2). The blocker occupancy curves reflect nSSO occupancy at $k_{on} =$ 1x10^5 M^{-1} s^{-1} (where $k_{on} << k_{onSS}$, as suggested from Table 1), and the peak occupancy is far below 50% at 5 μM. Nevertheless, even transient fractional occupancy approaching the ~45% level can be highly pro-arrhythmic [4]. (B) Plot of $B_{total}(\tau)$ (gray), $B_{free}(\tau)$ (blue) and $c(\tau)$ (gold) simulated using our logistic model (scenario 2) for a hERG blocker exhibiting $K_d =$ 5 μM ($k_{on} =$ 1x10^5 M^{-1} s^{-1} and $k_{off} =$

509 0.5 s^{-1}) and [free blocker] = 10 μM. k_i and k_{-i} were set to 13 s^{-1} and 2.1 s^{-1}, respectively,
510 so as to reproduce B_{max} at $\tau \approx$ 50 ms and $\Lambda \approx$ 350 ms. $B_{total}(\tau)$ and $c(\tau)$ are qualitatively
511 similar to the curves in A.

512 Table 3. L_0 (expressed as $n \cdot K_d$ and $n \cdot K_d'$) for a set of hypothetical hERG blockers
513 resulting in the pro-arrhythmic fractional channel occupancy levels predicted from our AP
514 simulations. Blocker $K_d =$ 5 μM in all cases, where k_{on} ranges between $1x10^4$ and $1x10^9$
515 M^{-1} s^{-1} and k_{off} between 0.005 and 5,000 (noting that the pro-arrhythmic occupancy level
516 increases as k_{off} speeds). $n \cdot K_d$ was back-calculated from the predicted pro-arrhythmic
517 occupancy using equation 19.

k_{on} (M^{-1} s^{-1})	$1x10^4$	$1x10^5$	$1x10^6$	$1x10^7$	$1x10^8$	$1x10^9$
k_{off} (s^{-1})	$5x10^{-2}$	$5x10^{-1}$	$5x10^0$	$5x10^1$	$5x10^2$	$5x10^3$
k_{off}' (s^{-1})	2	2	2	2	2	2
Fractional pro-arrhythmic hERG occupancy (%)	42	45	53	54	55	55
$n \cdot K_d'$ → **pro-arrhythmic occupancy (M)**	$2.6x10^{-4}$	$2.9x10^{-5}$	$7.8x10^{-6}$	$6.2x10^{-6}$	$6.0x10^{-6}$	$6.0x10^{-6}$
$n \cdot K_d$ → **pro-arrhythmic occupancy (M)**	$3.6x10^{-6}$	$4.1x10^{-6}$	$5.7x10^{-6}$	$5.9x10^{-6}$	$6.1x10^{-6}$	$6.1x10^{-6}$

518

519 ***Implications of binding dynamics for drug discovery***

520 Both drug-target and endogenous time-dependent binding partner occupancy are described by
521 similar biodynamics principles. Namely:

522 1) Extrinsic rates: the rates of buildup and decay of the binding site and ligand, which may
523 vary with conditions.

524 2) Intrinsic rates: k_{on} and k_{off}, which may also vary with conditions.

525 3) Fractional occupancy at each instant of time ($c(\tau)$). It is reasonable to assume that
526 molecular response (both efficacious and toxic) depends on $c(\tau) \geq$ a fractional occupancy
527 threshold during each binding site buildup/decay cycle (in general, ranging from a small
528 fraction to nearly 100%, case-by-case).

529 Our results suggest the paramount importance of tuning k_{on} and k_{off} to the rates of binding site
530 buildup and decay, respectively, for achieving the Goldilocks zone of efficacious target occupancy
531 and target/off-target selectivity (Fig 15). Constant maximal fractional occupancy is maintained
532 under the SSO profile at the lowest possible L (where $c(\tau)$ depends solely on $L = n \cdot K_d$). On the
533 other hand, fractional occupancy in the qSSO regime approaches a constant level only under
534 saturating conditions (i.e. at n >> 1) (S3 Fig). Target/off-target selectivity may be compromised
535 with the nSSO profile, depending on the ratio of $K_{d(target)}/K_{d(off-target)}$, keeping in mind that
536 nSSO may exist for the target, and SSO for one or more off-targets and/or competing endogenous
537 substrates.

538 Fig 15. Hypothetical plot of drug L versus time (red), showing a series of buildup-decay
539 cycles (one per dose) culminating in a steady-state condition, together with the efficacious
540 threshold of L (green), the safe upper limit of L (orange), and the toxic level of L (red). L
541 is maintained in the efficacious/sub-toxic "green zone" by overshooting and decaying back
542 to the efficacious level. Optimizing to the SSO regime affords the greatest chance of
543 achieving a therapeutic index in humans.

544 *Tuning kinetics to the qSSO profile*

545 Optimization of drug k_{off} or "residence time" (i.e. $t_{1/2} = \ln(2)/k_{off}$) does not translate to
546 increased occupancy when $k_{off} < k_i$ (unless k_{-i} is slowed in the bound state). We used equation
547 10 to test the effect of slowing k_{off} under qSSO versus SSO conditions (i.e. $k_{on} < k_{on\_ss}$ versus
548 $k_{on} \geq k_{on\_ss}$) at constant K_d (Fig 16).

549 Fig 16. Plot of $B_{total}(\tau)$ (gray), $c(\tau)$ at $L_0 = k_{off}/k_{on} =$ 1 nM and $\Lambda =$ 5 min ($k_i = k_{-i} =$
550 1x10^{-2} s^{-1}), in which k_{off} and k_{on} were sampled at 5x10^{-1} s^{-1}/5x10^{8} M^{-1} s^{-1} (blue), 5x10^{-7} s^{-1}/5x10^{5} M^{-1} s^{-1} (magenta), 5x10^{-2} s^{-1}/5x10^{8} M^{-1} s^{-1} (cyan), and 5x10^{-5} s^{-1}/5x10^{8} M^{-1} s^{-1} (olive)
552 (solid lines), and $B_{free}(\tau)$ (dotted lines correspond to the $c(\tau)$ color scheme). $c(\tau)$ is unaffected
553 by slowing k_{off} (magenta curve) when $k_{on} < k_{onSS}$. However, when $k_{on} \geq k_{onSS}$, $c(\tau)$
554 increases when k_{off} is further slowed (e.g. 5x10^{-1} s^{-1} → 5x10^{-2} s^{-1} (cyan curve) and 5x10^{-1} s^{-1}
555 → 5x10^{-5} s^{-1} (olive curve)).

556 Lastly, we used equation 10 to test the effect of increasing L_0 toward the qSSO profile at k_{on}
557 $< k_{on\_ss}$ (Fig 17 and S2 Fig).

558 Fig 17. (A) Plot of $B_{total}(\tau)$ (black), $B_{free}(\tau)$ (blue), and $c(\tau)$ at $L_0 = 0.5 \cdot K_d =$ 0.5 nM
559 and $\Lambda =$ 5 min ($k_i = k_{-i} =$ 1x10^{-3} s^{-1}, $k_{onSS} =$ 1x10^{8} M^{-1} s^{-1}), where $k_{off} =$ 1x10^{-1} s^{-1}/k_{on}
560 $=$ 1x10^{8} M^{-1} s^{-1} (gold). (B) Same as A, except at $L_0 = K_d =$ 1 nM, and $k_{off} =$ 3x10^{-4} s^{-1}/$k_{on} =$ 3x10^{5} M^{-1} s^{-1}. Although $c(\tau)$ reaches ~c_{31} in both cases, the steady-state scenario
562 in A reaches ~c_{31} at all instants of time (an example of kinetically tuned binding), whereas
563 the nSSO scenario results in considerably greater $B_{free}(\tau)$ prior to c_{max} (an example of non-
564 kinetically tuned binding). (C) Plot of $B_{total}(\tau)$ (gray), $c(\tau)$ at $K_d =$ 1 nM, $\Lambda =$ 5 min ($k_i =$
565 $k_{-i} =$ 1x10^{-3} s^{-1}, $k_{onSS} =$ 1x10^{8} M^{-1} s^{-1}), $k_{off} =$ 1x10^{-5} s^{-1}, and $k_{on} =$ 1x10^{4} M^{-1} s^{-1}, in

566 which L_0 was sampled between 1 nM and 2 μM (solid lines), and $B_{free}(\tau)$ (dotted lines
567 correspond to the $c(\tau)$ color scheme). Slow k_{on} is only compensated at sufficiently high L_0,
568 which in this case, approaches SSO conditions at $L_0 =$ 1 μM.

569

570 *The putative effects of competition and drug pharmacokinetics (PK) on drug-target occupancy*

571 Although we have not considered the effects of endogenous ligand competition and time-
572 dependent drug concentration (L(t)) on dynamic drug-target occupancy, these factors can only
573 serve to further increase k_{on_ss}. The rates of binding site and drug buildup within the target-
574 containing compartment (which may or may not be slower than the rate of drug buildup within the
575 central compartment) should ideally be synchronized to ensure that L is always $\geq K_d$. Fractional
576 drug-target occupancy is decreased by $L_e \cdot K_i/K_e$ in the presence of endogenous ligand
577 competition, as is apparent from the following equation [23]:

$$\gamma = L/(L + K_i + \left(\frac{K_i \cdot L_e}{K_e}\right)) \quad (20)$$

578

579 where L_e, K_e, and K_i are the free endogenous ligand concentration and K_d, and inhibitory drug K_d,
580 respectively. For example, drug SSO = 50% is achieved at $L_{50} = K_i + L_e$ when $K_i = K_e$, and L_{50}
581 further increases with increasing L_e (or synchronization with binding site buildup) and/or
582 decreasing K_e. It is further apparent that qSSO is achieved at higher L than in the non-competitive
583 case, and that competition between endogenous ligand binding via the SSO profile would be
584 greatly favored over inhibitory drug binding via the nSSO profile (more the reason for optimizing
585 to $k_{on} \geq k_{on\_ss}$).

The binding kinetics profiles of marketed drugs are consistent with non-equilibrium drug-target binding

We set about to test the relative importance of k_{on_ss} versus k_{off} in the human setting using measured k_{on} and K_d data curated by Dahl and Akrud for 32 marketed drugs [29] (reproduced in Table 3). We assume that marketed drugs observe steady-state or quasi-steady-state occupancy for targets with fast k_i and $k_{\_i}$, or bind to targets that build and decay slowly (i.e. kinetics-agnostic occupancy). The data can be summarized as follows:

1) k_{on} ranges between 1.4x10^{1} and 9.2x10^{7} M^{-1} s^{-1}, with $k_{on} \geq$ 1x10^{5} M^{-1} s^{-1} occurring in ~72% of the cases, sufficient for achieving the SSO profile for binding site buildup times between 1 m $\lesssim t_{1/2} \lesssim$ 19 h (blue text in Table 3).

2) k_{off} ranges between 4.8x10^{-6} and 2.8 s^{-1}, with k_{off} < 3.9x10^{-4} s^{-1} ($t_{1/2} \gtrsim$ 30 min) occurring in ~47% of the cases (green text in Table 3).

3) K_d < 1 nM was achieved in ~44% of the cases (red text in Table 3), which is due to k_{off} < 3.9x10^{-4} s^{-1} in 57% of those cases (i.e. extreme potency is not driven by slow k_{off}).

4) k_{off} > 3.9x10^{-4} s^{-1} and k_{on} > 1x10^{5} M^{-1} s^{-1} (i.e. k_{on}-driven occupancy) occurs in ~44% of the cases.

5) k_{off} < 3.9x10^{-4} s^{-1} and k_{on} < 1x10^{5} M^{-1} s^{-1} (i.e. k_{off}-driven occupancy) occurs in only ~19% of the cases, of which 4 are receptors, 2 are NS3 protease, and 1 is HIV-1 RT (noting that k_{on} is near our cutoff in the receptor ligand telmisartan, and the NS3 inhibitor ciluprevir exhibits fast k_{on}).

These observations (and numbers 4 and 5 in particular) are consistent with our claim that high dynamic occupancy under non-equilibrium conditions found *in vivo* depends first and foremost on fast k_{on}, and further suggest that the rates of buildup of many of the targeted binding sites are $\geq$ 1x10^{-5} s^{-1} (based on Table 1), assuming that k_{on} was, in fact, wittingly or unwittingly optimized to k_{on_ss}. This contrasts with the claim of Dahl and Akrud [29] and Folmer [30] that the drugs were optimized on the basis of K_d (noting that Folmer acknowledges the greater contribution of fast k_{on} over slow k_{off} to drug success [30]).

Table 3. Published k_{on}, k_{off}, and K_d values for a set of marketed drugs [29]. The drugs are grouped and color-coded by target. Cases of $K_d < 1$ nM are color-coded with red text, $k_{on} >$ 1x10^5 M^{-1} s^{-1} are color-coded with blue text, and $t_{1/2} > 30$ min are color-coded with green text.

Drug	Target	k_{on} (M^{-1} s^{-1})	k_{off} (s^{-1})	$t_{1/2}$ (min)	K_d (M)
Aliskiren	Renin	4.00E+05	1.1E-04	105	3.00E-10
Aclidinium	Muscarinic M3 receptor	1.10E+06	2.0E-05	578	1.80E-11
Ipratropium	Muscarinic M3 receptor	4.10E+06	1.1E-03	11	2.60E-10
Tiotropium	Muscarinic M3 receptor	7.60E+05	7.2E-06	1604	9.50E-12
Candesartan	Human angiotensin II type 1 receptor	2.60E+04	1.9E-04	61	7.40E-09
Telmisartan	Human angiotensin II type 1 receptor	9.10E+04	1.5E-04	77	1.70E-09
Granisetron	5-HT3	7.50E+05	7.5e-04	15	1.00E-09
Lapatinib	ERBB2/EGFR	1.30E+04	3.9e-05	296	3.00E-09
Desloratadine	Histamine H1 receptor	3.20E+04	3.2e-05	361	1.00E-09
Amlodipine	L-type calcium channel	1.50E+05	3.0E-04	39	2.00E-09
Verapamil	L-type calcium channel	9.20E+07	2.8E0	0.004	3.00E-08
Phenytoin	Na+ channel	2.50E+04	5.0E-01	0.02	2.00E-05

Amprenavir	HIV-1 protease	4.40E+06	4.9E-03	2	1.10E-09
Atazanavir	HIV-1 protease	1.70E+06	6.9E-04	17	4.00E-10
Indinavir	HIV-1 protease	1.50E+06	1.6e-03	7	1.10E-09
Lopinavir	HIV-1 protease	6.60E+06	6.5E-04	18	1.00E-10
Ritonavir	HIV-1 protease	3.90E+06	2.2E-03	5	6.10E-10
Saqunavir	HIV-1 protease	8.20E+05	2.3E-04	50	3.20E-10
Nelfinavir	HIV-1 protease	6.60E+05	6.7E-04	17	1.60E-09
Boceprevir	Hepatitis C virus nonstructural protease (NS3)	2.40E+03	4.9E-05	236	2.00E-08
Ciluprevir	Hepatitis C virus nonstructural protease (NS3)	9.10E+05	7.3E-04	16	6.20E-09
Telaprevir	Hepatitis C virus nonstructural protease (NS3)	2.20E+03	9.6E-05	120	4.30E-08
Deoxy-conformycin	Adenosine deaminase	2.40E+06	4.8E-06	2,406	2.00E-12
Efavirenz	HIV-1 reverse transcriptase	1.40E+01	6.8E-05	170	5.00E-06
Elvitegravir	HIV integrase	2.10E+06	8.3e-03	1	4.00E-09
Raltegravir	HIV integrase	2.50E+05	2.5e-03	5	1.00E-08
Methotrexate	Chicken dihydrofolate reductase	3.70E+07	3.3e-04	35	9.00E-12
Trimethoprim	Escherichia coli dihydrofolate reductase	7.20E+07	1.4e-03	8	2.00E-11
Oseltamivir	Viral neuraminidase	7.90E+05	2.5e-04	46	3.10E-10
Saxagliptin	Human dipeptidyl-peptidase IV	1.60E+05	5.4e-05	214	3.50E-10
Vildagliptin	Human dipeptidyl-peptidase IV	8.70E+04	9.8e-04	12	1.10E-08
Triclosan	Enoyl-ACP reductase and Francisella tularensis	8.20E+06	4.2e-04	28	5.10E-11

618

619 **Discussion**

620 The fundamental mechanisms by which molecular properties are transduced into cellular structure-
621 function are poorly understood. Molecules are an unruly lot, whose states are distributed randomly
622 in the absence of transducible energy inputs to achieve maximal configurational entropy. The

relevant energy inputs consist largely of: 1) H-bond losses and gains among solvating water molecules (versus other liquid solvents); and 2) continual/continuous production and decay of the participating species needed to maintain non-equilibrium conditions. Furthermore, dynamic counter-balancing is essential for overcoming the inherent susceptibility of exponential molecular state transitions to under- and overshooting. Our biodynamics theory, in which cellular structure-function is predicated on a molecular form of analog computing, is well-aligned with these principles. Multiple levels of integrated dynamic contributions underlying cellular function, dysfunction, pharmacodynamics, and drug PK are addressed by our theory, the implications of which are summarized in the following sections.

The rates of change in binding partner levels/states are sensed via binding dynamics

The bound fraction of binding or catalytic sites can be calculated under strictly equilibrium conditions using the Hill and Michaelis-Menten equations, respectively. However, binding sites undergo transient buildup and decay driven by synthesis/degradation, translocation, or conformational state transitions to/from their binding-competent states. The lifetimes of many proteins range from single-digit minutes to hours [21] (e.g. PCSK9 is on the order of 5 min [24], and tumor cell line-derived NIK ranges from ~5-30 min [31]). The lifetimes of binding competent states can range from μs (e.g. mRNA) or ms (e.g. voltage-gated ion channels) to the lifetime of the molecule itself. Here, we have shown that dynamic occupancy is greatly influenced by the time window of binding site availability, where the SSO profile is only achieved when k_{on} is on the order of k_i. We assume that the association and dissociation rate constants for endogenous partners are kinetically tuned to the dynamic ranges of $B_{total}(t)$ and $L(t)$. Perturbations to partner states/levels can be sensed through binding dynamics, and specifically, kinetic tuning/de-tuning of $C(t)$ via:

1) Modulation of the maximum time-dependent binding partner levels ($B_{total}(t)$) (the "extrinsic" rates [1]).

2) Slowing/speeding of k_i and k_{-i} thereby shifting the k_{on} threshold for achieving the SSO profile (i.e. k_{onSS}) or the qSSO profile.

3) Modulation of partner-specific association and dissociation rate constants (k_{on} and k_{off}) (the "intrinsic" rates [1]).

Sensitivity of cellular function to the bound state depends on:

1) The dynamic range in B_{total}(t):

    a) Constitutively low $B_{total}(t)$ levels may result in undetectable levels of the bound state.

    b) Constitutively high B_{total}(t) levels may result in reduced sensitivity of the bound state to changes in concentration of the other partner(s).

2) k_{on} (subject to allosteric modulation, case-by-case).

    a) Very fast k_{on} (>> k_{on_ss}) diminishes the sensitivity of the bound state to changes in partner concentration.

    b) Very slow k_{on} (<< k_{on_ss}) may result in undetectable levels of the bound state at lower partner concentrations.

We assume that cellular systems operate within the binding sensitive regime, such that the buildup and decay of binding partners and the bound states thereof remain in phase over time. Although

665 we have assumed a constant free ligand concentration in constructing our analytical dynamic
666 occupancy expressions, it is apparent that this condition rarely occurs *in vivo* (noting that buildup
667 and decay of the binding partners may proceed at different rates, and in an in- or out-of-phase
668 relationship). As such, variable ligand concentration introduces potentially far greater kinetic
669 demands on dynamic occupancy, which is likely underestimated in our approach.

670 ***The implications of biodynamics for pharmacodynamics and drug discovery***

671 Efficacious and toxic drug levels are conventionally defined in terms of the equilibrium scenario
672 (equation 20), which rests on the assumptions that drug-target occupancy, drug exposure within
673 the target compartment (typically intra- or extracellular), and target level are quasi-time-
674 independent quantities, when in fact, they are not:

675 1) Biomolecular species underlying cellular function undergo continuous
676 production/degradation and state transitions (including drug targets).

677 2) Drug levels build and decay based on PK principles (S7 Fig).

678 3) Drug-target binding builds and decays based on binding dynamics principles.

679 4) Drug-target binding alters the rates of dysfunction promoting processes (i.e.
680 pharmacodynamics).

681 Pharmacodynamics may be taken as the mitigation of Yin-Yang imbalances [1] via the insertion
682 of one or more exogenous MDEs into afflicted system(s) (where inhibition and stimulation
683 effectively slow and speed target buildup, respectively). As for endogenous complexes:

684 1) Buildup of drug-target occupancy is on-rate driven, and the bound state must rebuild with
685 each target buildup/decay cycle due to loss of the bound drug-target population.

686 2) On-rate may be driven by k_{on} and/or free drug concentration.

687 3) The SSO profile is achievable, in practice, for kinetically tuned binding, in which k_{on} is
688 optimized to $\geq k_{onSS}$, as dictated by the lifetime of the target or binding site (Fig 18). Under
689 these conditions, efficacious or toxic occupancy, which can conceivably vary from << 50%
690 to 95+% is expected at a free drug concentration $= n \cdot K_d$ (e.g. n = 19 yields 95%
691 occupancy), noting that the putative safe range of trappable hERG blocker occupancy
692 ranges between 0-3% [4]. Conversely, achieving the qSSO profile (converging to ~95%
693 occupancy) may require considerably larger n than the SSO profile.

694 4) In the absence of kinetic tuning, the SSO profile is unachievable via escalation of drug
695 concentration, although the qSSO profile is conceivable at sub-toxic exposures. This
696 constitutes a potential source of *in vitro-in vivo* disconnects and clinical failures due to loss
697 of the therapeutic index. The worst-case scenario consists of a drug that is kinetically
698 mistuned to its target, while being kinetically tuned to one or more off-targets, and that
699 competes for the target with an endogenous kinetically tuned partner.

700 5) Residence time (i.e. $\ln(2)/k_{off}$ below the rate of binding site decay adds no benefit to
701 occupancy (target dynamics are not considered by other workers advocating k_{off}
702 optimization [32,33]).

703 Fig 18. Optimization of dynamic occupancy is achieved by first speeding k_{on} to $\geq k_{onSS}$
704 (based on the binding site lifetime), followed by slowing k_{off} to $k_{\_i}$, a process we refer to
705 as "kinetic tuning." The ultimate objective is to achieve the highest occupancy at the lowest

706 free drug concentration (i.e. the SSO profile), affording the greatest chance for achieving
707 a therapeutic index in humans.

708

709 **Conclusion**

710 In our previous work [1], we outlined a first principles theoretical framework (referred to herein
711 as biodynamics) that explains the general mechanisms of cellular analog computing on the basis
712 of non-equilibrium biomolecular state transitions, as well as the key implications of our theory for:

713 1) The transformation of chemical systems into living cells capable of maintaining non-
714 equilibrium conditions, harnessing exponential behavior, and exploiting water H-bond
715 energy to generate state transition barriers.

716 2) The origin of disease-causing cellular dysfunction (Yin-Yang imbalances), and the
717 pharmacological mitigation thereof (insertion of exogenous MDEs capable of fully or
718 partially restoring the normal Yin-Yang balance).

719 The current work is focused on the interplay between two key biodynamics contributions
720 consisting of molecular dynamics and binding dynamics. We used a simplified analytical model
721 that qualitatively captures these contributions to explore the possible effects of non-equilibrium
722 conditions (namely, binding site buildup and decay) on dynamic occupancy. Our results suggest
723 that:

724 1) Achieving the SSO profile as a function of diminishing binding site lifetime depends on
725 increasingly faster k_{on} (noting that nSSO → the qSSO profile is achievable only at high L
726 compared with SSO).

727 2) Nature has likely tuned k_{on} to achieve SSO or qSSO binding for endogenous partners (i.e.
728 maximal binding efficiency).

729 Our findings challenge the conventional equilibrium binding paradigm on which much of modern
730 drug discovery is based, as follows:

731 1) Knowledge of target and binding site buildup and decay rates is essential for achieving the
732 SSO profile on a non-trial-and-error basis.

733 2) Binding site lifetimes ranging from single-digit hours to milliseconds require increasingly
734 faster k_{on} to achieve the SSO profile (i.e. kinetic tuning versus potency optimization).

735 3) Increased drug exposure (i.e. PK) is a poor substitute for kinetically tuned binding, in which
736 the qSSO profile is only asymptotically approached. As such, dose escalation during
737 clinical trials is an extremely risky proposition from the safety standpoint.

738 **Acknowledgements**

739 We gratefully acknowledge Xin Chen and Andrei Golosov for helpful discussions and comments
740 on this manuscript.

References

1. Pearlstein RARA, McKay DJJDJJ, Hornak V, Dickson C, Golosov A, Harrison T, et al. Building New Bridges between In Vitro and In Vivo in Early Drug Discovery: Where Molecular Modeling Meets Systems Biology. Curr Top Med Chem. 2017;17: 1–1. doi:10.2174/1568026617666170414152311

2. Daniel R, Rubens JR, Sarpeshkar R, Lu TK. Synthetic analog computation in living cells. Nature. Nature Publishing Group; 2013;497: 619–623. doi:10.1038/nature12148

3. Howe RM. Fundamentals of the Analog Computer. IEEE Control Syst Mag. 2005; 29–36.

4. Pearlstein RA, MacCannell KA, Erdemli G, Yeola S, Helmlinger G, Hu Q-Y, et al. Implications of dynamic occupancy, binding kinetics, and channel gating kinetics for hERG blocker safety assessment and mitigation. Curr Top Med Chem. 2016;16.

5. O'Hara T, Virág L, Varró A, Rudy Y. Simulation of the undiseased human cardiac ventricular action potential: model formulation and experimental validation. PLoS Comput Biol. 2011;7: e1002061. doi:10.1371/journal.pcbi.1002061

6. Willis WT, Jackman MR, Messer JI, Kuzmiak-Glancy S, Glancy B. A simple hydraulic analog model of oxidative phosphorylation. Med Sci Sports Exerc. 2016;48: 990–1000. doi:10.1249/MSS.0000000000000884

7. Alon U. An introduction to systems biology : design principles of biological circuits. Chapman & Hall/CRC; 2007.

8. Keener J, Sneyd J, editors. Mathematical Physiology [Internet]. New York, NY: Springer New York; 2009. doi:10.1007/978-0-387-75847-3

9. Keener JP. Mathematical physiology 2009 : systems physiology ii. 2nd revise. Springer; 2008.

10. Beard DA. Biosimulation : simulation of living systems [Internet]. Cambridge University Press; 2012. Available: https://books.google.com/books?id=PPl3yNpij9gC&pg=PR4&lpg=PR4&dq=Daniel+A.+Beard.+Biosimulation:+Simulation+of+Living+Systems.+Cambridge+University+Press,+Cambridge,+UK.,+2012.+ISBN+978-0-521-76823-8.&source=bl&ots=RKhaR4C26H&sig=WXszESobIMh3VrWyH9lDX8nuZ

11. Voit EO. A first course in systems biology. Garland Science; 2013.

12. Pearlstein RA, Hu Q-Y, Zhou J, Yowe D, Levell J, Dale B, et al. New hypotheses about the structure-function of proprotein convertase subtilisin/kexin type 9: Analysis of the epidermal growth factor-like repeat A docking site using WaterMap. Proteins Struct Funct Bioinforma. Wiley-Blackwell; 2010;78: 2571–2586. doi:10.1002/prot.22767

13. Pearlstein RA, Sherman W, Abel R. Contributions of water transfer energy to protein-ligand association and dissociation barriers: Watermap analysis of a series of p38α MAP kinase inhibitors. Proteins Struct Funct Bioinforma. 2013;81. doi:10.1002/prot.24276

14. Tran Q-T, Williams S, Farid R, Erdemli G, Pearlstein R. The translocation kinetics of antibiotics through porin OmpC: Insights from structure-based solvation mapping using WaterMap. Proteins Struct Funct Bioinforma. 2013;81. doi:10.1002/prot.24185

15. Velez-Vega C, McKay DJJ, Kurtzman T, Aravamuthan V, Pearlstein RA, Duca JS. Estimation of solvation entropy and enthalpy via analysis of water oxygen-hydrogen

correlations. J Chem Theory Comput. 2015;11. doi:10.1021/acs.jctc.5b00439

16. Pratt JM, Petty J, Riba-Garcia I, Robertson DHL, Gaskell SJ, Oliver SG, et al. Dynamics of Protein Turnover , a Missing Dimension in Proteomics. 2002; 579–591. doi:10.1074/mcp.M200046-MCP200

17. Hopper AK, Patel M, Furia BS, Peltz SW, Trotta CR, Trotta CR, et al. Proteome Half-Life Dynamics in Living Human Cells. 2011; 764–769.

18. Yen HS, Xu Q, Chou DM, Zhao Z, Elledge SJ. Global Protein Stability Profiling in Mammalian Cells. 2008;322: 918–924.

19. Rothman S. How is the balance between protein synthesis and degradation achieved ? 2010; 1–11.

20. Jiang X, Coffino P, Li X. Development of a method for screening short-lived proteins using green fluorescent protein. 2004;

21. Loriaux PM, Hoffmann A, Haugh JM. A Protein Turnover Signaling Motif Controls the Stimulus-Sensitivity of Stress Response Pathways. PLoS Comput Biol. 2013;9. doi:10.1371/journal.pcbi.1002932

22. Hoor M ten. " Are we there yet ?"… Can Equilibrium ever be Achieved ? ChemEd NZ. 2009; 7–8. Available: http://nzic.org.nz/chemed-nz/issue-archive.html

23. Invitrogen Corporation. Theory of Binding Data Analysis. Fluoresc Polariz Tech Resour Guid Chapter 7. 2008; 1–18. Available: www.invitrogen.com/drugdiscovery

24. Grefhorst A, Mcnutt MC, Lagace TA, Horton JD. Plasma PCSK9 preferentially reduces

liver LDL receptors in mice. 2008;49: 1303–1311. doi:10.1194/jlr.M800027-JLR200

25. Benjannet S, Rhainds D, Essalmani R, Mayne J, Wickham L, Jin W, et al. NARC-1/PCSK9 and Its Natural Mutants ZYMOGEN CLEAVAGE AND EFFECTS ON THE LOW DENSITY LIPOPROTEIN (LDL) RECEPTOR AND LDL CHOLESTEROL*. 2004; doi:10.1074/jbc.M409699200

26. Schulz R, Schluter KD, Laufs U. Molecular and cellular function of the proprotein convertase subtilisin/kexin type 9 (PCSK9). Basic Res Cardiol. 2015;110. doi:10.1007/s00395-015-0463-z

27. Gustafsen C, Olsen D, Vilstrup J, Lund S, Reinhardt A, Wellner N, et al. Heparan sulfate proteoglycans present PCSK9 to the LDL receptor. Nat Commun. Springer US; 2017;8: 1–14. doi:10.1038/s41467-017-00568-7

28. Stork D, Timin EN, Berjukow S, Huber C, Hohaus a, Auer M, et al. State dependent dissociation of HERG channel inhibitors. Br J Pharmacol. 2007;151: 1368–1376. doi:10.1038/sj.bjp.0707356

29. Dahl G, Akerud T. Pharmacokinetics and the drug-target residence time concept. Drug Discov Today. 2013;18: 697–707. doi:10.1016/j.drudis.2013.02.010

30. Folmer RHAA. Drug target residence time: a misleading concept. Drug Discov Today. 2017;00: 1–5. doi:10.1016/j.drudis.2017.07.016

31. Annunziata CM, Davis RE, Demchenko Y, Bellamy W, Zhan F, Lenz G, et al. Frequent engagement of the classical and alternative NF-κB pathways by diverse genetic abnormalities in multiple myeloma. Cancer Cell. 2007;12: 115–130.

824 doi:10.1016/j.ccr.2007.07.004.Frequent

825 32. Copeland RA, Pompliano DL, Meek TD. Drug–target residence time and its implications
826 for lead optimization. Nat Rev Drug Discov. 2006;5: 730–739. doi:10.1038/nrd2082

827 33. Schoop A, Dey F. On-rate based optimization of structure-kinetic relationship - Surfing
828 the kinetic map. Drug Discov Today Technol. Elsevier Ltd; 2015;17: 9–15.
829 doi:10.1016/j.ddtec.2015.08.003

830

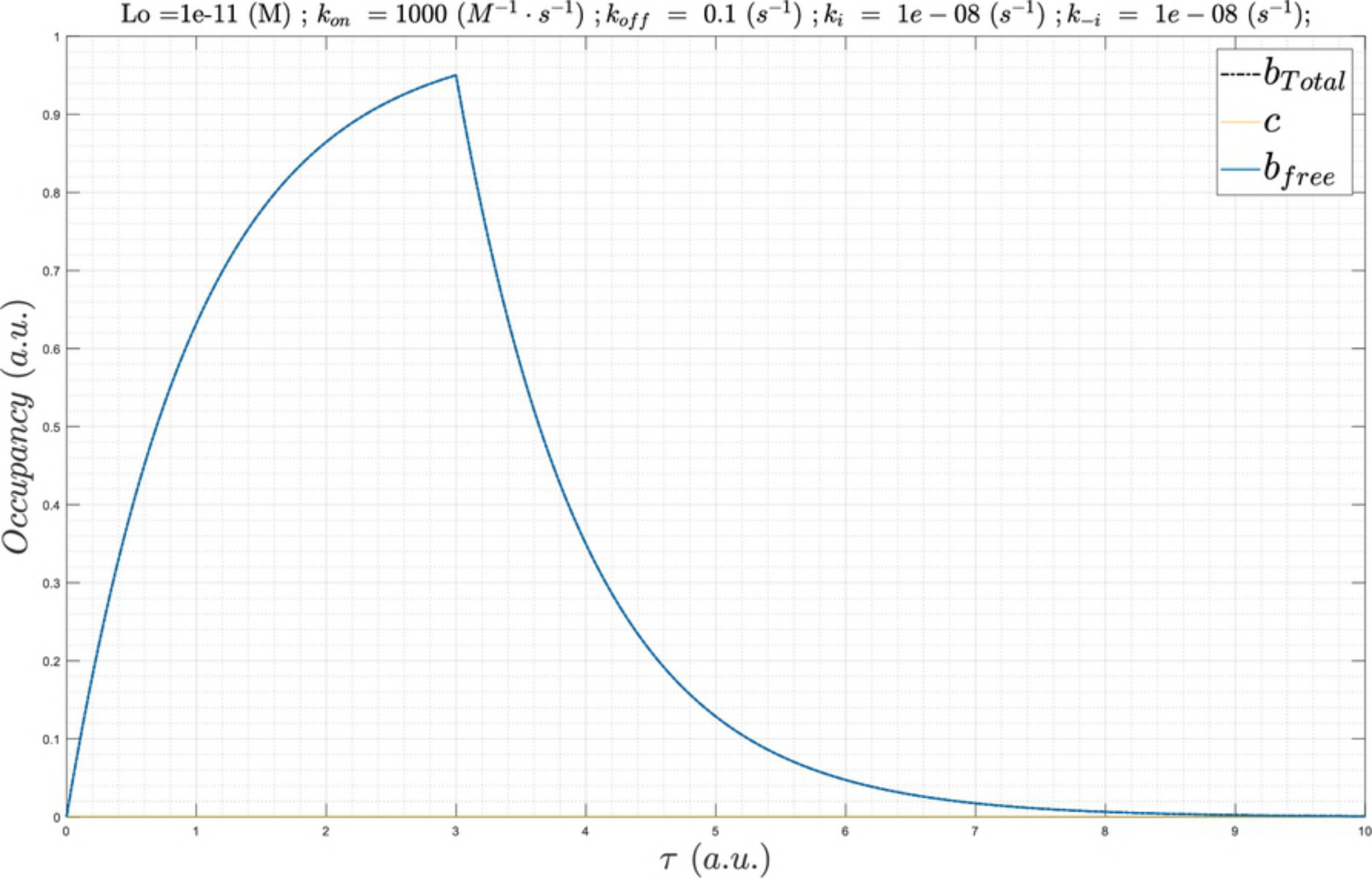
Lo =1e-11 (M) ; $k_{on} = 1000\ (M^{-1} \cdot s^{-1})$; $k_{off} = 0.1\ (s^{-1})$; $k_i = 1e-08\ (s^{-1})$; $k_{-i} = 1e-08\ (s^{-1})$;
b_{Total}
c
b_{free}
Occupancy (a.u.)
τ (a.u.)
0
0.1
0.2
0.3
0.4
0.5
0.6
0.7
0.8
0.9
1
0
1
2
3
4
5
6
7
8
9
10

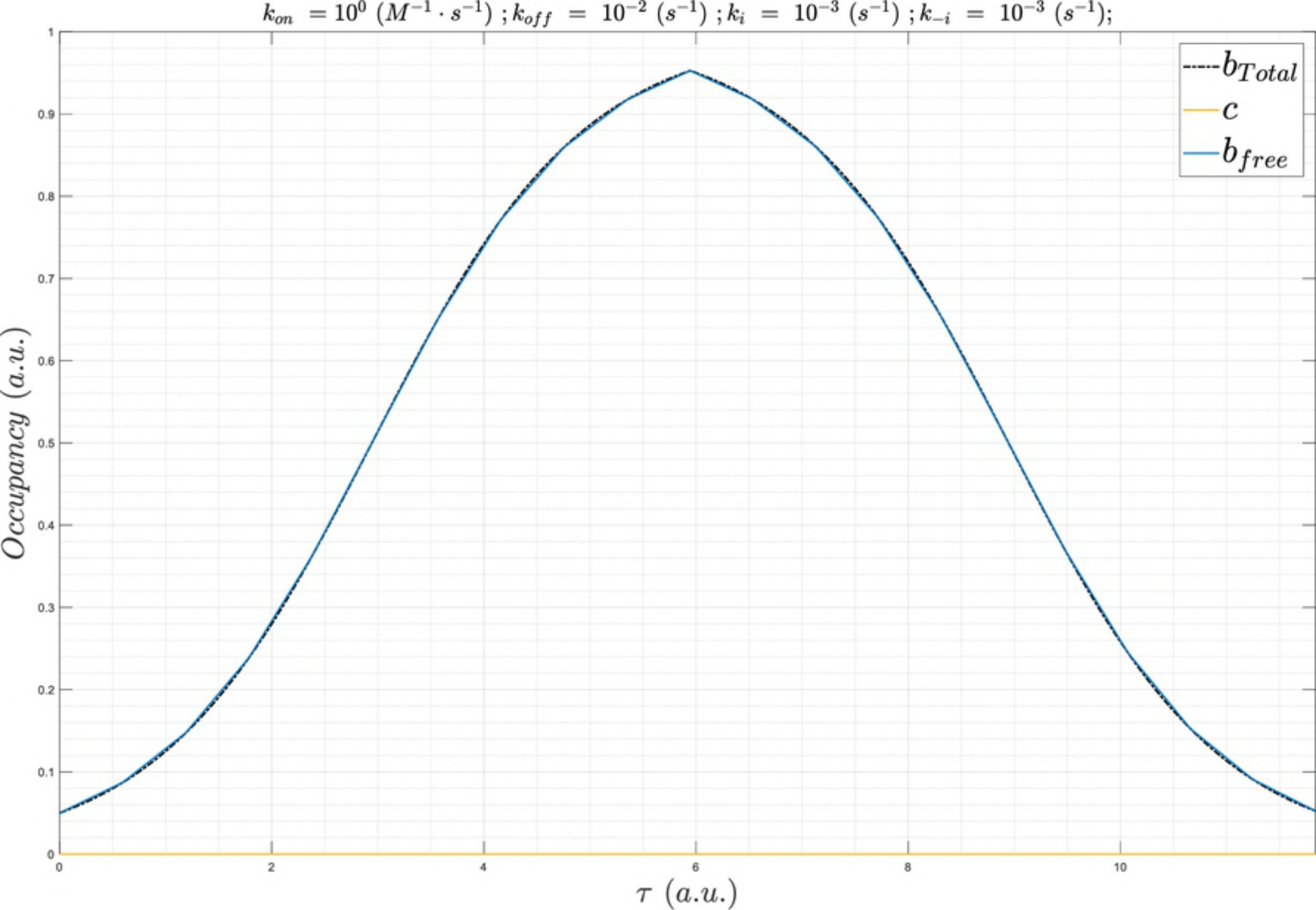
$k_{on} = 10^{0}\ (M^{-1} \cdot s^{-1})\ ; k_{off} = 10^{-2}\ (s^{-1})\ ; k_{i} = 10^{-3}\ (s^{-1})\ ; k_{-i} = 10^{-3}\ (s^{-1});$
b_{Total}
c
b_{free}
$Occupancy\ (a.u.)$
$\tau\ (a.u.)$
0
0.1
0.2
0.3
0.4
0.5
0.6
0.7
0.8
0.9
1
0
2
4
6
8
10

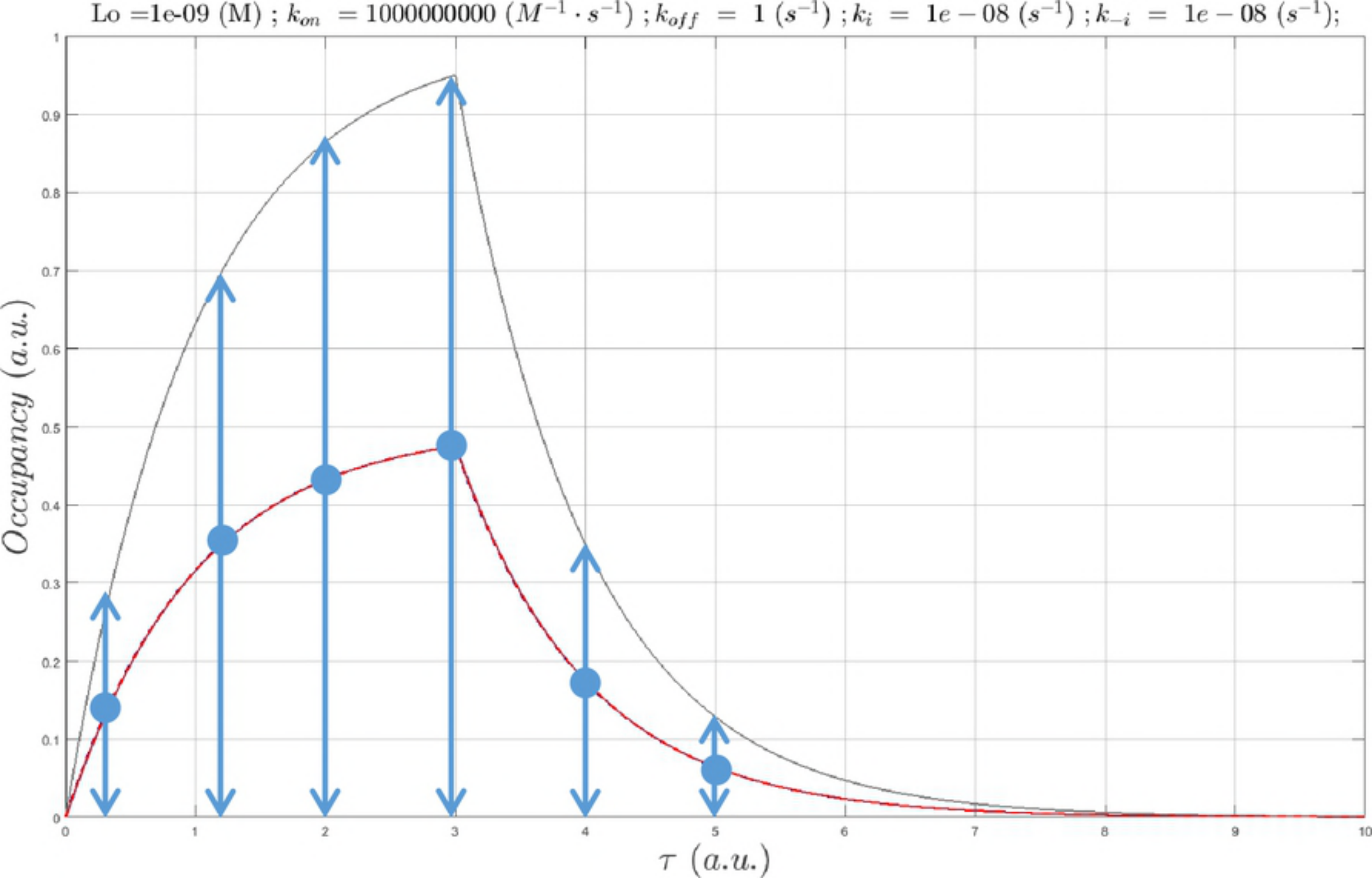
Lo =1e-09 (M) ; k_{on} = 1000000000 ($M^{-1} \cdot s^{-1}$) ; k_{off} = 1 (s^{-1}) ; k_i = 1e − 08 (s^{-1}) ; k_{-i} = 1e − 08 (s^{-1});
Occupancy (a.u.)
τ (a.u.)
0
0.1
0.2
0.3
0.4
0.5
0.6
0.7
0.8
0.9
1
0
1
2
3
4
5
6
7
8
9
10

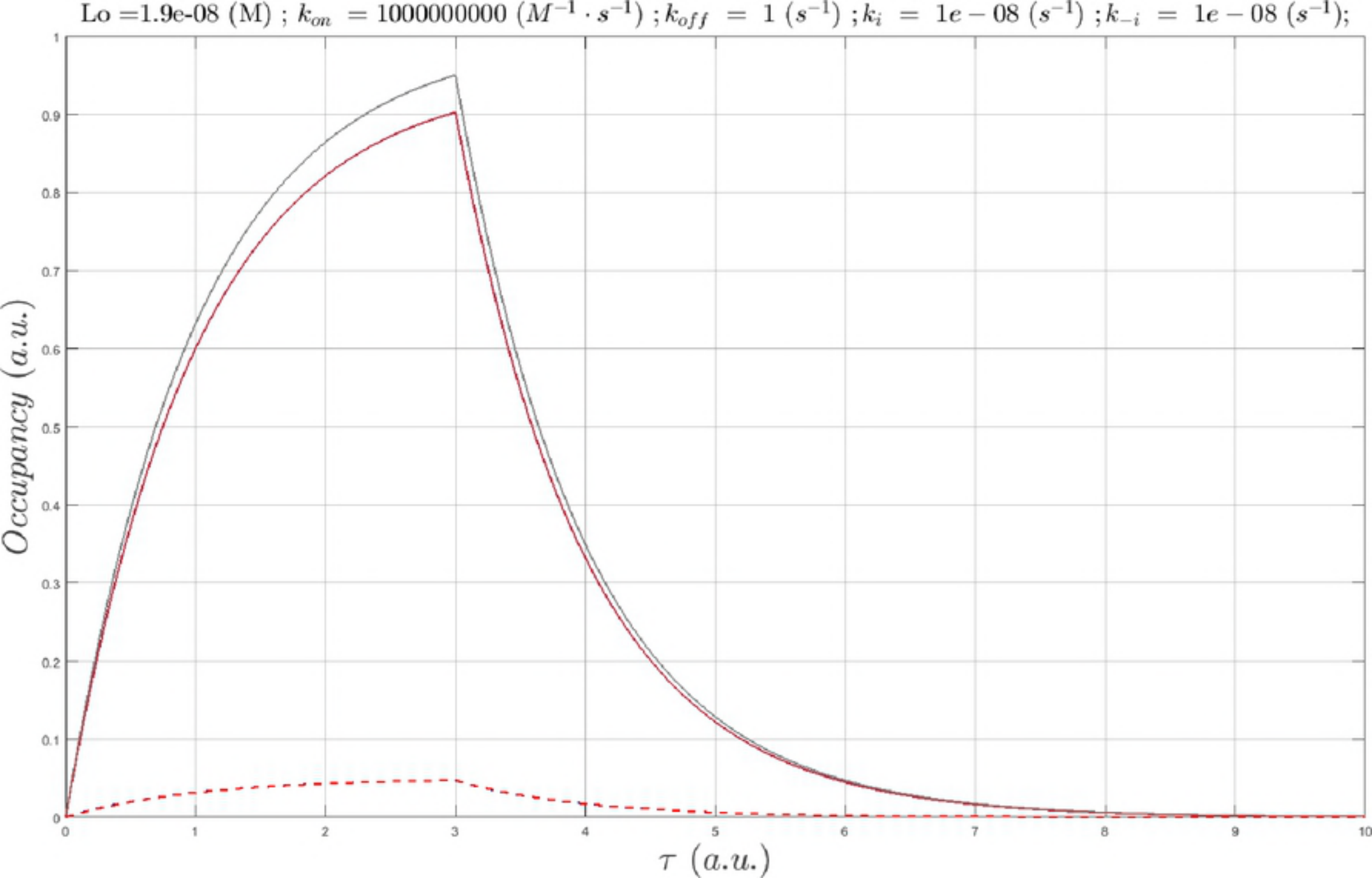
Lo =1.9e-08 (M) ; $k_{on} = 1000000000\ (M^{-1} \cdot s^{-1})$; $k_{off} = 1\ (s^{-1})$; $k_i = 1e-08\ (s^{-1})$; $k_{-i} = 1e-08\ (s^{-1})$;
Occupancy (a.u.)
τ (a.u.)
0
0.1
0.2
0.3
0.4
0.5
0.6
0.7
0.8
0.9
1
0
1
2
3
4
5
6
7
8
9
10

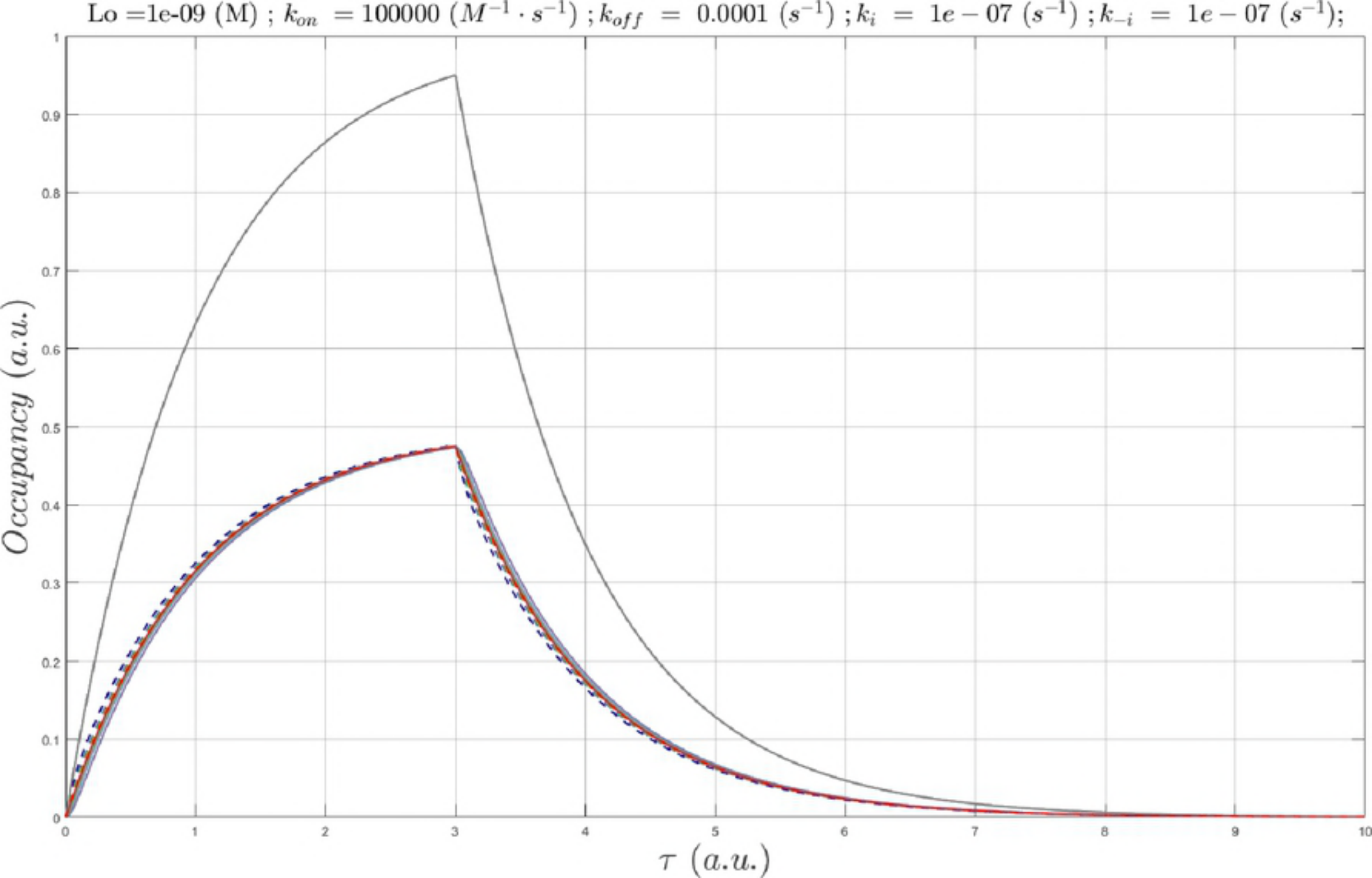
Lo =1e-09 (M) ; k_{on} = 100000 ($M^{-1} \cdot s^{-1}$) ; k_{off} = 0.0001 (s^{-1}) ; k_i = $1e-07$ (s^{-1}) ; k_{-i} = $1e-07$ (s^{-1});
Occupancy (a.u.)
τ (a.u.)
0
0.1
0.2
0.3
0.4
0.5
0.6
0.7
0.8
0.9
1
0
1
2
3
4
5
6
7
8
9
10

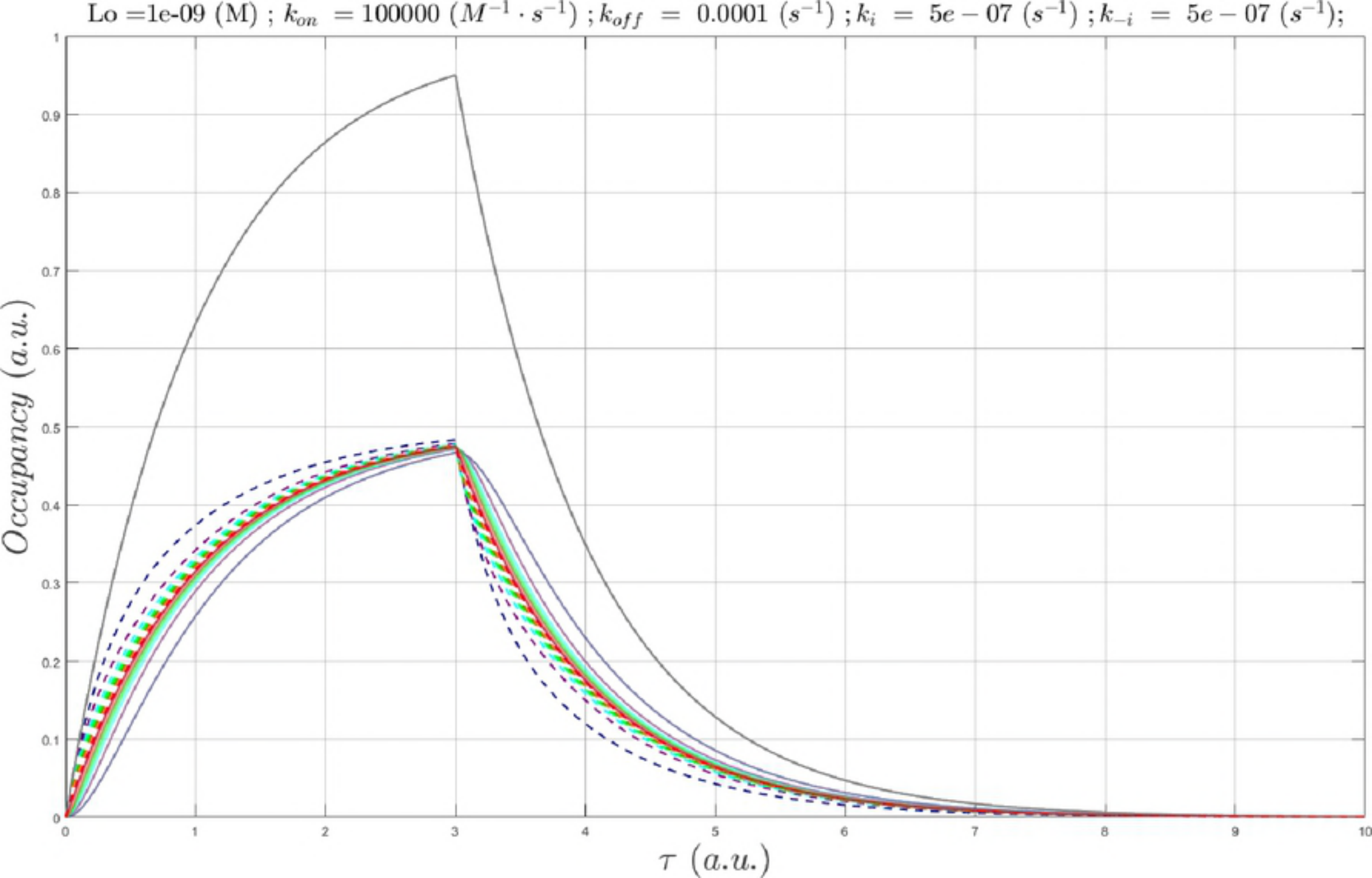
Lo =1e-09 (M) ; k_{on} = 100000 ($M^{-1} \cdot s^{-1}$) ; k_{off} = 0.0001 (s^{-1}) ; k_i = $5e-07$ (s^{-1}) ; k_{-i} = $5e-07$ (s^{-1});
Occupancy (a.u.)
τ (a.u.)
0
0.1
0.2
0.3
0.4
0.5
0.6
0.7
0.8
0.9
1
0
1
2
3
4
5
6
7
8
9
10

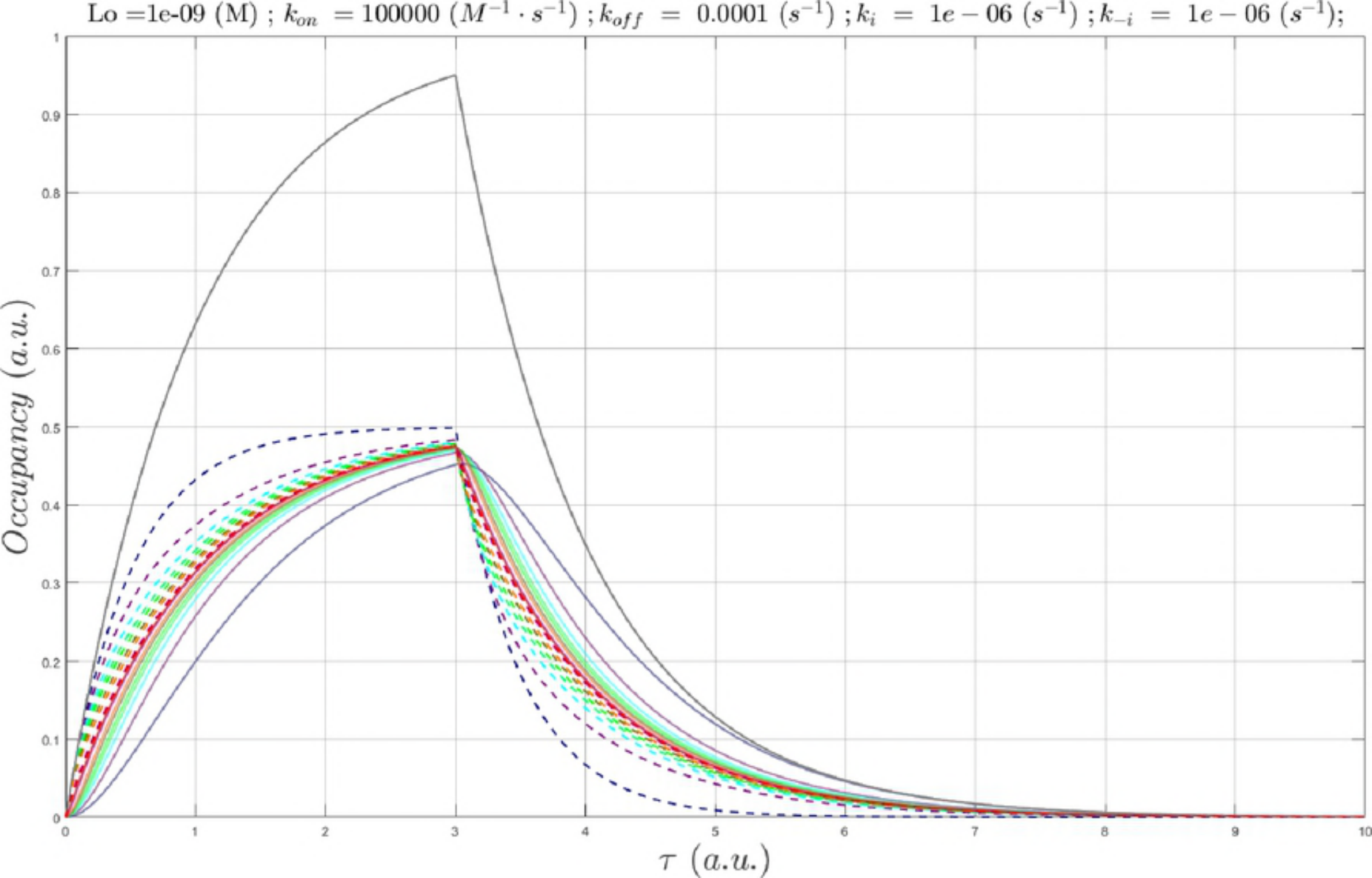
Lo =1e-09 (M) ; $k_{on} = 100000\ (M^{-1} \cdot s^{-1})$; $k_{off} = 0.0001\ (s^{-1})$; $k_i = 1e-06\ (s^{-1})$; $k_{-i} = 1e-06\ (s^{-1})$;
Occupancy (a.u.)
τ (a.u.)
0
0.1
0.2
0.3
0.4
0.5
0.6
0.7
0.8
0.9
1
0
1
2
3
4
5
6
7
8
9
10

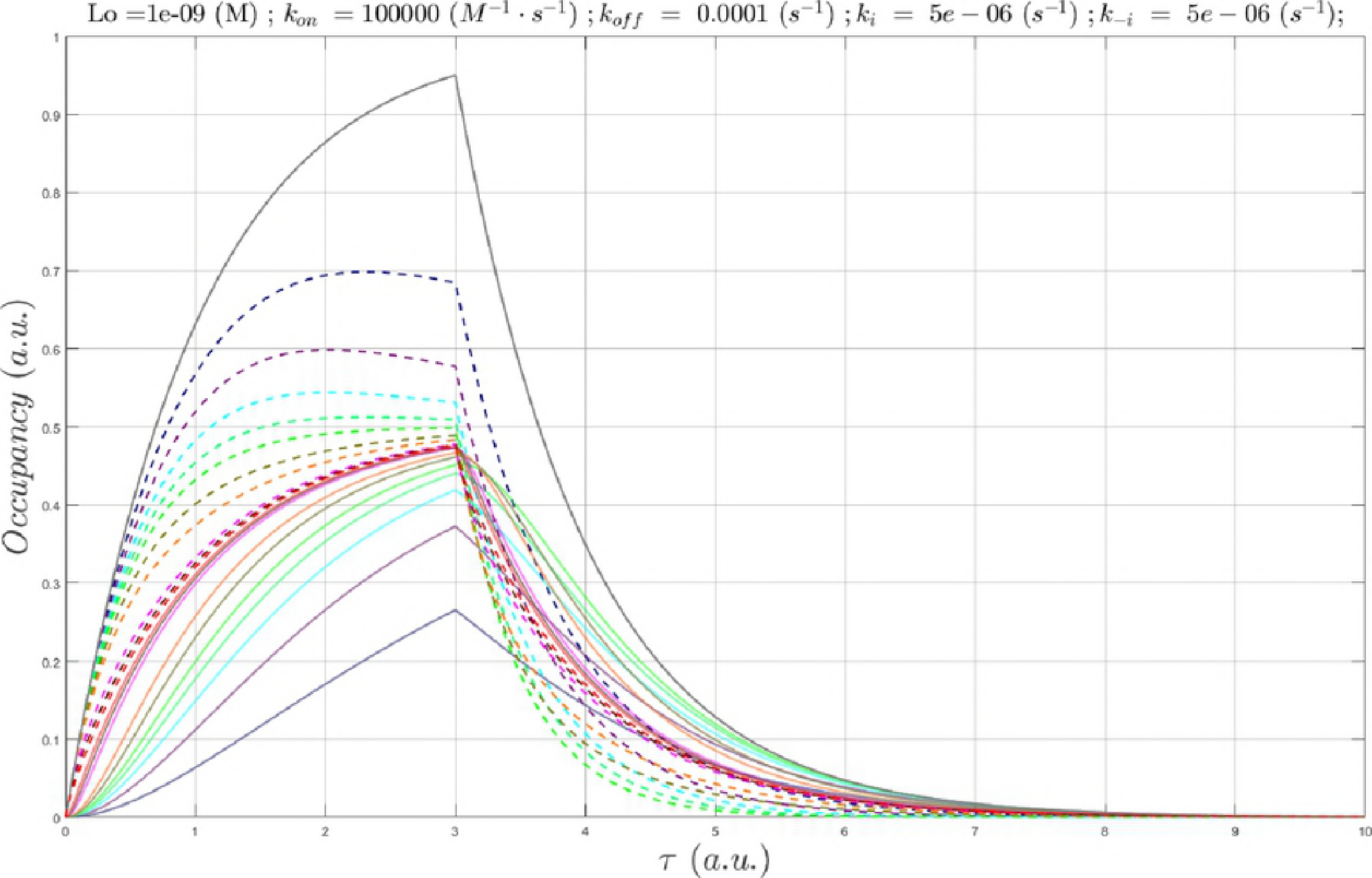
Lo =1e-09 (M) ; k_{on} = 100000 ($M^{-1} \cdot s^{-1}$) ; k_{off} = 0.0001 (s^{-1}) ; k_i = 5e − 06 (s^{-1}) ; k_{-i} = 5e − 06 (s^{-1});
Occupancy (a.u.)
τ (a.u.)
0
0.1
0.2
0.3
0.4
0.5
0.6
0.7
0.8
0.9
1
0
1
2
3
4
5
6
7
8
9
10

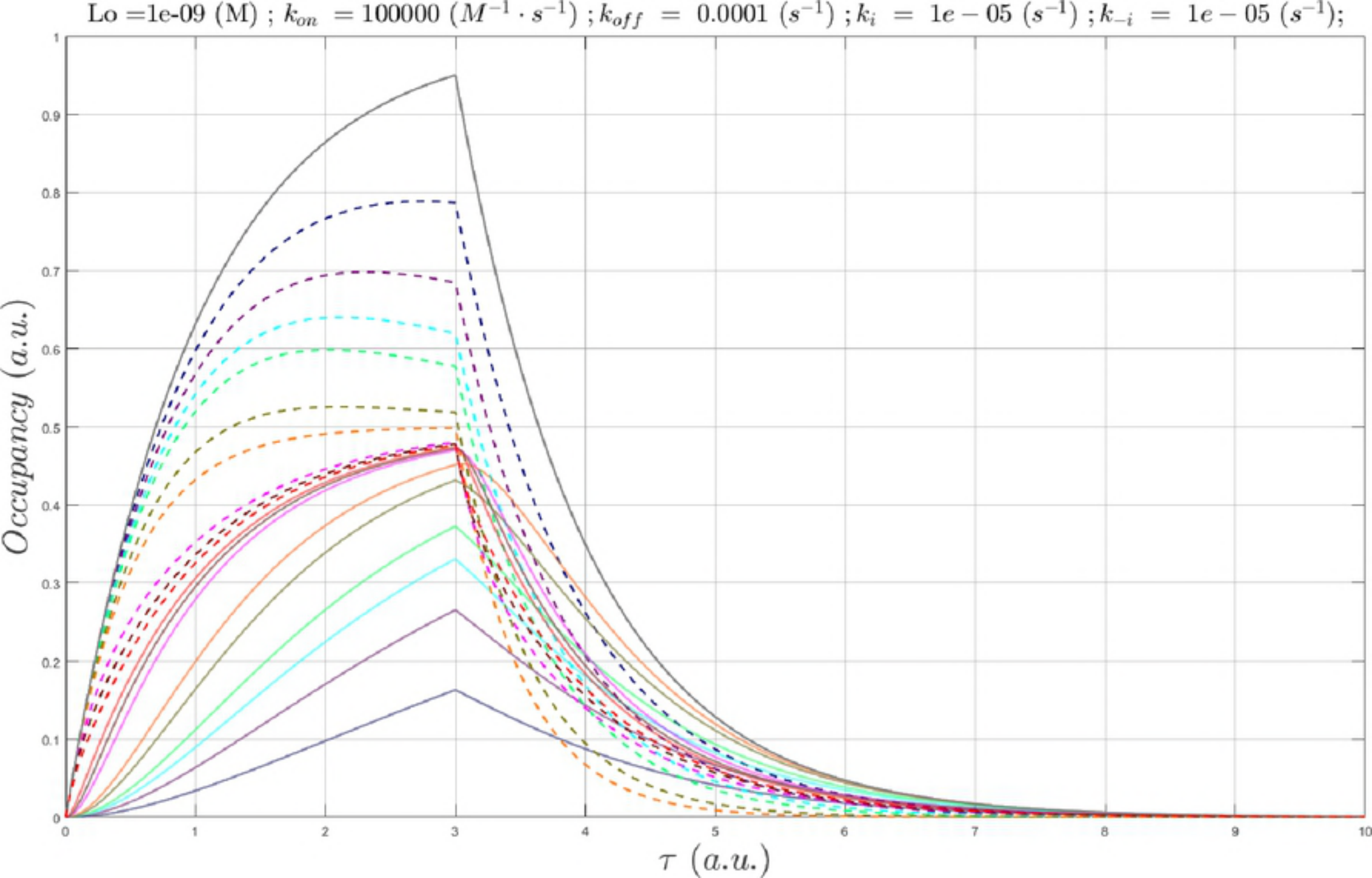
Lo =1e-09 (M) ; k_{on} = 100000 ($M^{-1} \cdot s^{-1}$) ; k_{off} = 0.0001 (s^{-1}) ; k_i = $1e-05$ (s^{-1}) ; k_{-i} = $1e-05$ (s^{-1});
Occupancy (a.u.)
τ (a.u.)
0
0.1
0.2
0.3
0.4
0.5
0.6
0.7
0.8
0.9
1
0
1
2
3
4
5
6
7
8
9
10

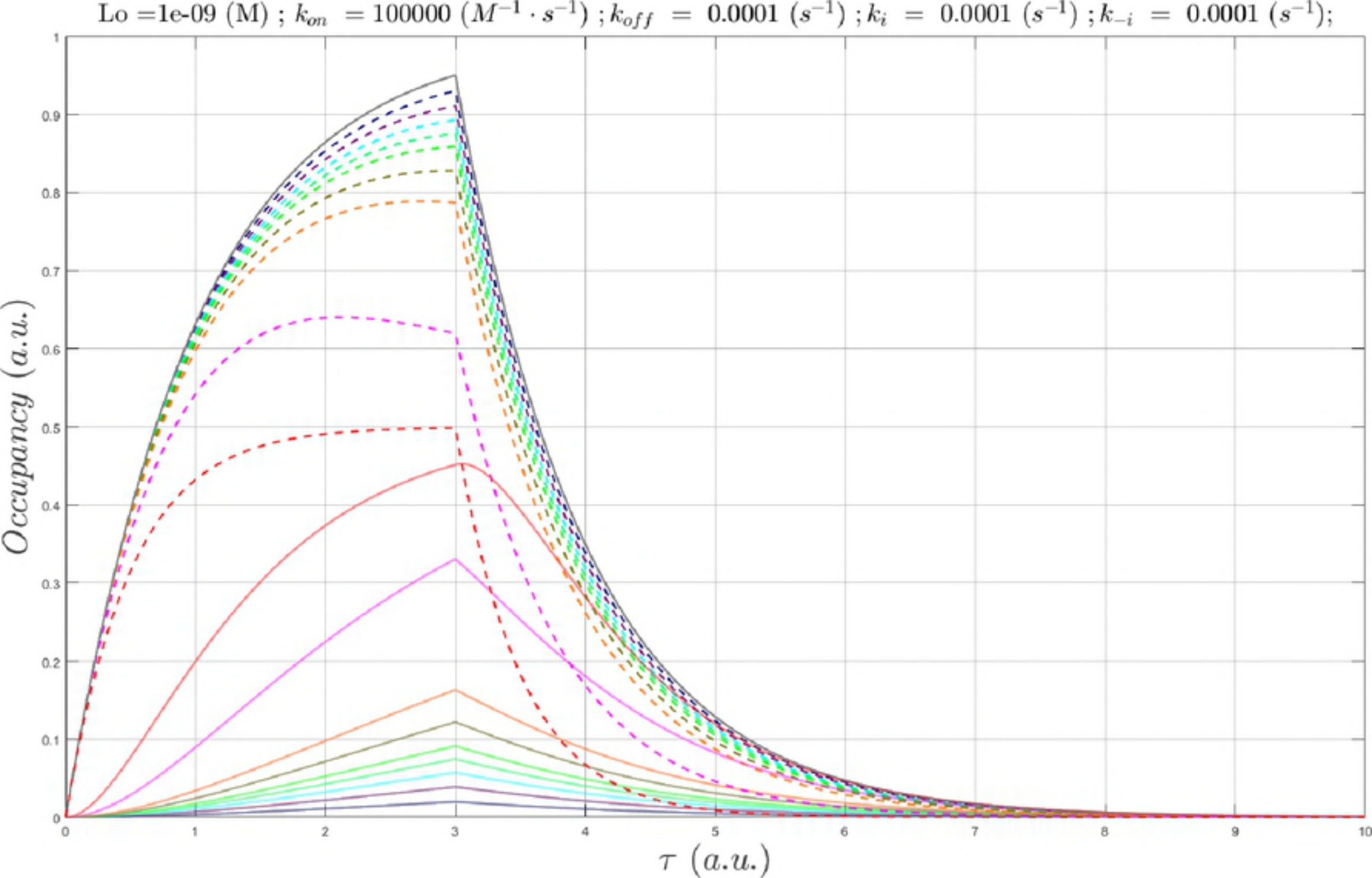
Lo =1e-09 (M) ; k_{on} = 100000 ($M^{-1} \cdot s^{-1}$) ; k_{off} = 0.0001 (s^{-1}) ; k_i = 0.0001 (s^{-1}) ; k_{-i} = 0.0001 (s^{-1});
Occupancy (a.u.)
τ (a.u.)
0
0.1
0.2
0.3
0.4
0.5
0.6
0.7
0.8
0.9
1
0
1
2
3
4
5
6
7
8
9
10

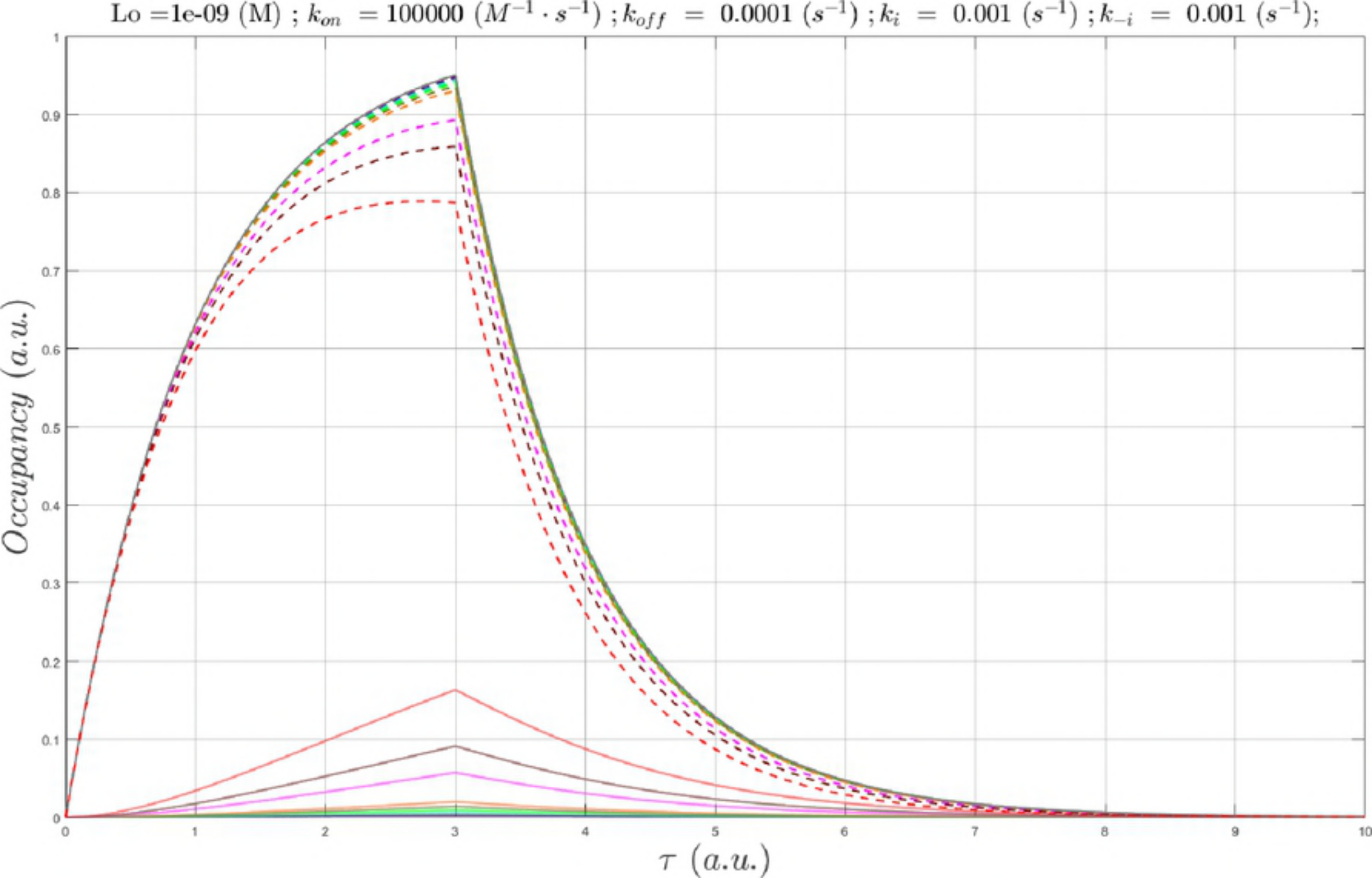
Lo =1e-09 (M) ; k_{on} = 100000 ($M^{-1} \cdot s^{-1}$) ; k_{off} = 0.0001 (s^{-1}) ; k_i = 0.001 (s^{-1}) ; k_{-i} = 0.001 (s^{-1});
Occupancy (a.u.)
τ (a.u.)
0
0.1
0.2
0.3
0.4
0.5
0.6
0.7
0.8
0.9
1
0
1
2
3
4
5
6
7
8
9
10

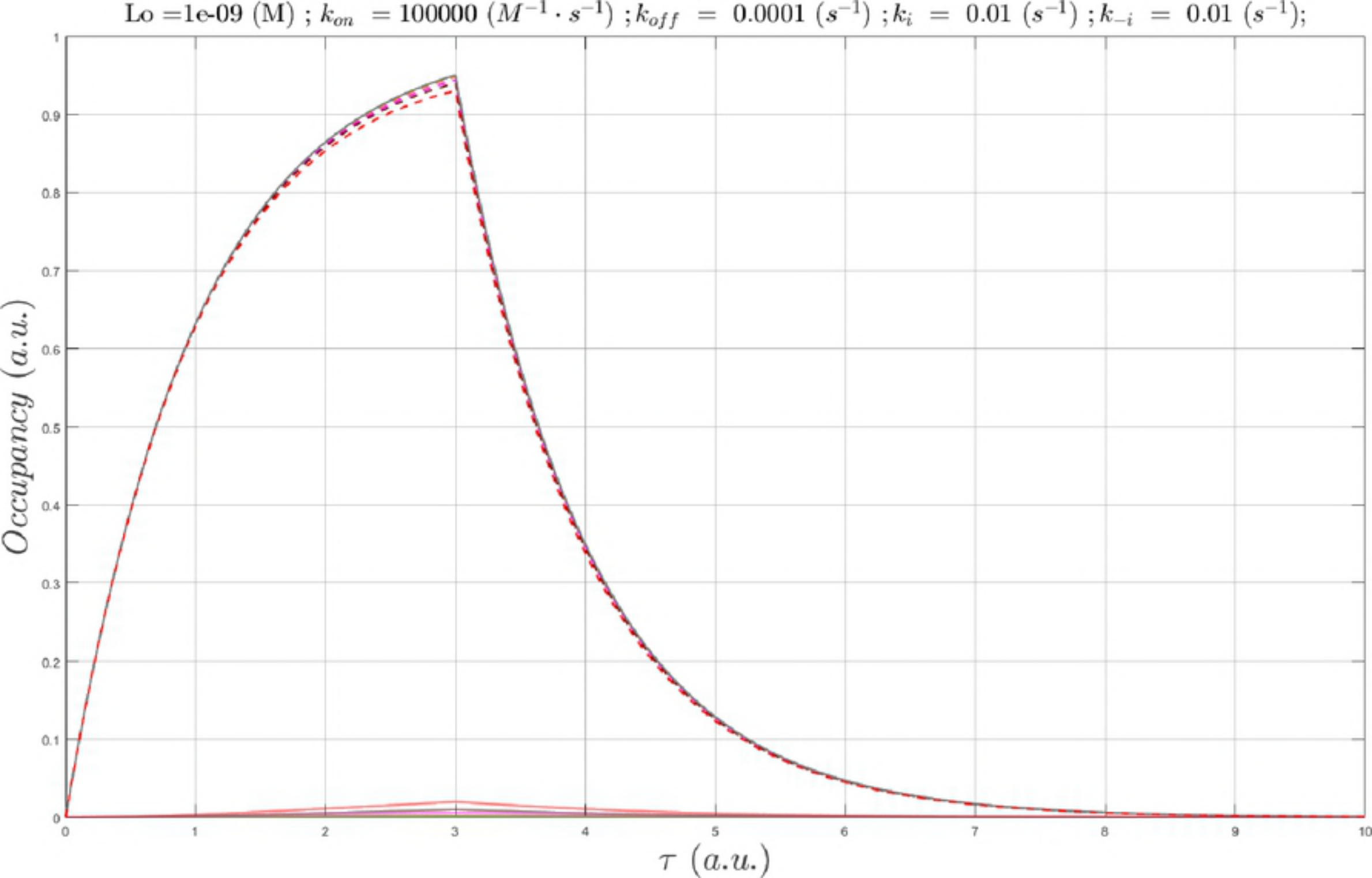
Lo =1e-09 (M) ; k_{on} = 100000 $(M^{-1} \cdot s^{-1})$; k_{off} = 0.0001 (s^{-1}) ; k_i = 0.01 (s^{-1}) ; k_{-i} = 0.01 (s^{-1});
Occupancy (a.u.)
τ (a.u.)
0
0.1
0.2
0.3
0.4
0.5
0.6
0.7
0.8
0.9
1
0
1
2
3
4
5
6
7
8
9
10

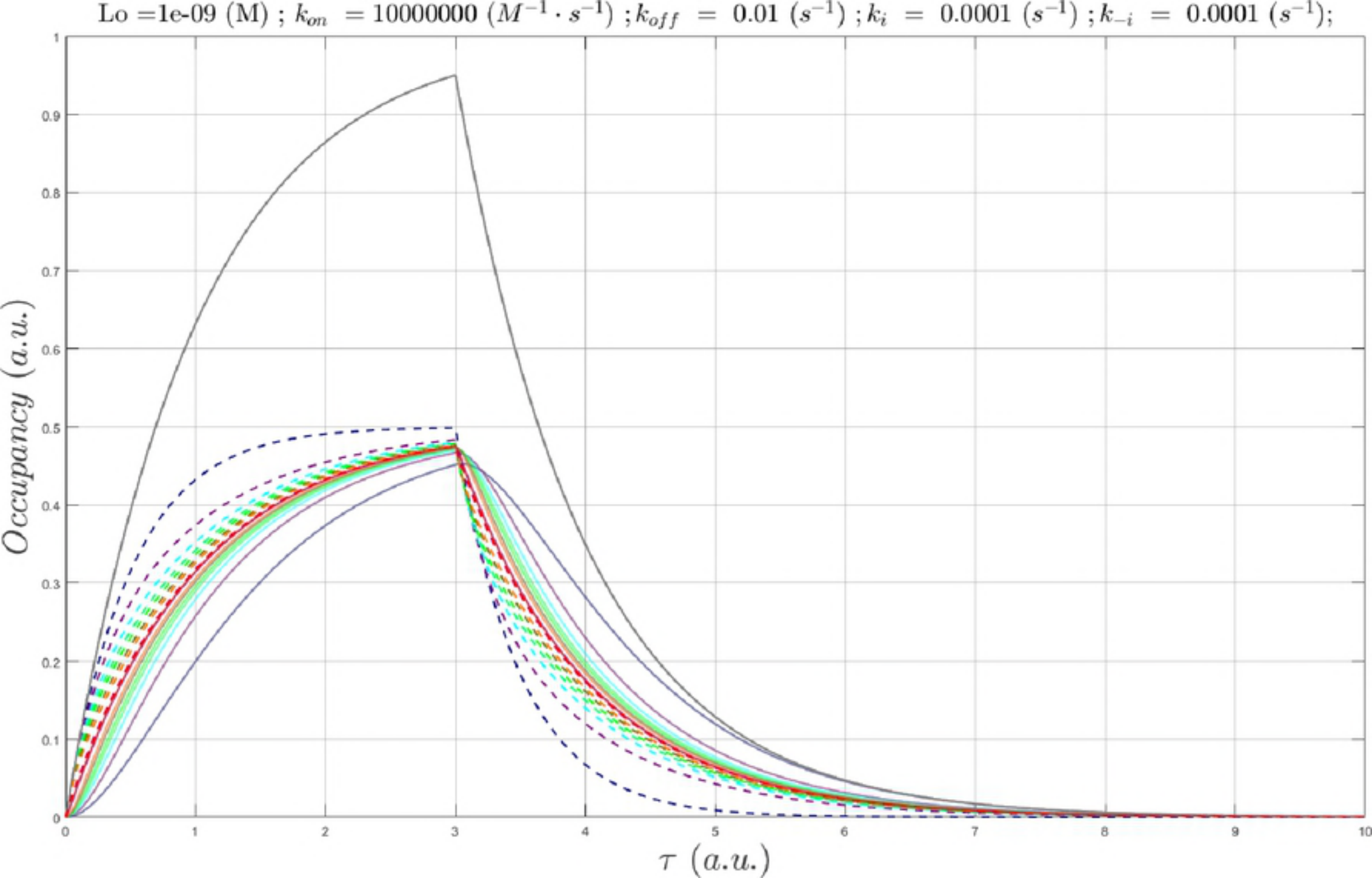
Lo =1e-09 (M) ; k_{on} = 10000000 $(M^{-1} \cdot s^{-1})$; k_{off} = 0.01 (s^{-1}) ; k_i = 0.0001 (s^{-1}) ; k_{-i} = 0.0001 (s^{-1});
Occupancy (a.u.)
τ (a.u.)
0
0.1
0.2
0.3
0.4
0.5
0.6
0.7
0.8
0.9
1
0
1
2
3
4
5
6
7
8
9
10

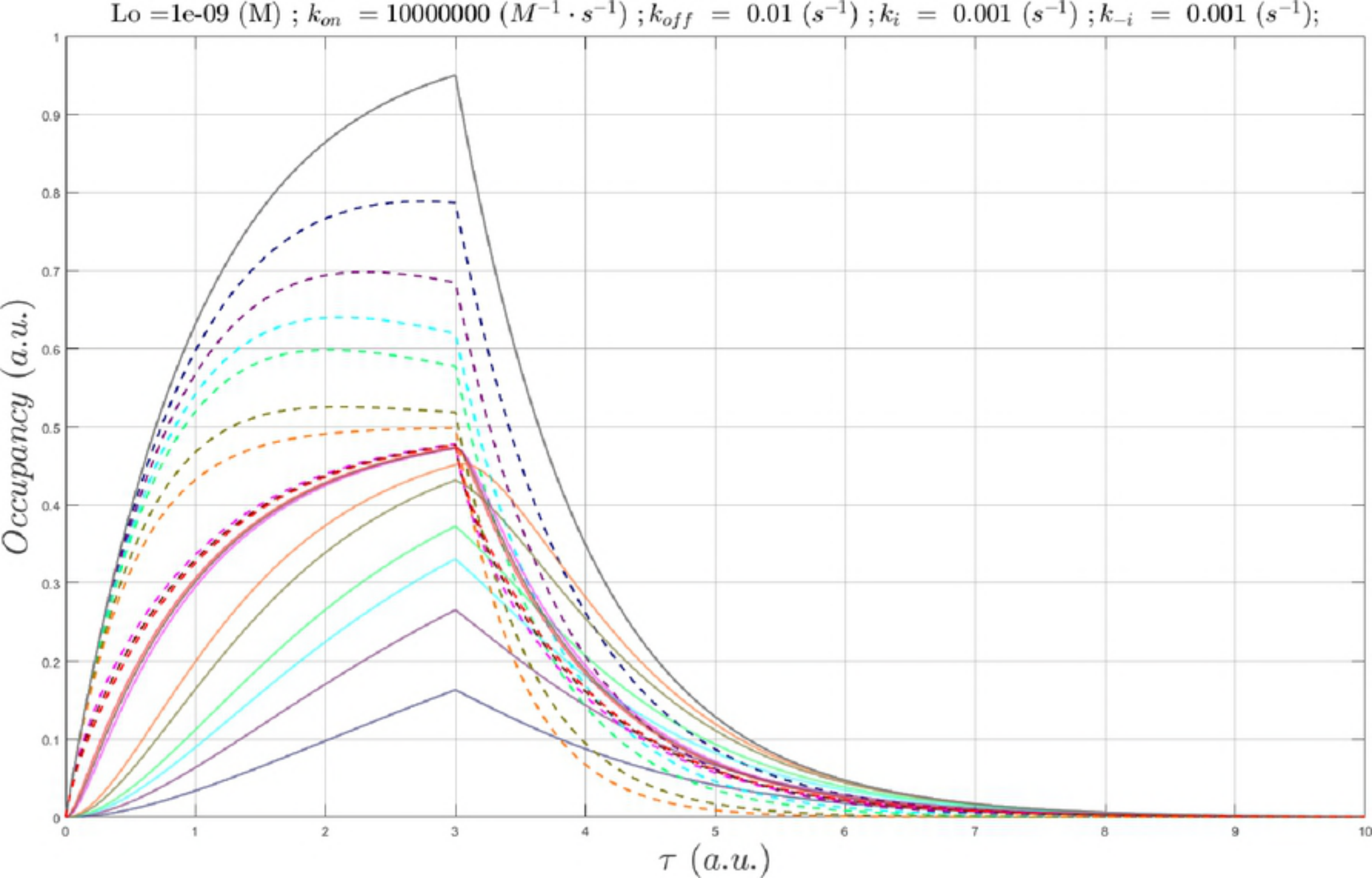
Lo =1e-09 (M) ; k_{on} = 10000000 ($M^{-1} \cdot s^{-1}$) ; k_{off} = 0.01 (s^{-1}) ; k_i = 0.001 (s^{-1}) ; k_{-i} = 0.001 (s^{-1});
Occupancy (a.u.)
τ (a.u.)
0
0.1
0.2
0.3
0.4
0.5
0.6
0.7
0.8
0.9
1
0
1
2
3
4
5
6
7
8
9
10

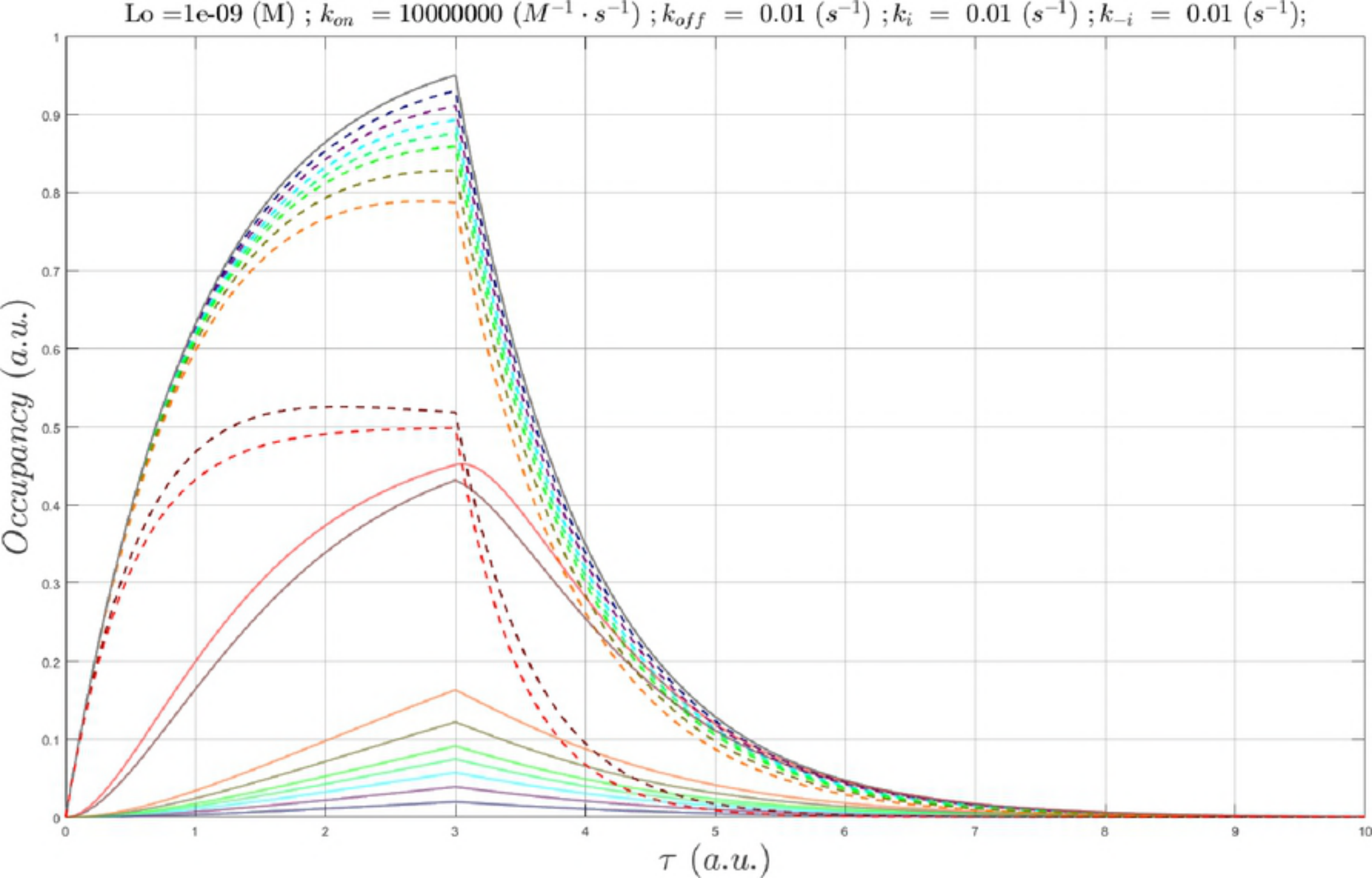
Lo =1e-09 (M) ; k_{on} = 10000000 ($M^{-1} \cdot s^{-1}$) ; k_{off} = 0.01 (s^{-1}) ; k_i = 0.01 (s^{-1}) ; k_{-i} = 0.01 (s^{-1});
Occupancy (a.u.)
τ (a.u.)
0
0.1
0.2
0.3
0.4
0.5
0.6
0.7
0.8
0.9
1
0
1
2
3
4
5
6
7
8
9
10

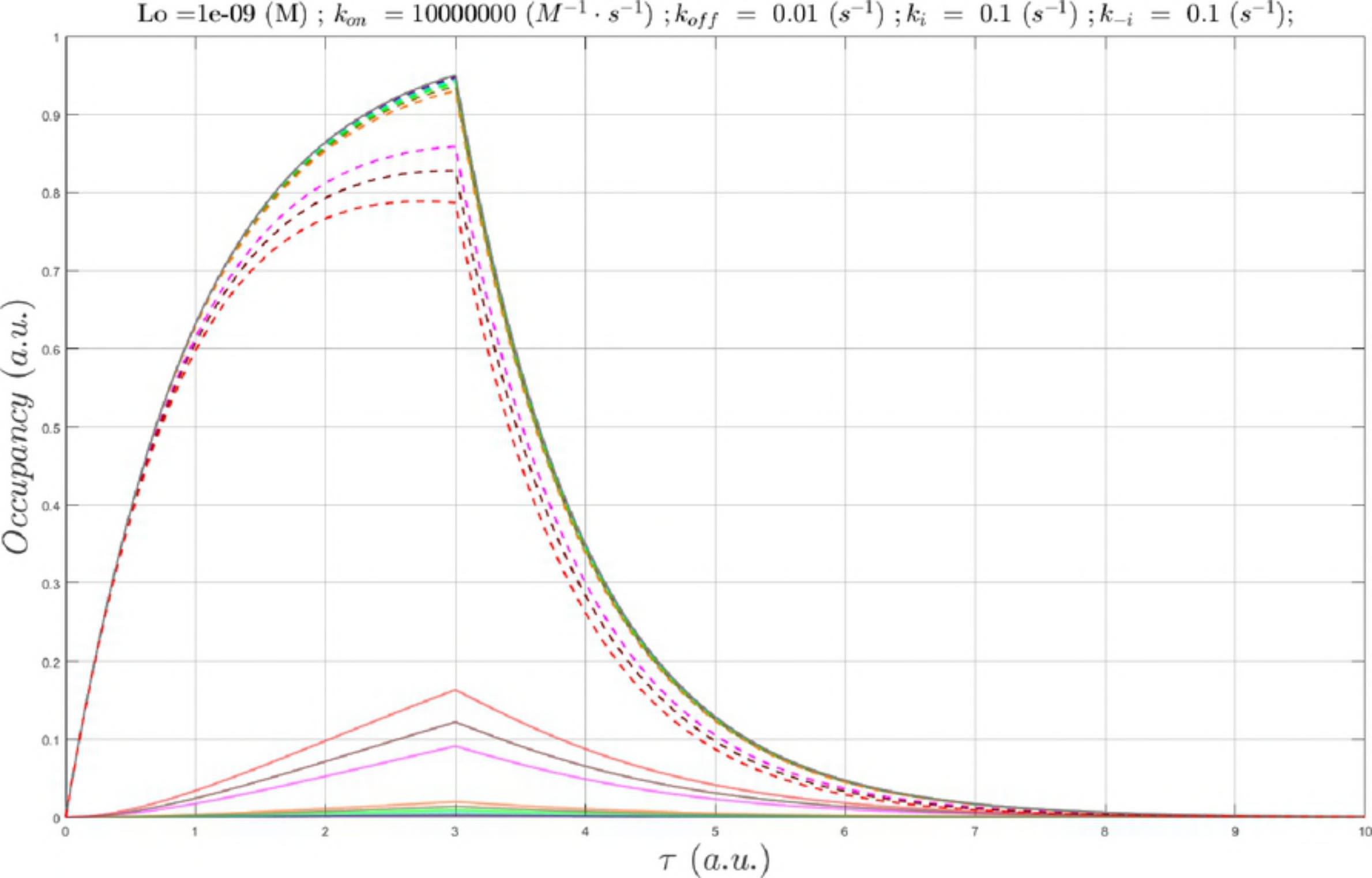
Lo =1e-09 (M) ; k_{on} = 10000000 $(M^{-1} \cdot s^{-1})$; k_{off} = 0.01 (s^{-1}) ; k_i = 0.1 (s^{-1}) ; k_{-i} = 0.1 (s^{-1});
Occupancy (a.u.)
τ (a.u.)
0
0.1
0.2
0.3
0.4
0.5
0.6
0.7
0.8
0.9
1
0
1
2
3
4
5
6
7
8
9
10

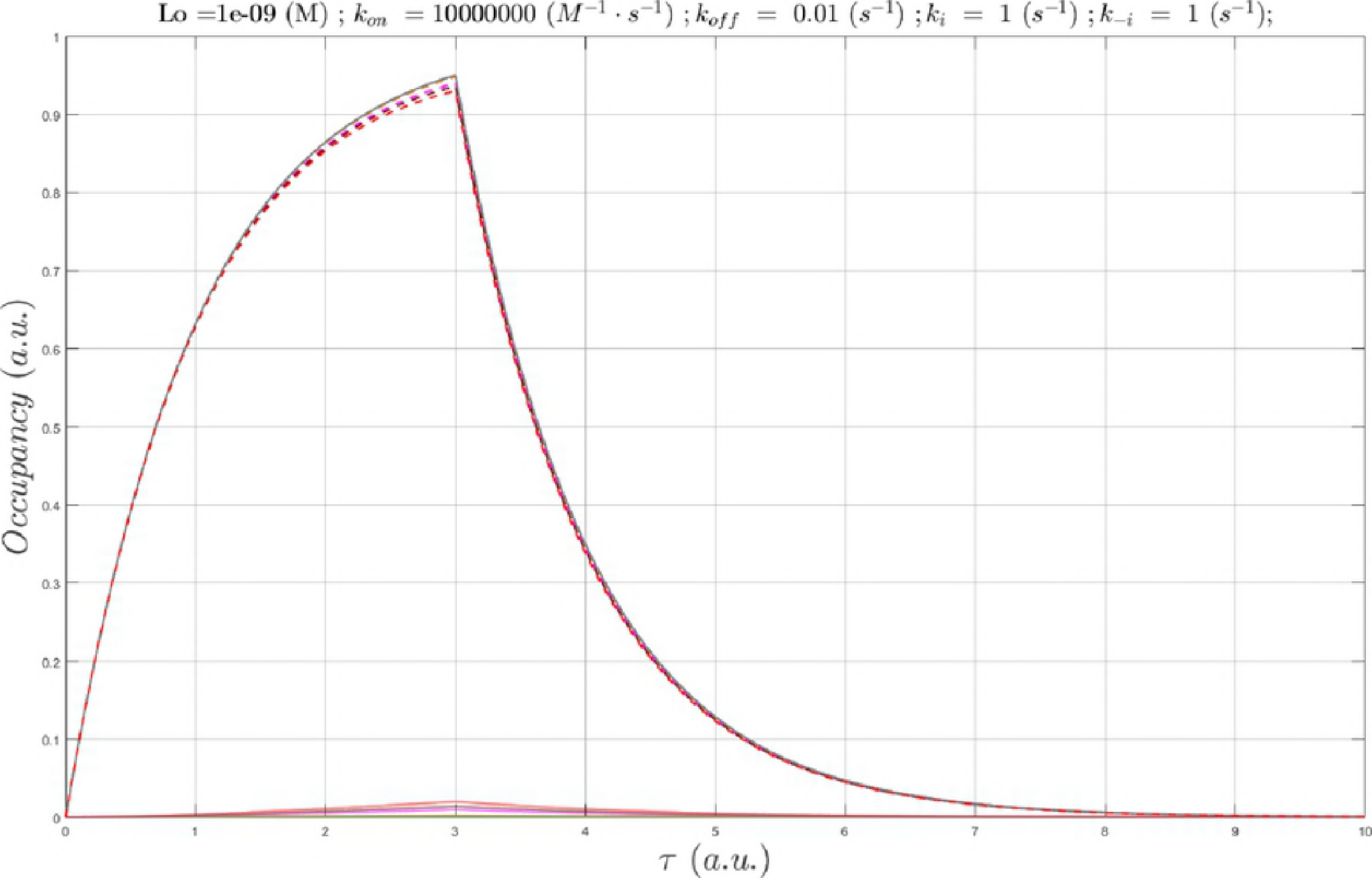
Lo =1e-09 (M) ; k_{on} = 10000000 ($M^{-1} \cdot s^{-1}$) ; k_{off} = 0.01 (s^{-1}) ; k_i = 1 (s^{-1}) ; k_{-i} = 1 (s^{-1});
Occupancy (a.u.)
τ (a.u.)
0
0.1
0.2
0.3
0.4
0.5
0.6
0.7
0.8
0.9
1
0
1
2
3
4
5
6
7
8
9
10

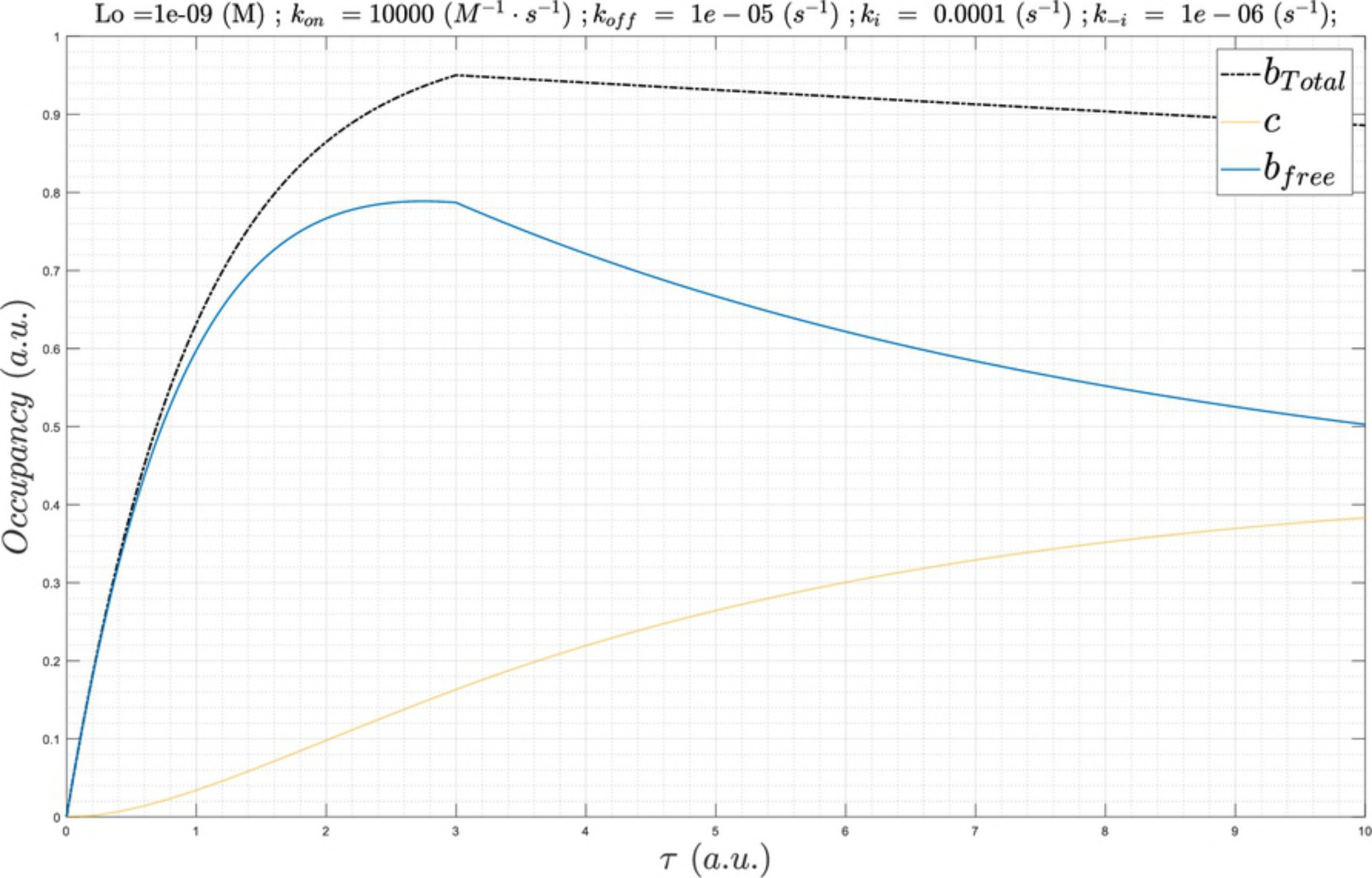
Lo =1e-09 (M) ; k_{on} = 10000 ($M^{-1} \cdot s^{-1}$) ; k_{off} = $1e-05$ (s^{-1}) ; k_i = 0.0001 (s^{-1}) ; k_{-i} = $1e-06$ (s^{-1});
b_{Total}
c
b_{free}
Occupancy (a.u.)
τ (a.u.)
0
0.1
0.2
0.3
0.4
0.5
0.6
0.7
0.8
0.9
1
0
1
2
3
4
5
6
7
8
9
10

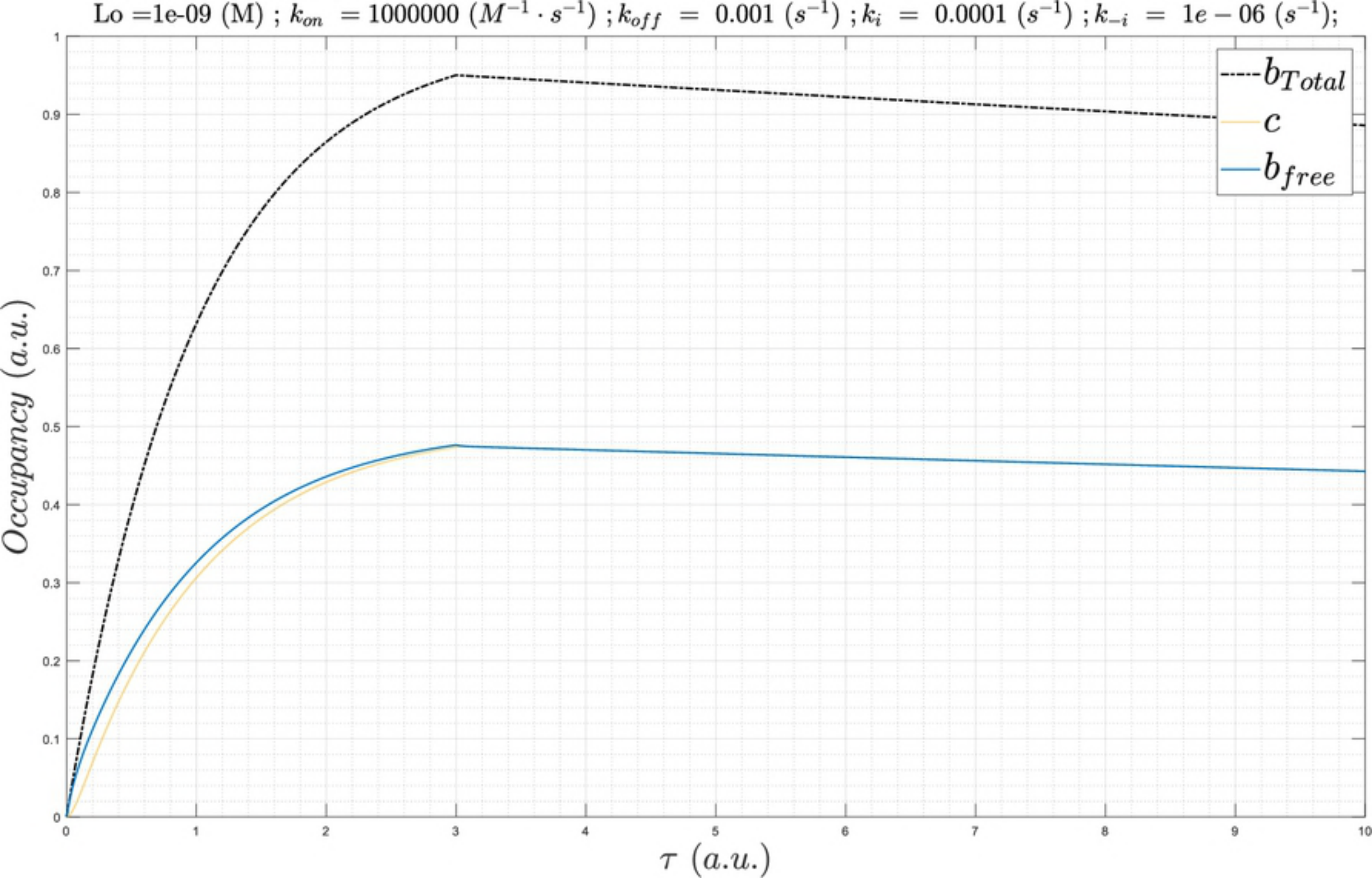
Lo =1e-09 (M) ; k_{on} = 1000000 ($M^{-1} \cdot s^{-1}$) ; k_{off} = 0.001 (s^{-1}) ; k_i = 0.0001 (s^{-1}) ; k_{-i} = $1e-06$ (s^{-1});
b_{Total}
c
b_{free}
Occupancy (a.u.)
τ (a.u.)
0
0.1
0.2
0.3
0.4
0.5
0.6
0.7
0.8
0.9
1
0
1
2
3
4
5
6
7
8
9
10

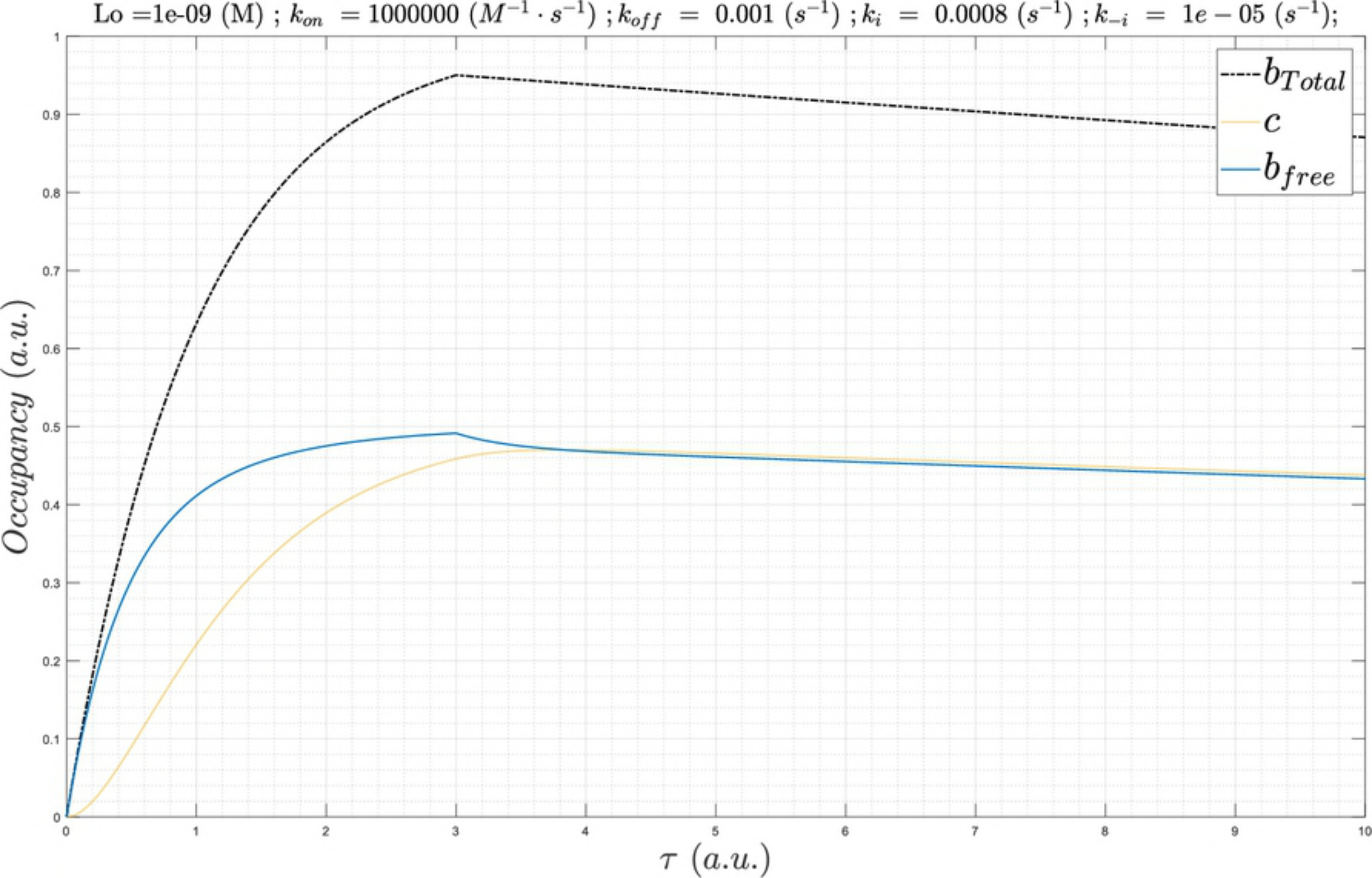
Lo =1e-09 (M) ; k_{on} = 1000000 ($M^{-1} \cdot s^{-1}$) ; k_{off} = 0.001 (s^{-1}) ; k_i = 0.0008 (s^{-1}) ; k_{-i} = $1e-05$ (s^{-1});
b_{Total}
c
b_{free}
Occupancy (a.u.)
τ (a.u.)
0
0.1
0.2
0.3
0.4
0.5
0.6
0.7
0.8
0.9
1
0
1
2
3
4
5
6
7
8
9
10

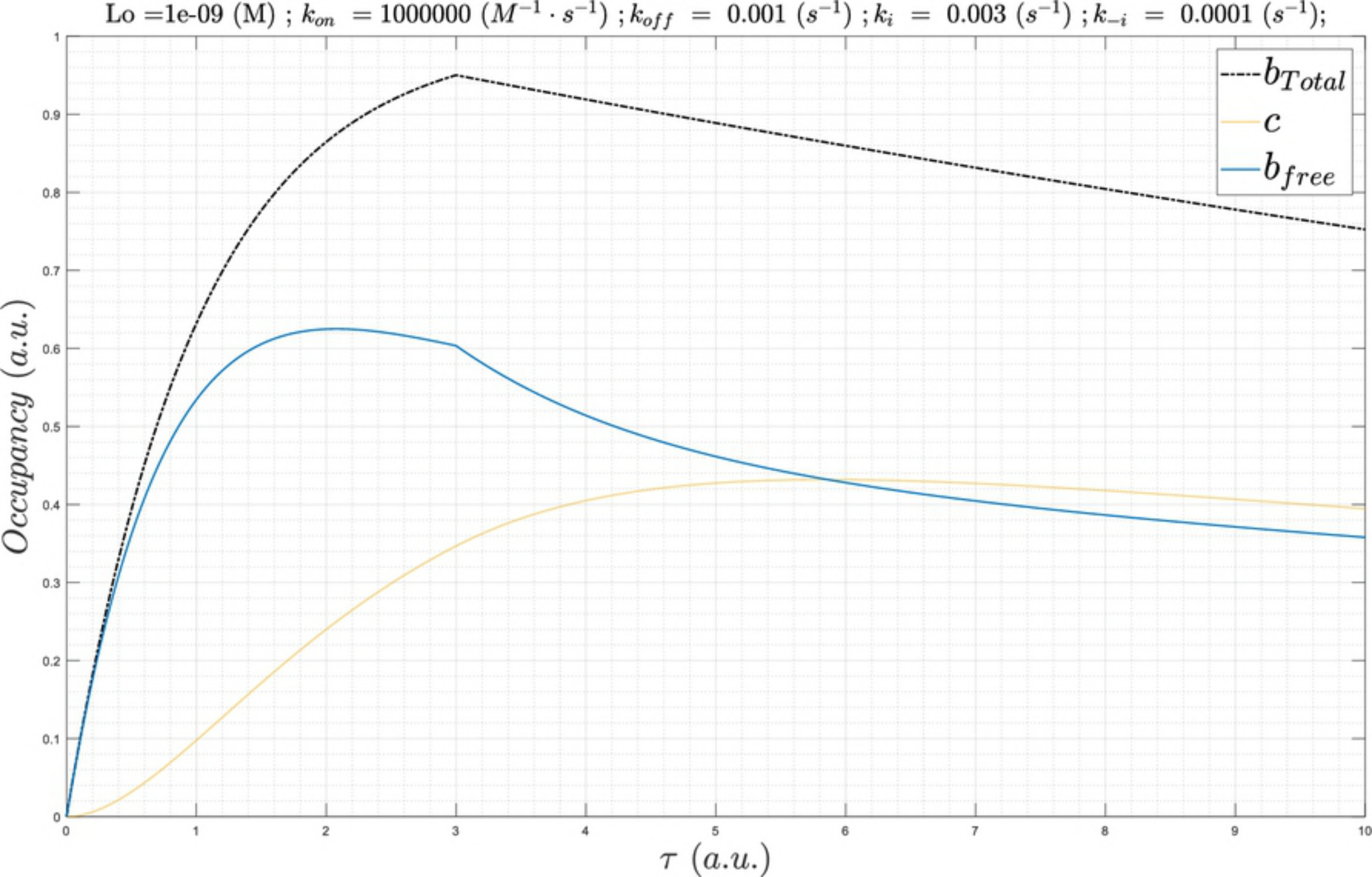
Lo =1e-09 (M) ; k_{on} = 1000000 ($M^{-1} \cdot s^{-1}$) ; k_{off} = 0.001 (s^{-1}) ; k_i = 0.003 (s^{-1}) ; k_{-i} = 0.0001 (s^{-1});
b_{Total}
c
b_{free}
Occupancy (a.u.)
τ (a.u.)
0
0.1
0.2
0.3
0.4
0.5
0.6
0.7
0.8
0.9
1
0
1
2
3
4
5
6
7
8
9
10

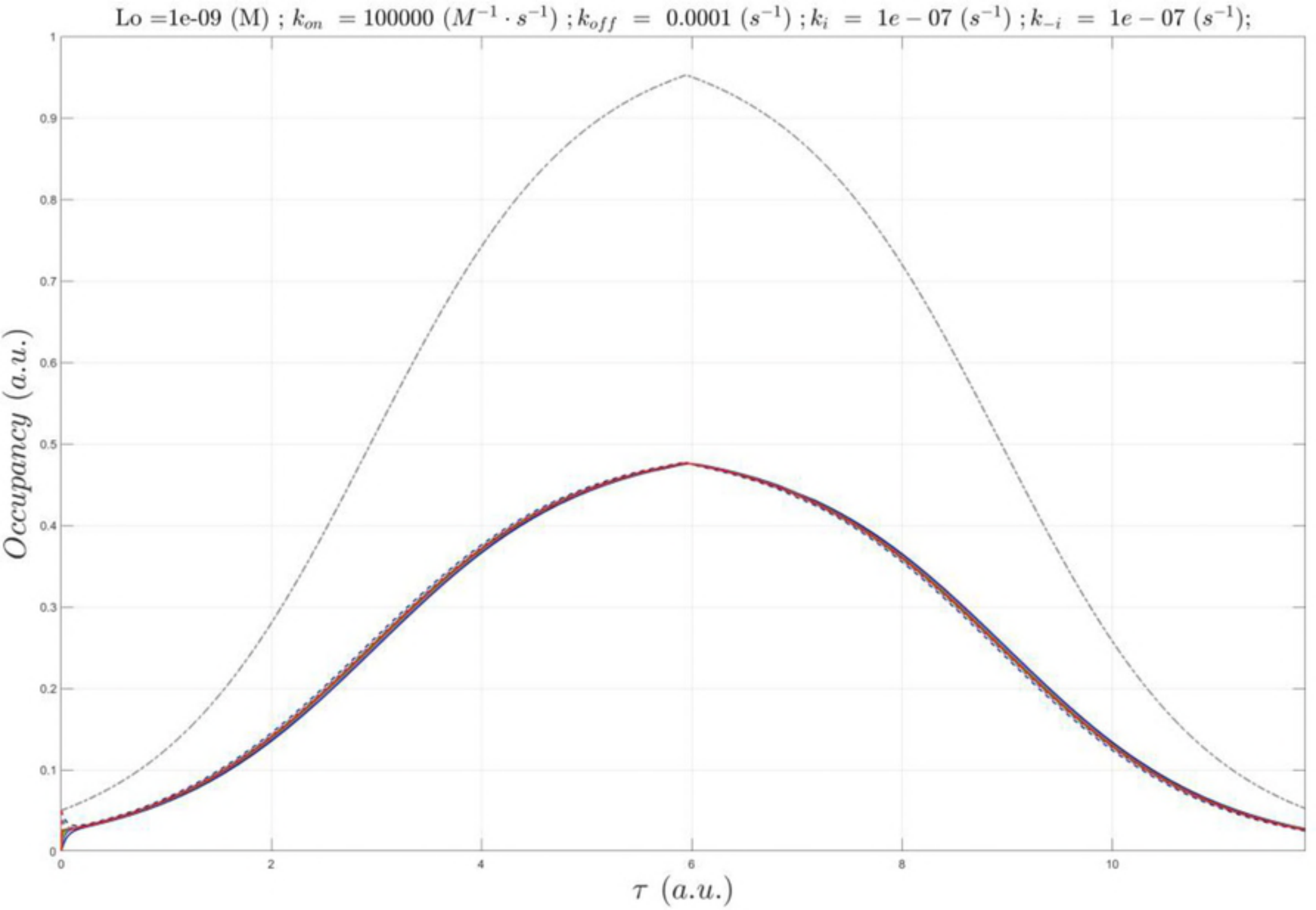
Lo =1e-09 (M) ; k_{on} = 100000 ($M^{-1} \cdot s^{-1}$) ; k_{off} = 0.0001 (s^{-1}) ; k_i = $1e-07$ (s^{-1}) ; k_{-i} = $1e-07$ (s^{-1});
Occupancy (a.u.)
τ (a.u.)
0
0.1
0.2
0.3
0.4
0.5
0.6
0.7
0.8
0.9
1
0
2
4
6
8
10

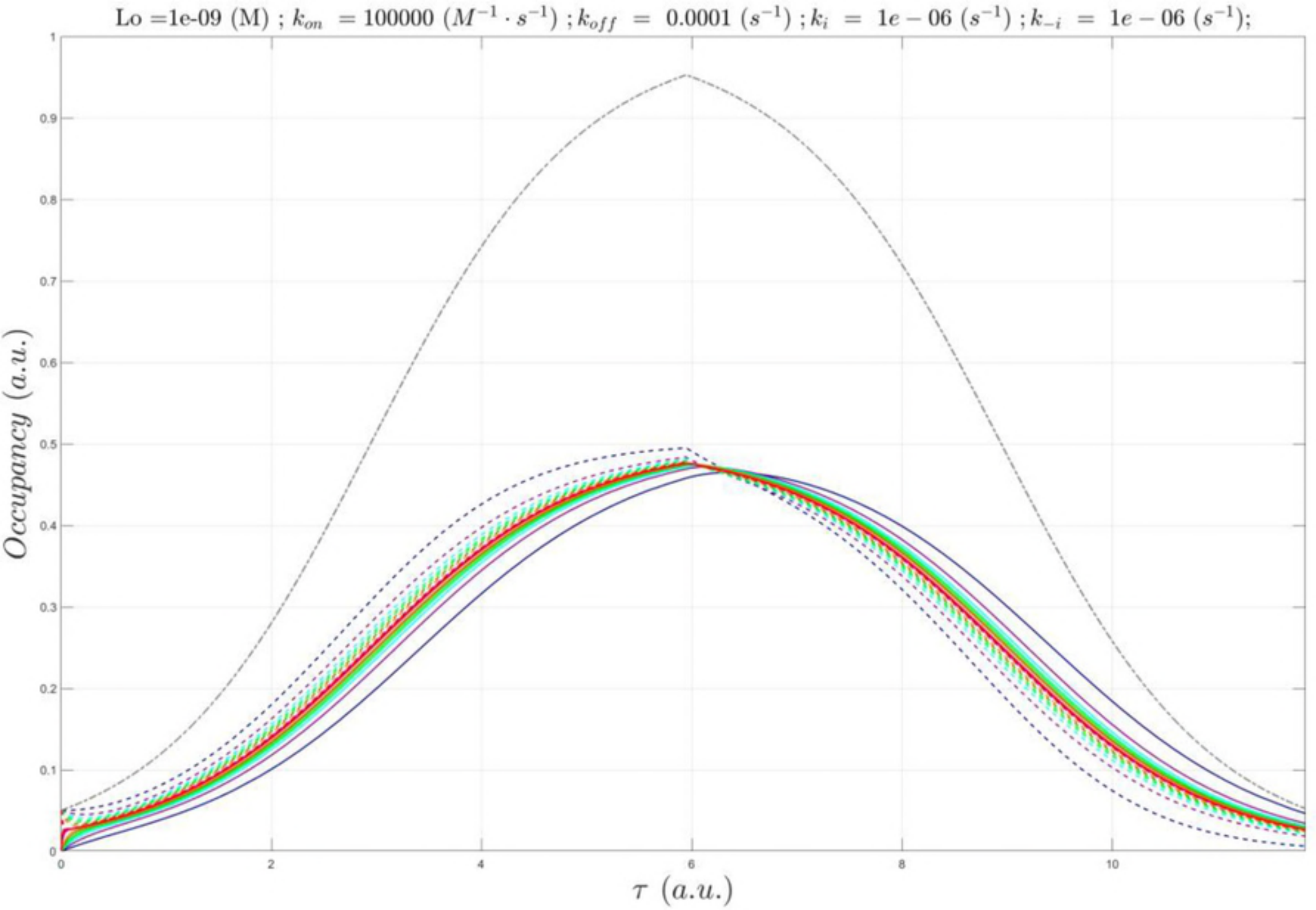
Lo =1e-09 (M) ; k_{on} = 100000 ($M^{-1} \cdot s^{-1}$) ; k_{off} = 0.0001 (s^{-1}) ; k_i = $1e-06$ (s^{-1}) ; k_{-i} = $1e-06$ (s^{-1});
Occupancy (a.u.)
τ (a.u.)
0
0.1
0.2
0.3
0.4
0.5
0.6
0.7
0.8
0.9
1
0
2
4
6
8
10

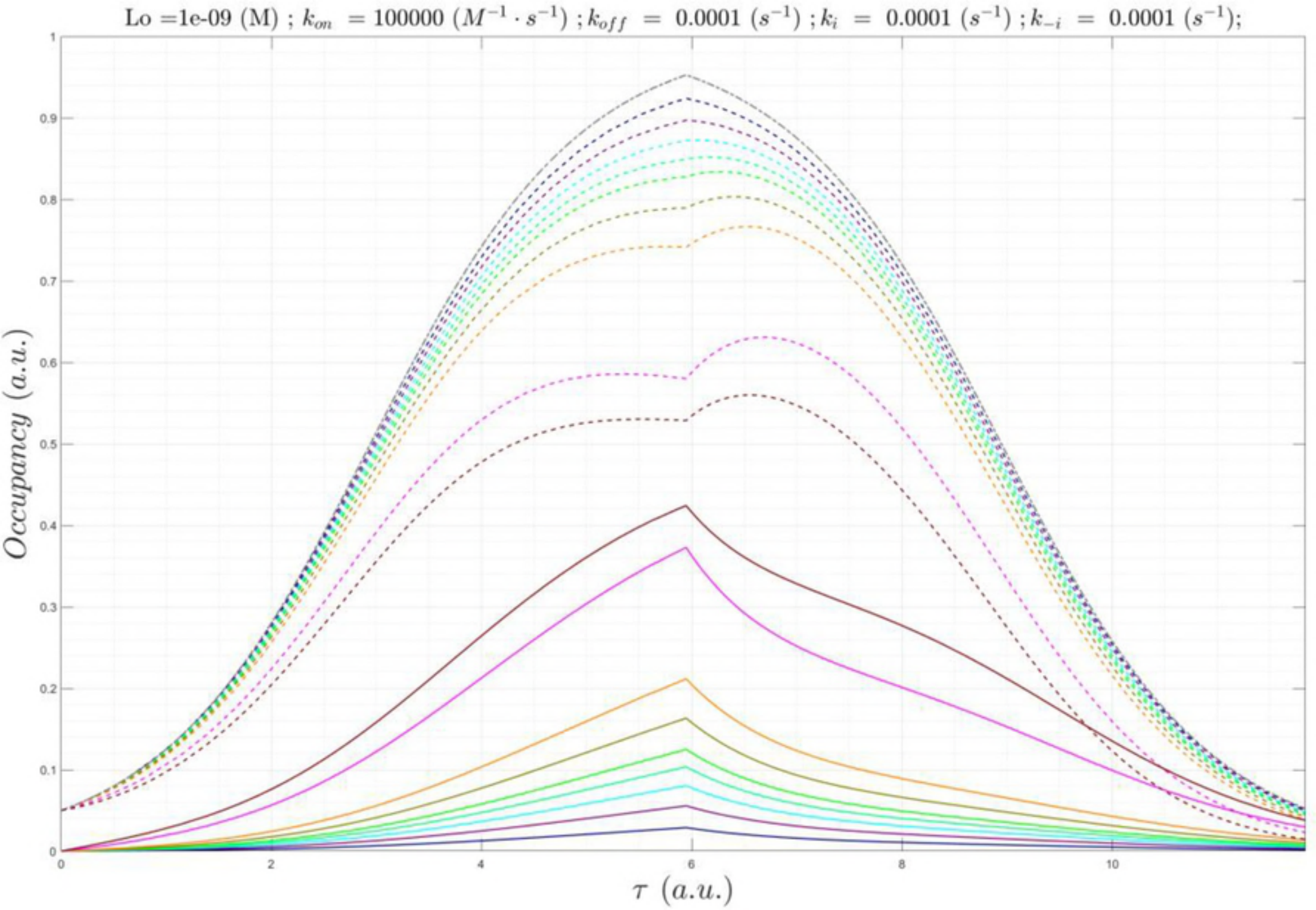
Lo =1e-09 (M) ; k_{on} = 100000 $(M^{-1} \cdot s^{-1})$; k_{off} = 0.0001 (s^{-1}) ; k_i = 0.0001 (s^{-1}) ; k_{-i} = 0.0001 (s^{-1});
Occupancy (a.u.)
τ (a.u.)
0
0.1
0.2
0.3
0.4
0.5
0.6
0.7
0.8
0.9
1
0
2
4
6
8
10

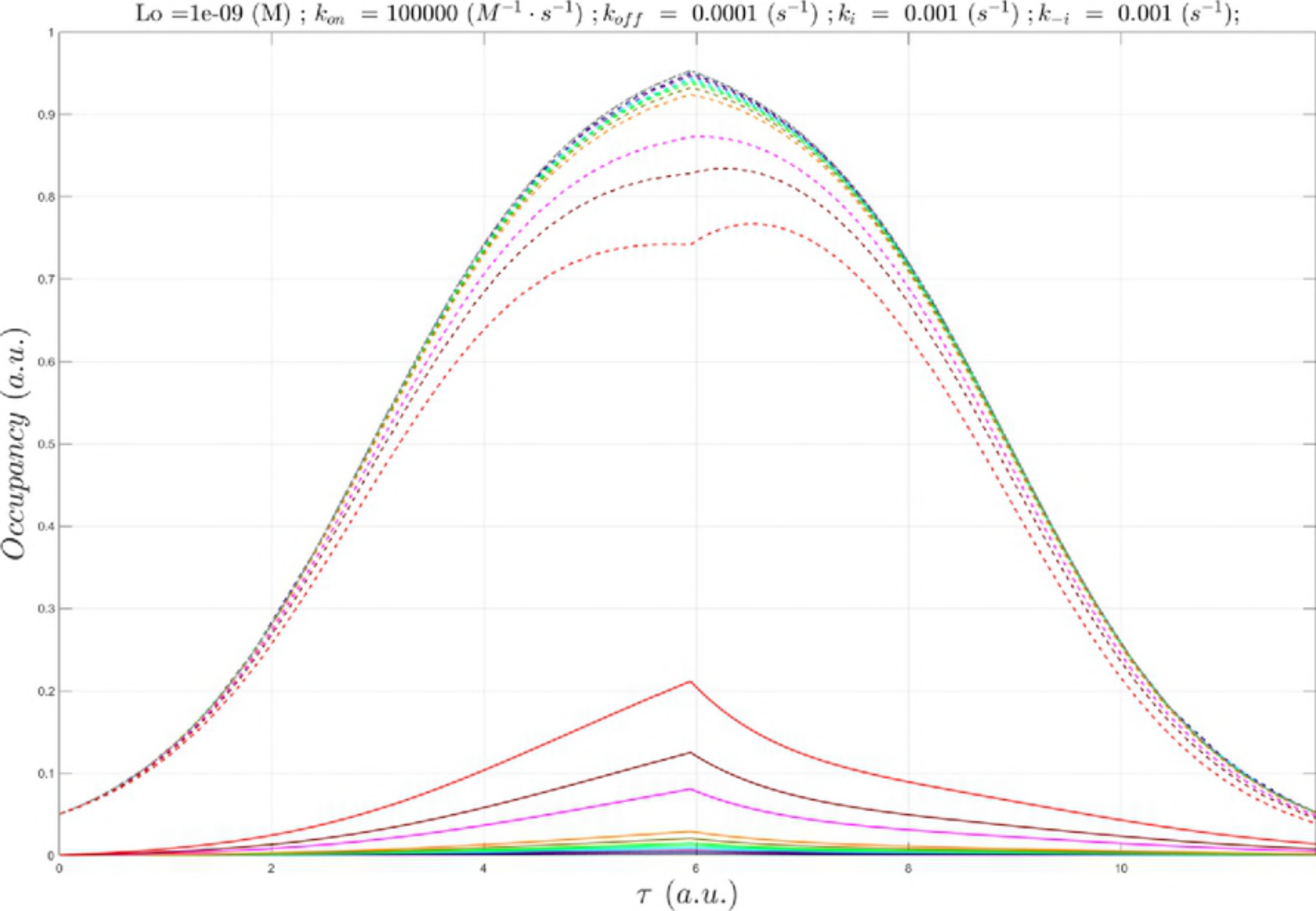
Lo =1e-09 (M) ; k_{on} = 100000 $(M^{-1} \cdot s^{-1})$; k_{off} = 0.0001 (s^{-1}) ; k_i = 0.001 (s^{-1}) ; k_{-i} = 0.001 (s^{-1});
Occupancy (a.u.)
τ (a.u.)
0
0.1
0.2
0.3
0.4
0.5
0.6
0.7
0.8
0.9
1
0
2
4
6
8
10

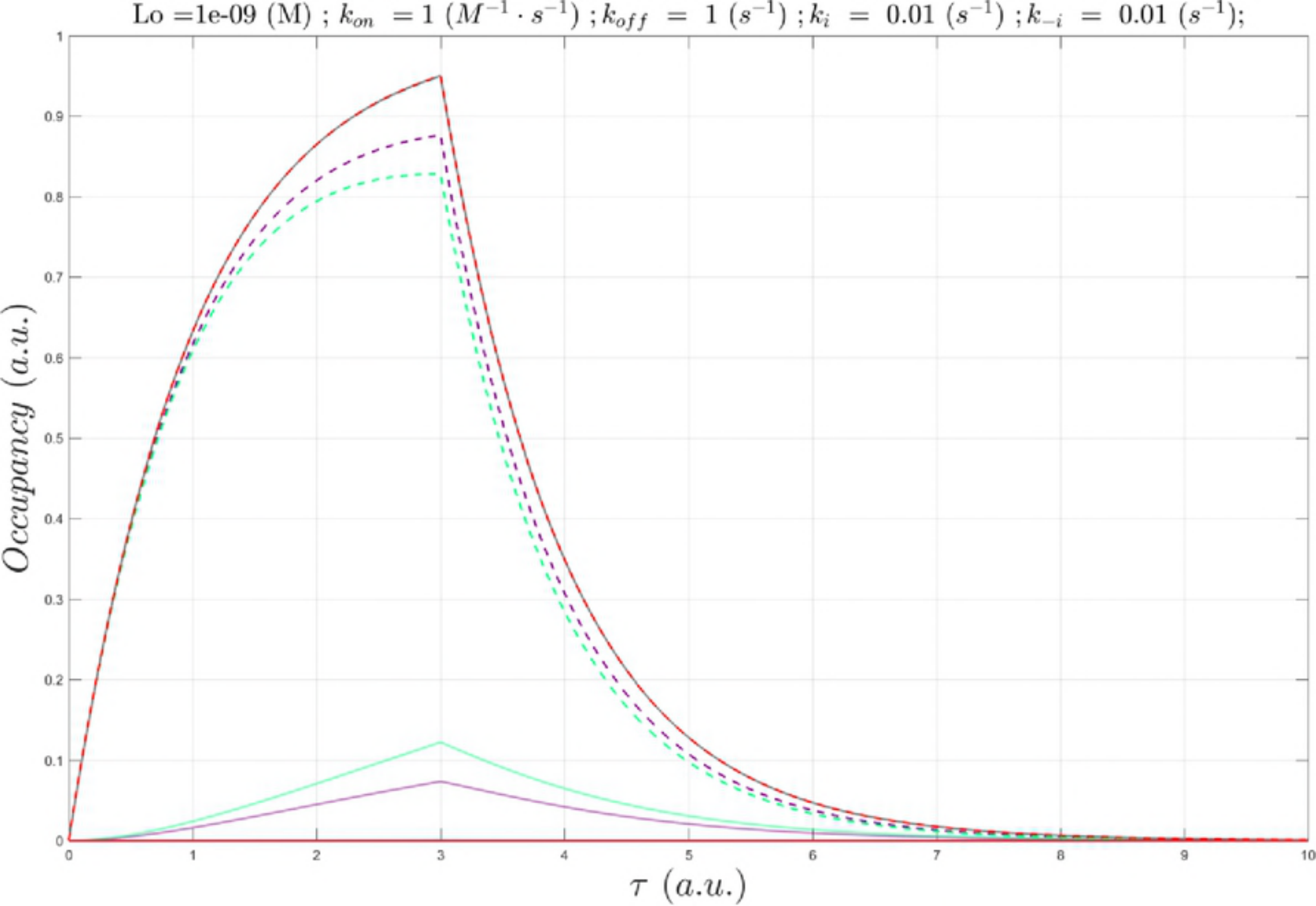
Lo =1e-09 (M) ; $k_{on} = 1\ (M^{-1} \cdot s^{-1})$; $k_{off} = 1\ (s^{-1})$; $k_i = 0.01\ (s^{-1})$; $k_{-i} = 0.01\ (s^{-1})$;
Occupancy (a.u.)
τ (a.u.)
0
0.1
0.2
0.3
0.4
0.5
0.6
0.7
0.8
0.9
1
0
1
2
3
4
5
6
7
8
9
10

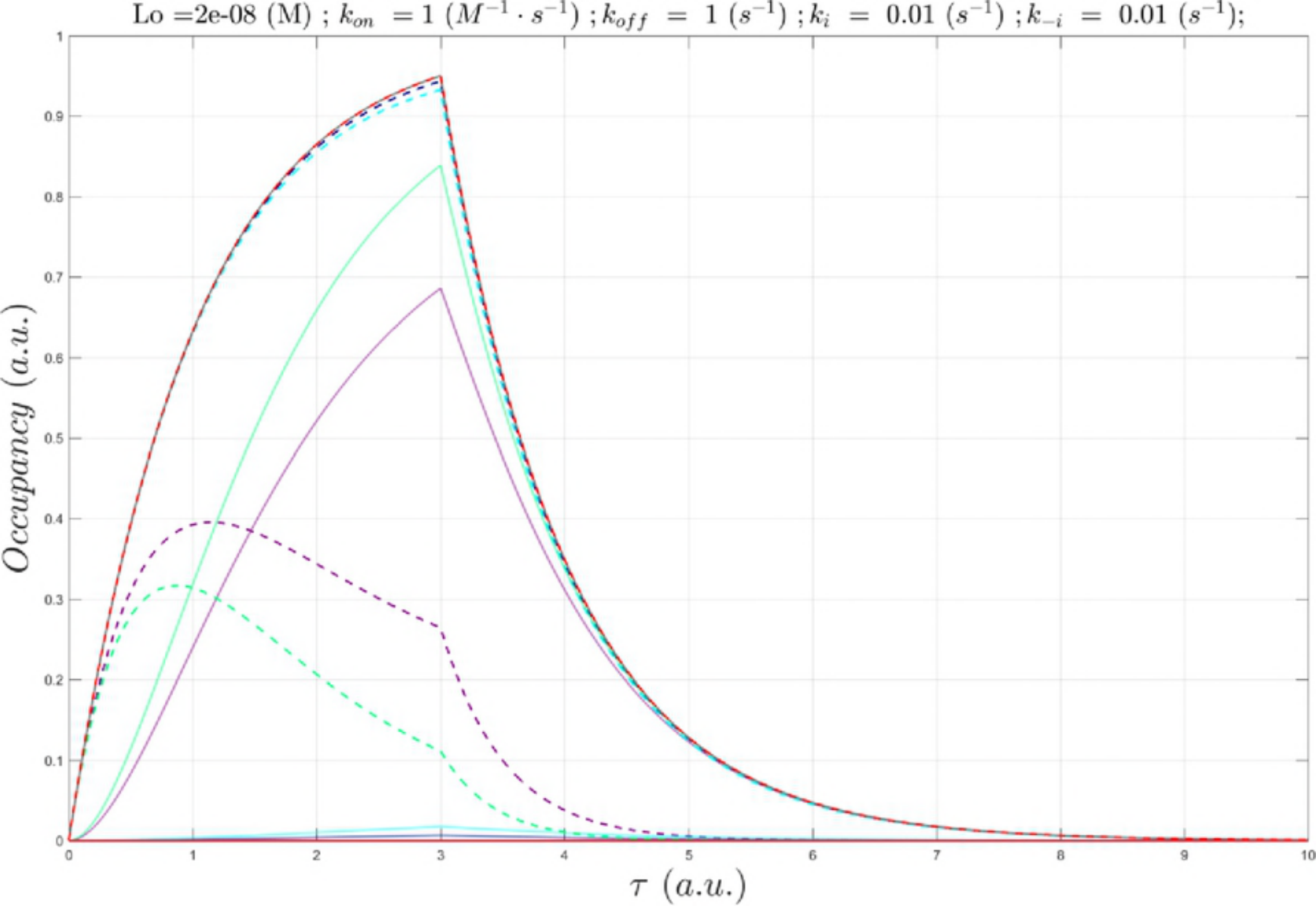
Lo =2e-08 (M) ; $k_{on} = 1\ (M^{-1} \cdot s^{-1})$; $k_{off} = 1\ (s^{-1})$; $k_i = 0.01\ (s^{-1})$; $k_{-i} = 0.01\ (s^{-1})$;
Occupancy (a.u.)
τ (a.u.)
0
0.1
0.2
0.3
0.4
0.5
0.6
0.7
0.8
0.9
1
0
1
2
3
4
5
6
7
8
9
10

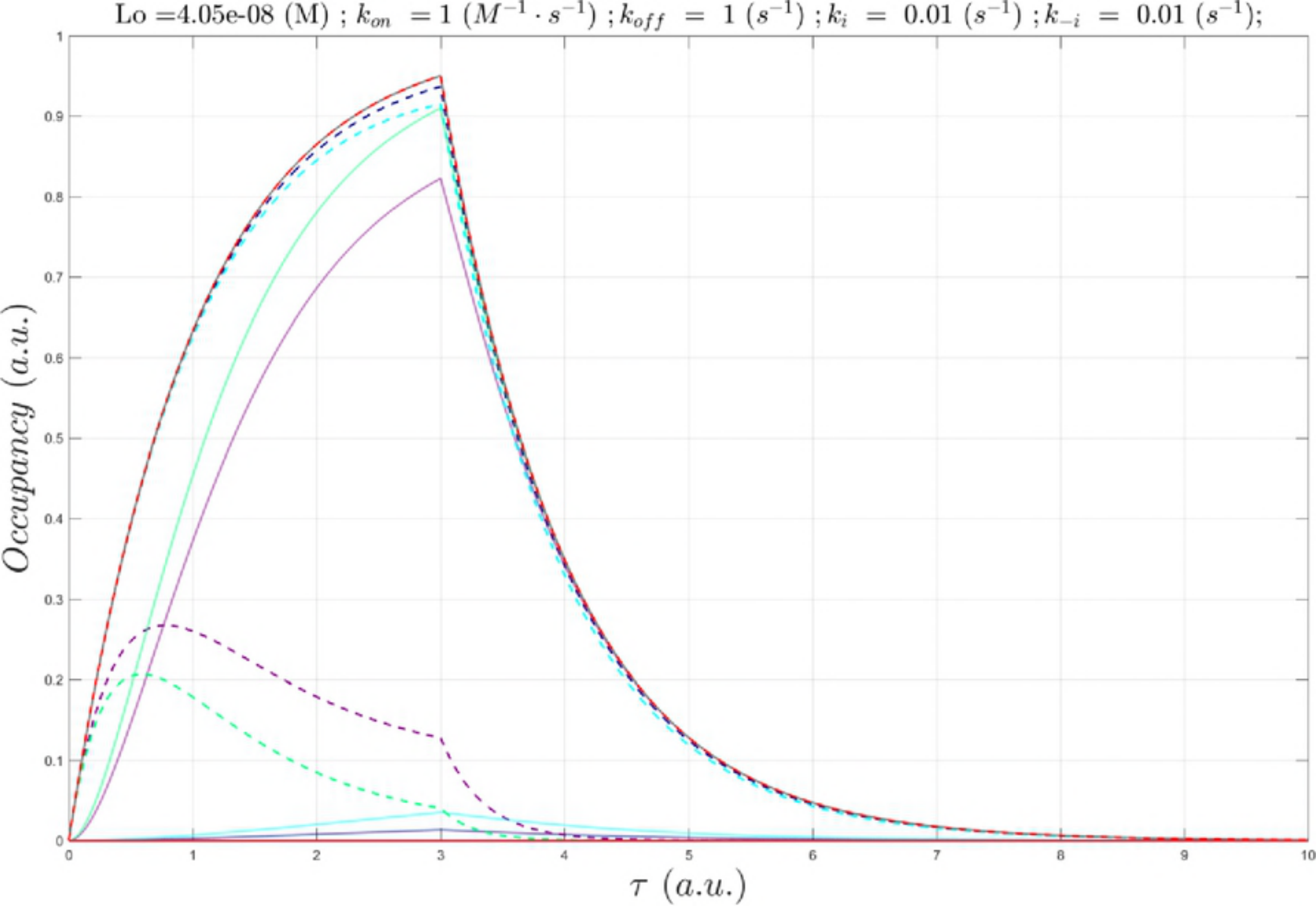
Lo =4.05e-08 (M) ; k_{on} = 1 ($M^{-1} \cdot s^{-1}$) ; k_{off} = 1 (s^{-1}) ; k_i = 0.01 (s^{-1}) ; k_{-i} = 0.01 (s^{-1});
Occupancy (a.u.)
τ (a.u.)
0
0.1
0.2
0.3
0.4
0.5
0.6
0.7
0.8
0.9
1
0
1
2
3
4
5
6
7
8
9
10

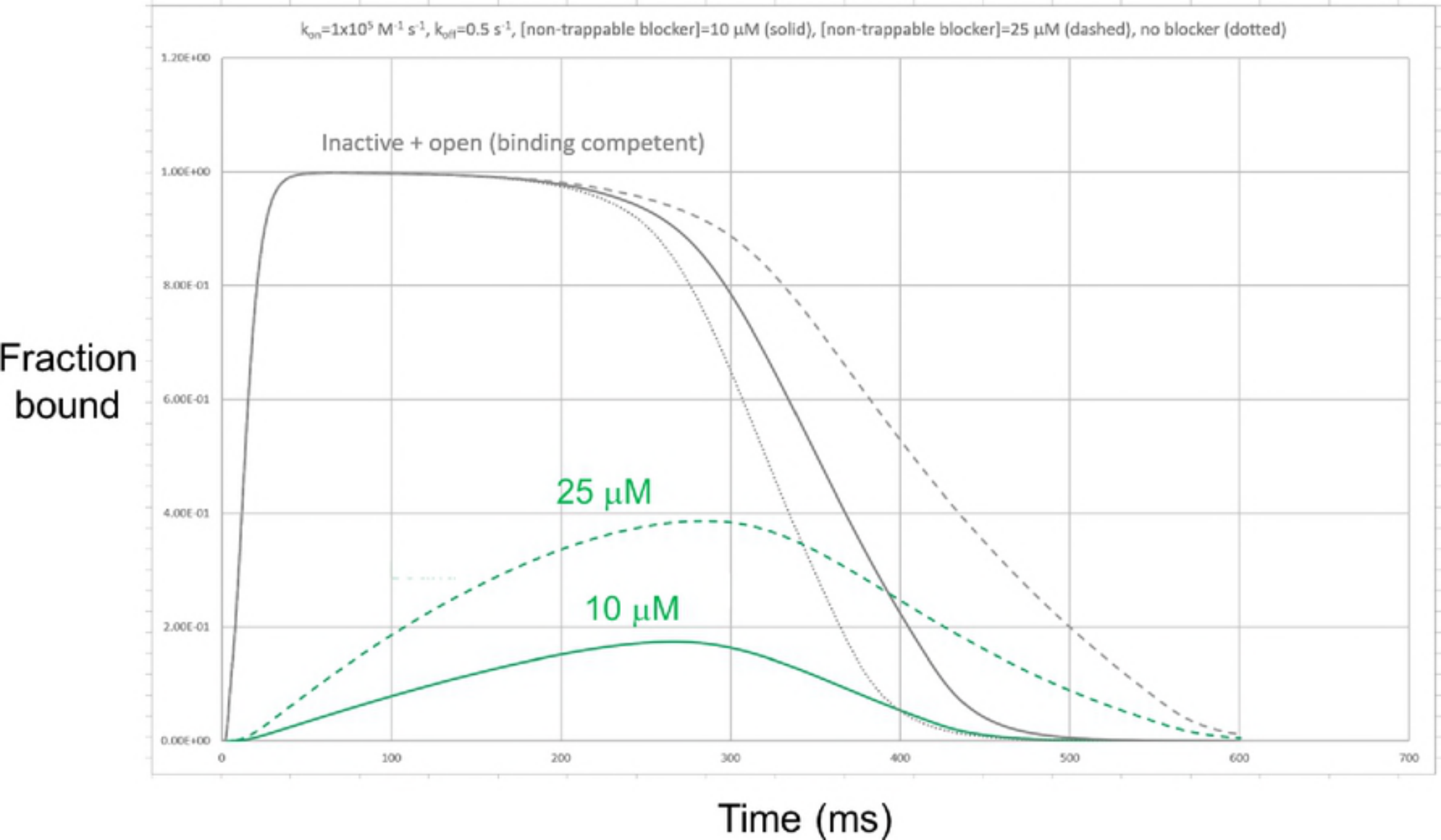
k_{on}=1x10^5 M^{-1} s^{-1}, k_{off}=0.5 s^{-1}, [non-trappable blocker]=10 µM (solid), [non-trappable blocker]=25 µM (dashed), no blocker (dotted)
Inactive + open (binding competent)
25 µM
10 µM
Fraction bound
Time (ms)
1.20E+00
1.00E+00
8.00E-01
6.00E-01
4.00E-01
2.00E-01
0.00E+00
0
100
200
300
400
500
600
700

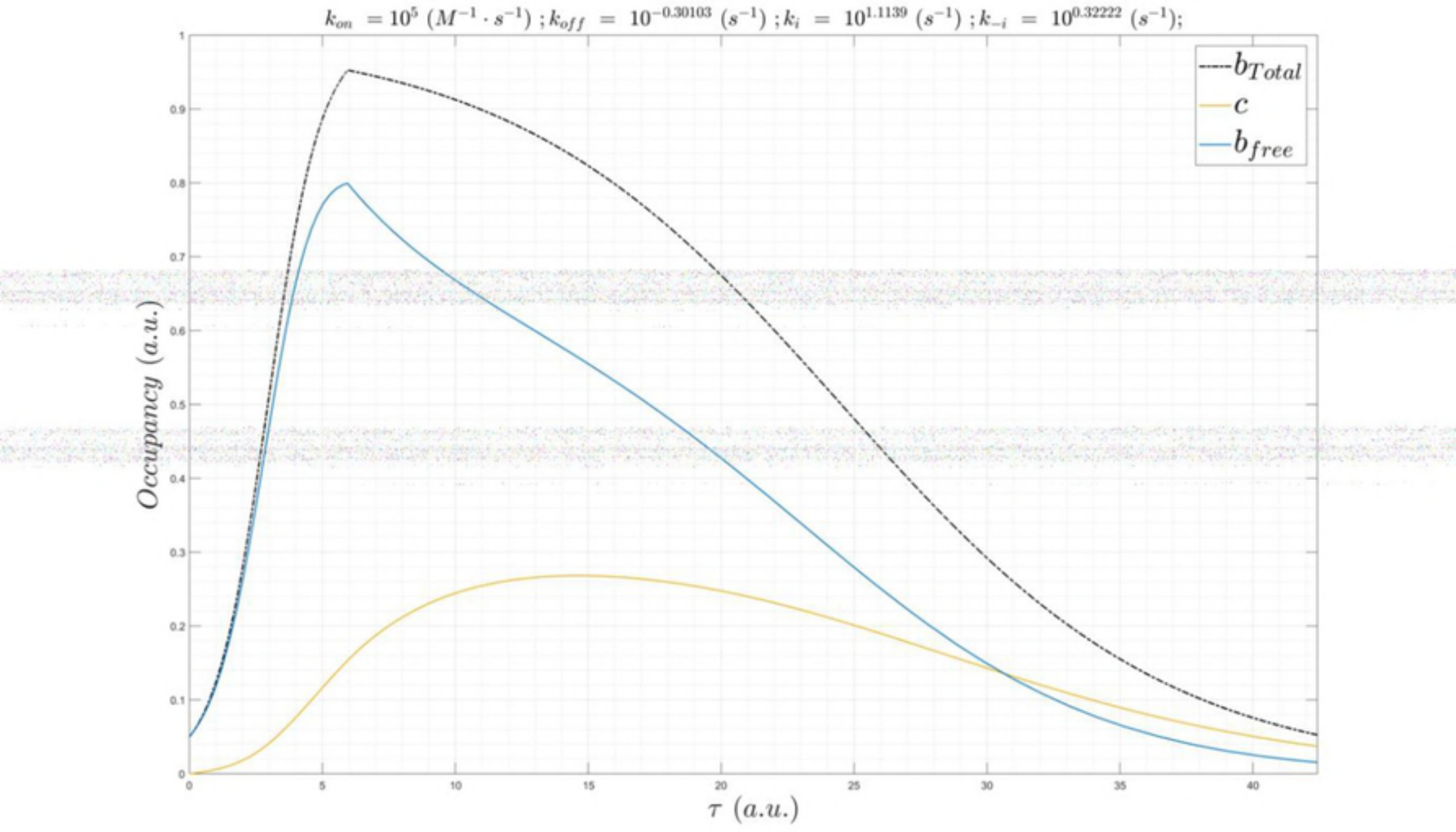
$k_{on} = 10^{5}\ (M^{-1} \cdot s^{-1})\ ; k_{off} = 10^{-0.30103}\ (s^{-1})\ ; k_i = 10^{1.1139}\ (s^{-1})\ ; k_{-i} = 10^{0.32222}\ (s^{-1});$
b_{Total}
c
b_{free}
Occupancy (a.u.)
τ (a.u.)
0
0.1
0.2
0.3
0.4
0.5
0.6
0.7
0.8
0.9
1
0
5
10
15
20
25
30
35
40

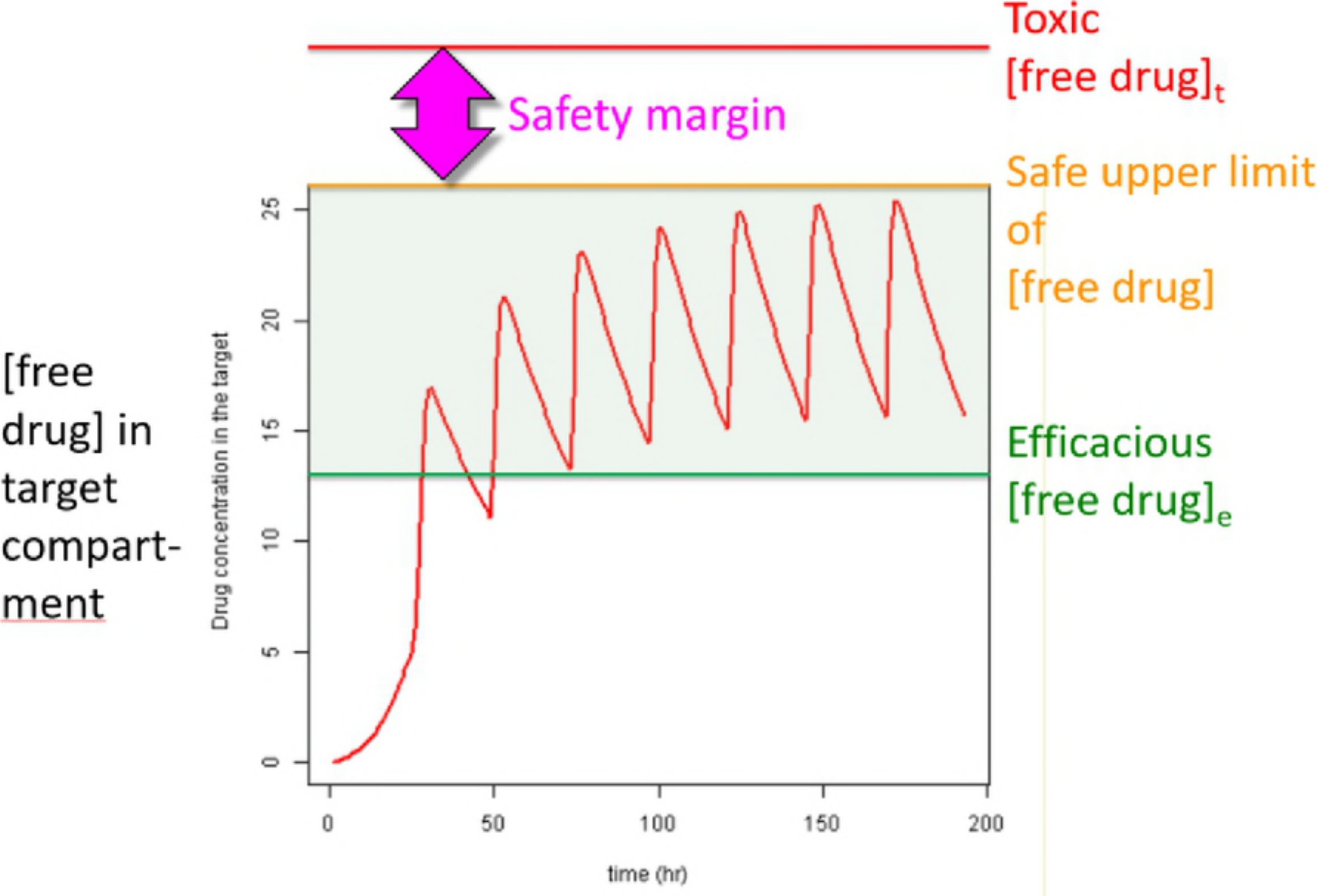
Toxic
[free drug]t
Safety margin
Safe upper limit
of
[free drug]
[free drug] in target compart-ment
Efficacious
[free drug]e
Drug concentration in the target
0
5
10
15
20
25
0
50
100
150
200
time (hr)

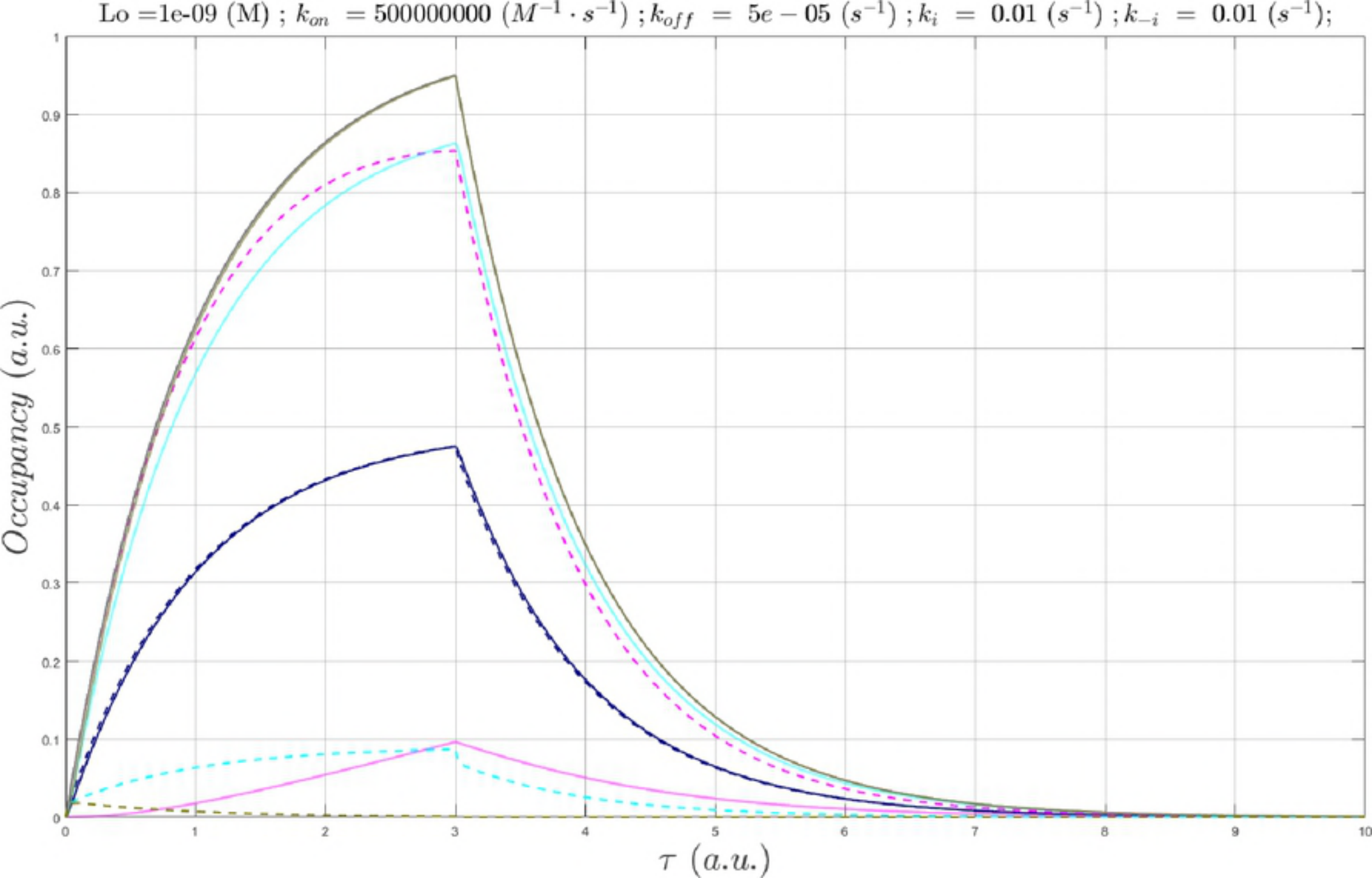
Lo =1e-09 (M) ; k_{on} = 500000000 $(M^{-1} \cdot s^{-1})$; k_{off} = 5e − 05 (s^{-1}) ; k_i = 0.01 (s^{-1}) ; k_{-i} = 0.01 (s^{-1});
Occupancy (a.u.)
τ (a.u.)
0
0.1
0.2
0.3
0.4
0.5
0.6
0.7
0.8
0.9
1
0
1
2
3
4
5
6
7
8
9
10

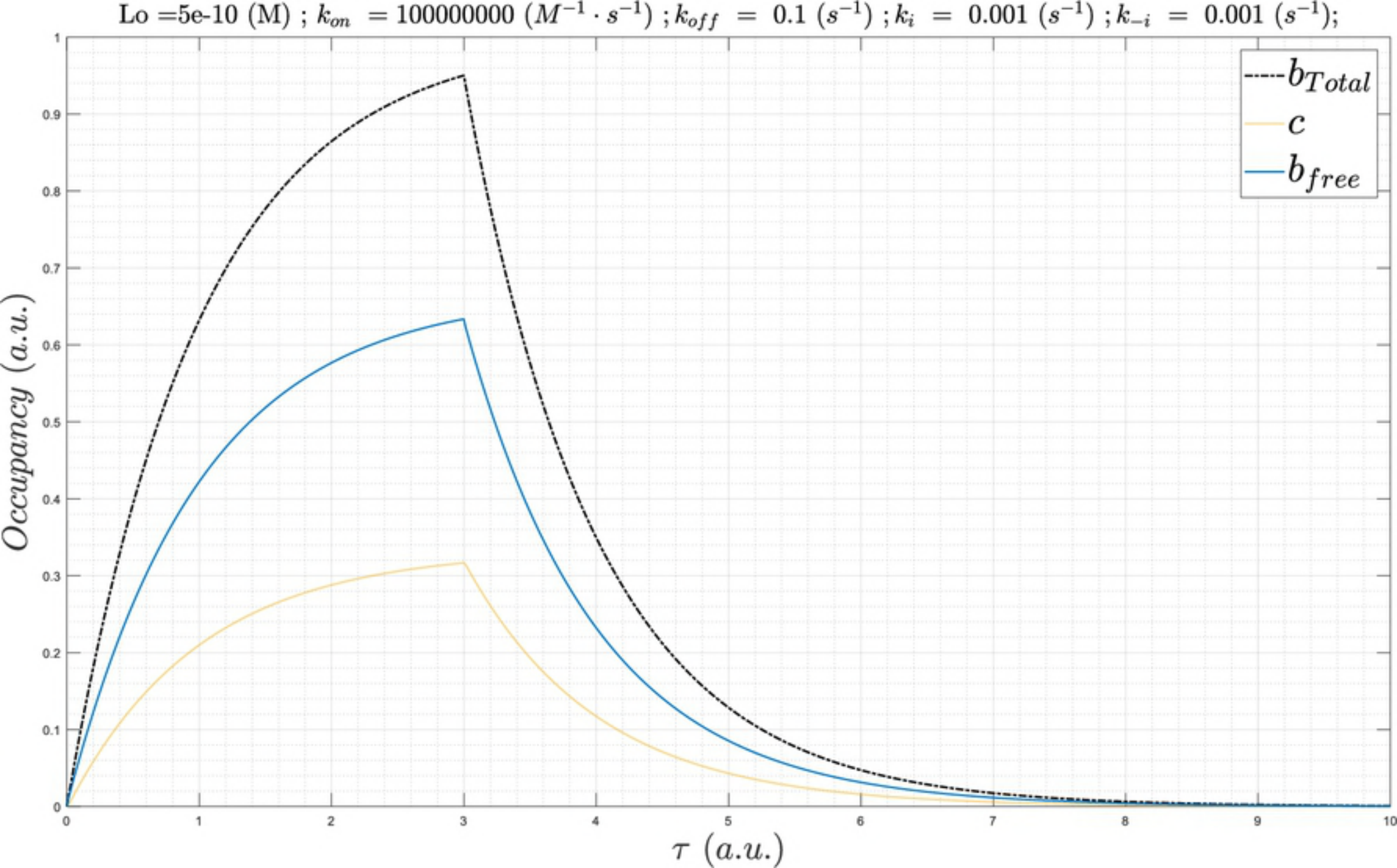
Lo =5e-10 (M) ; k_{on} = 100000000 ($M^{-1} \cdot s^{-1}$) ; k_{off} = 0.1 (s^{-1}) ; k_i = 0.001 (s^{-1}) ; k_{-i} = 0.001 (s^{-1});
b_{Total}
c
b_{free}
Occupancy (a.u.)
τ (a.u.)
0
0.1
0.2
0.3
0.4
0.5
0.6
0.7
0.8
0.9
1
0
1
2
3
4
5
6
7
8
9
10

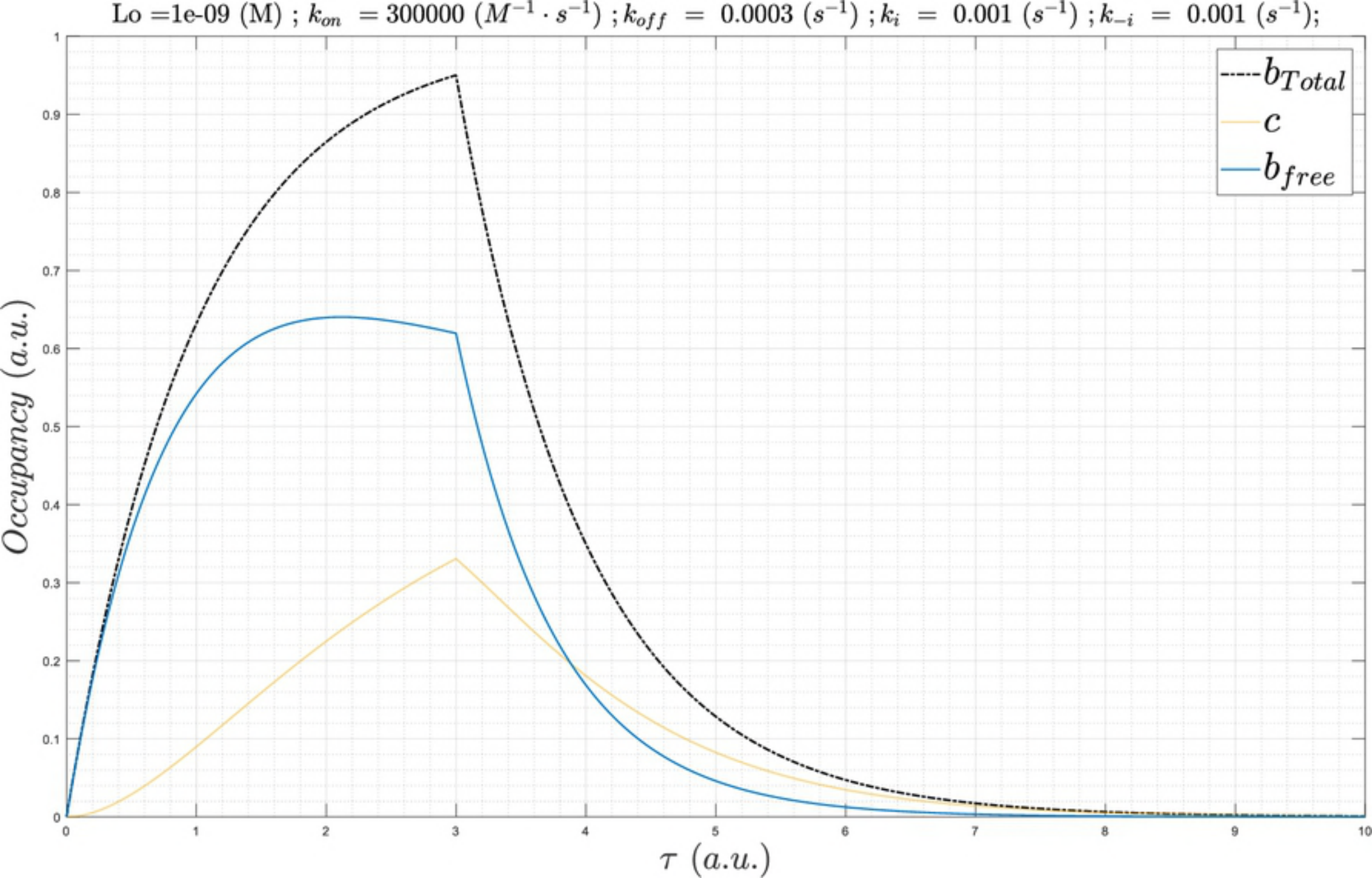
Lo =1e-09 (M) ; k_{on} = 300000 ($M^{-1} \cdot s^{-1}$) ; k_{off} = 0.0003 (s^{-1}) ; k_i = 0.001 (s^{-1}) ; k_{-i} = 0.001 (s^{-1});
b_{Total}
c
b_{free}
Occupancy (a.u.)
τ (a.u.)
0
0.1
0.2
0.3
0.4
0.5
0.6
0.7
0.8
0.9
1
0
1
2
3
4
5
6
7
8
9
10

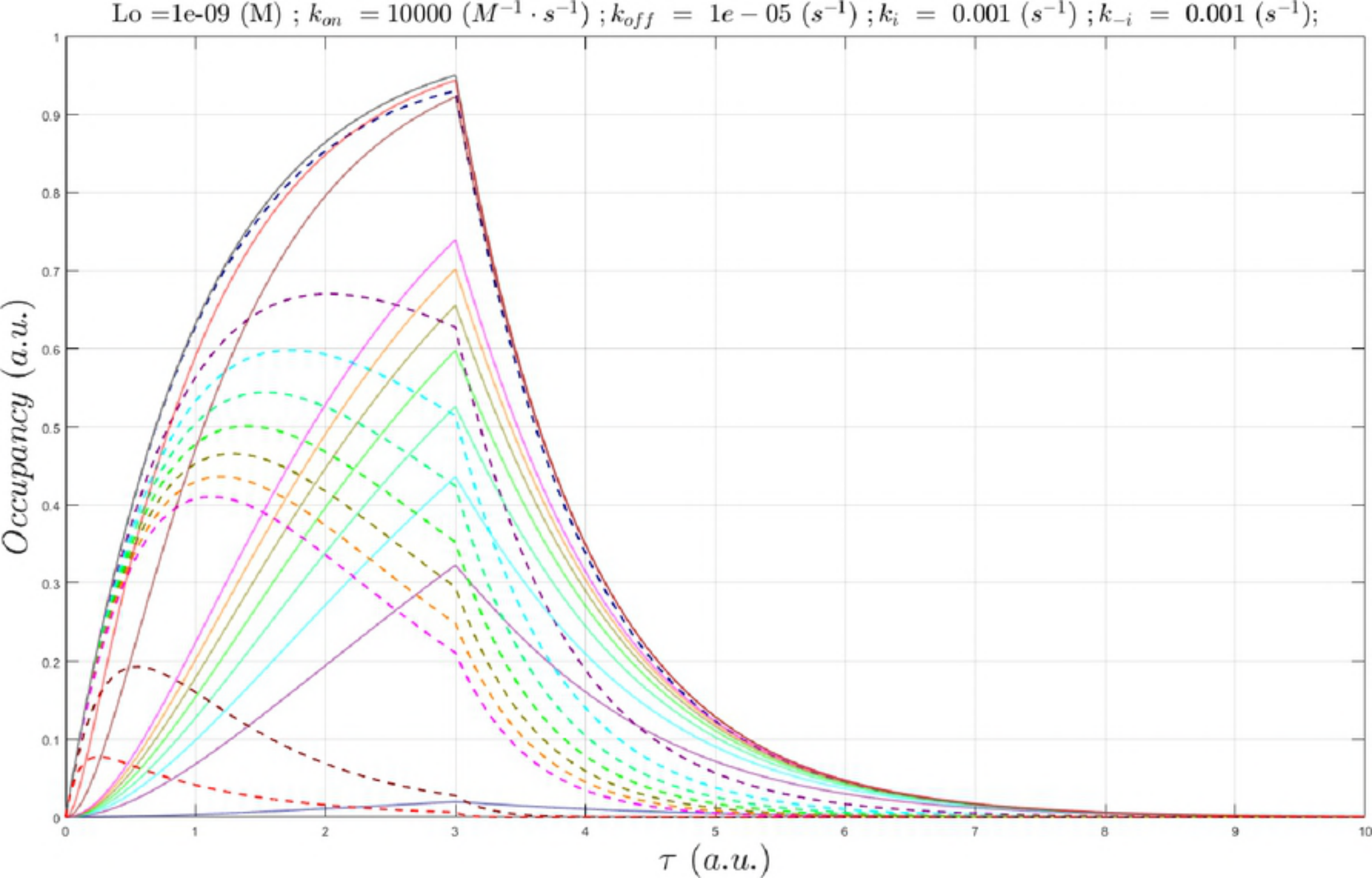
Lo =1e-09 (M) ; k_{on} = 10000 ($M^{-1} \cdot s^{-1}$) ; k_{off} = 1e − 05 (s^{-1}) ; k_i = 0.001 (s^{-1}) ; k_{-i} = 0.001 (s^{-1});
Occupancy (a.u.)
τ (a.u.)
0
0.1
0.2
0.3
0.4
0.5
0.6
0.7
0.8
0.9
1
0
1
2
3
4
5
6
7
8
9
10

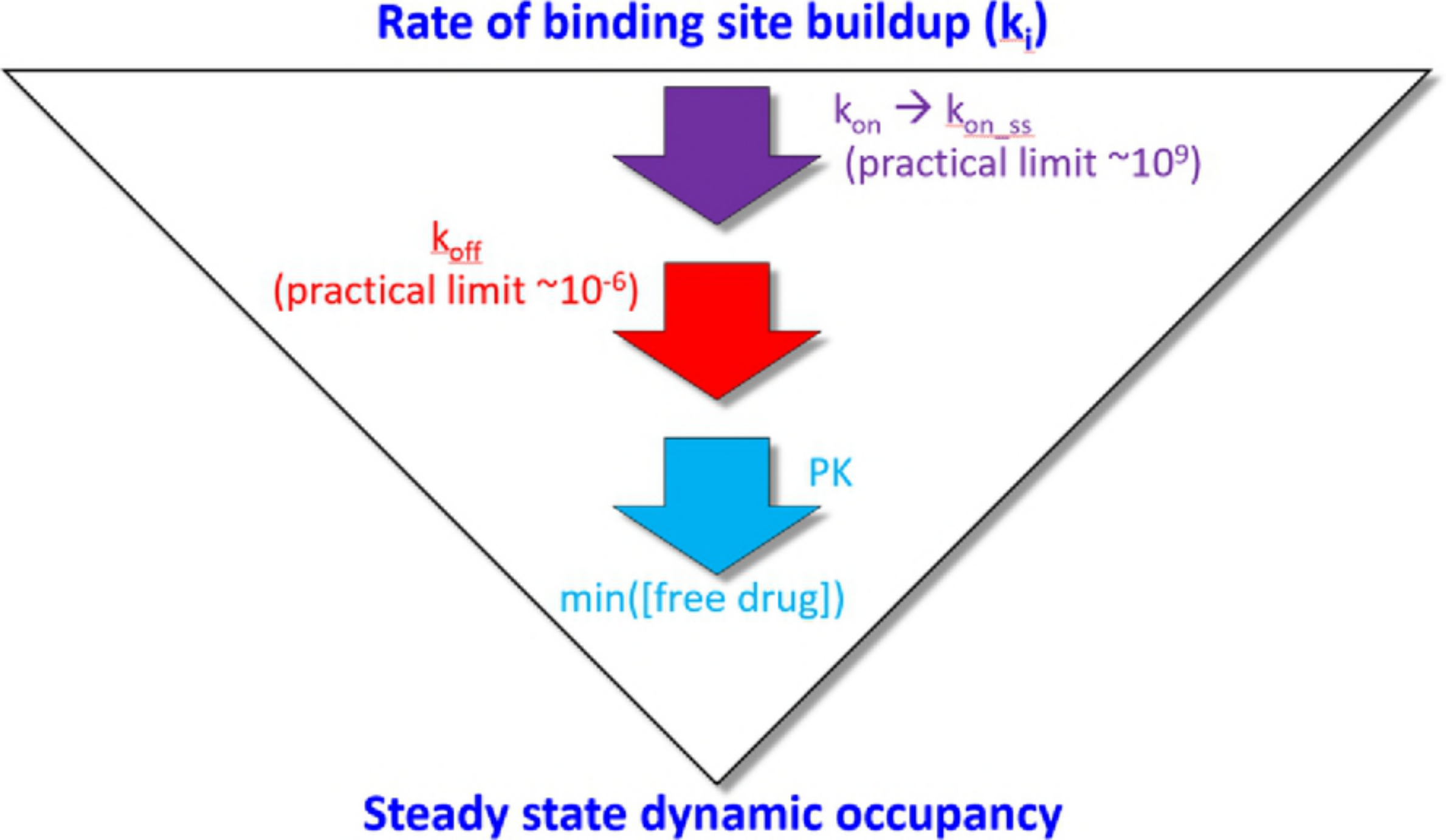
Rate of binding site buildup (k_i)
$k_{on} \rightarrow k_{on\_ss}$
(practical limit ~10^9)
k_{off}
(practical limit ~10^{-6})
PK
min([free drug])
Steady state dynamic occupancy

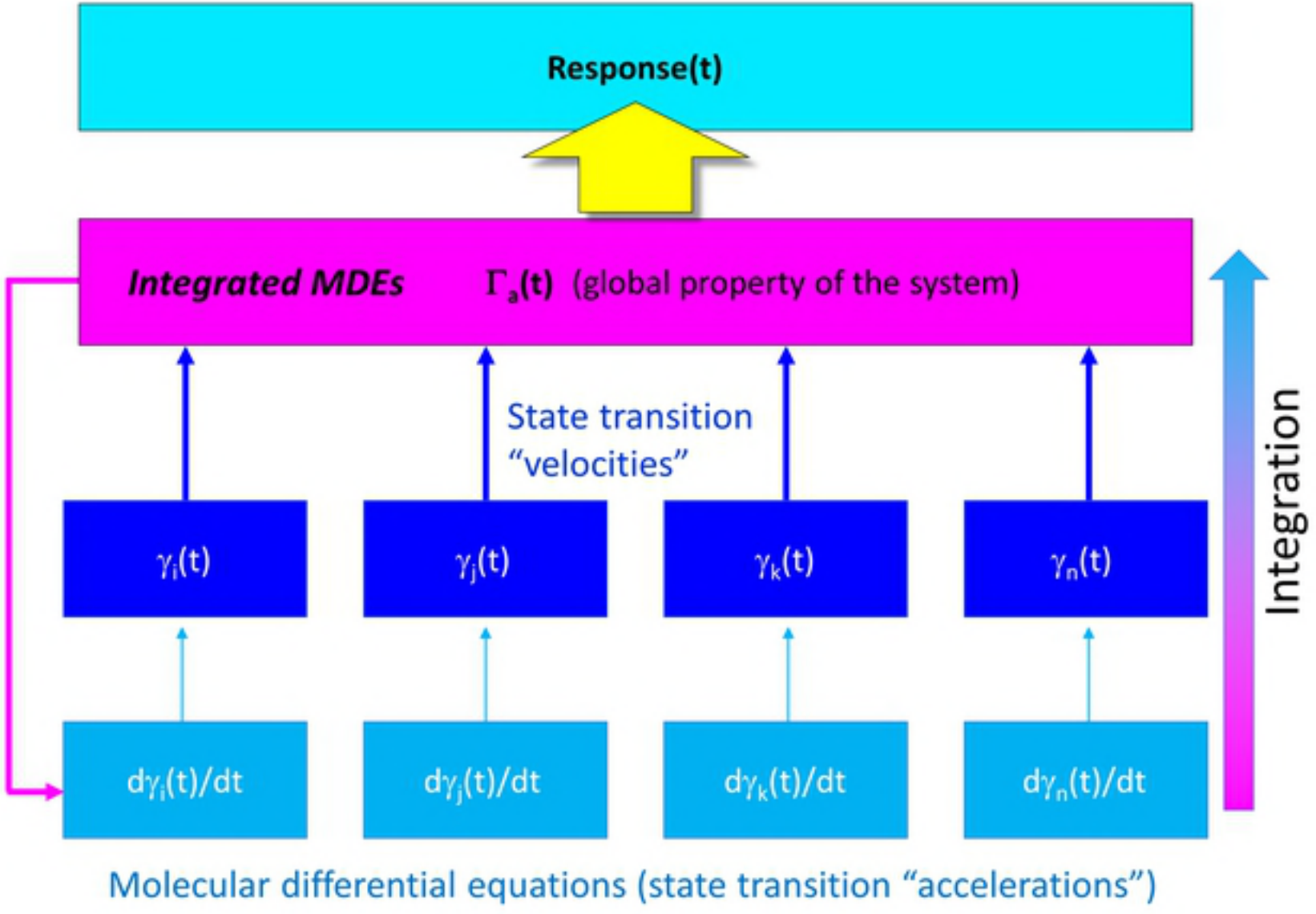
Response(t)
Integrated MDEs
$\Gamma_a(t)$ (global property of the system)
State transition
"velocities"
$\gamma_i(t)$
$\gamma_j(t)$
$\gamma_k(t)$
$\gamma_n(t)$
$d\gamma_i(t)/dt$
$d\gamma_j(t)/dt$
$d\gamma_k(t)/dt$
$d\gamma_n(t)/dt$
Integration
Molecular differential equations (state transition "accelerations")

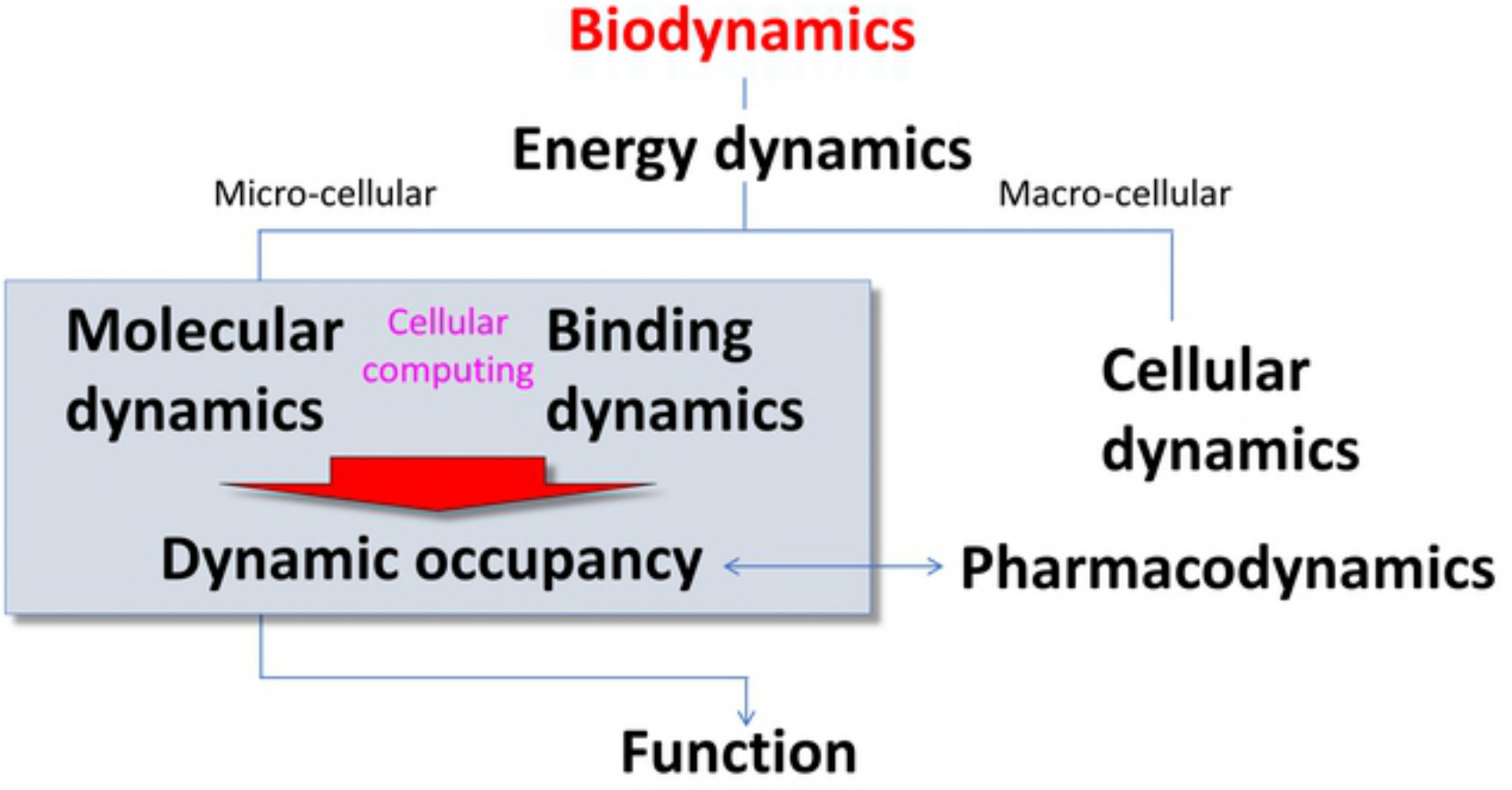
Biodynamics
Energy dynamics
Micro-cellular
Macro-cellular
Molecular dynamics
Cellular computing
Binding dynamics
Cellular dynamics
Dynamic occupancy
Pharmacodynamics
Function

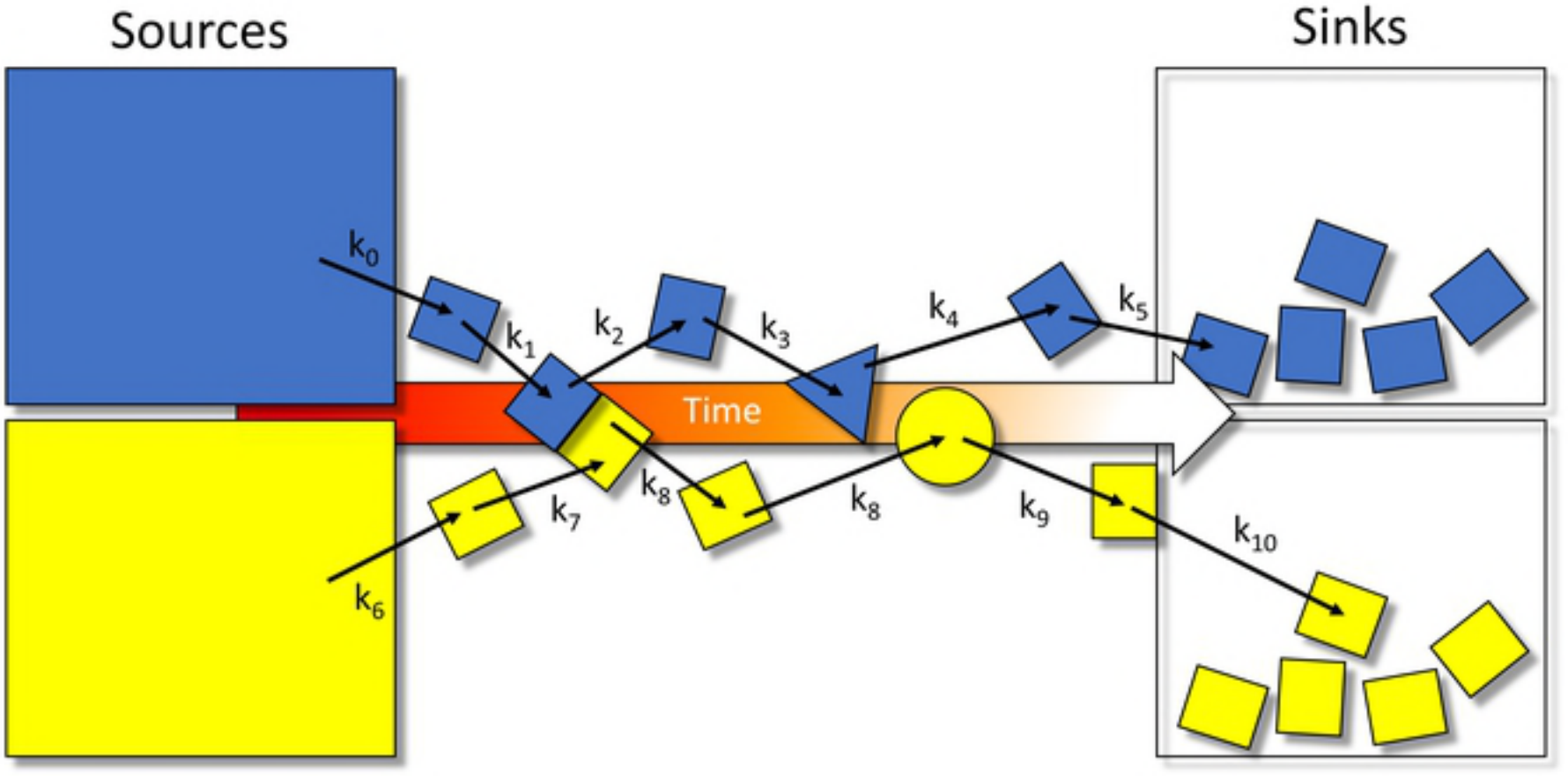
Sources
Sinks
Time
k_0
k_1
k_2
k_3
k_4
k_5
k_6
k_7
k_8
k_8
k_9
k_{10}

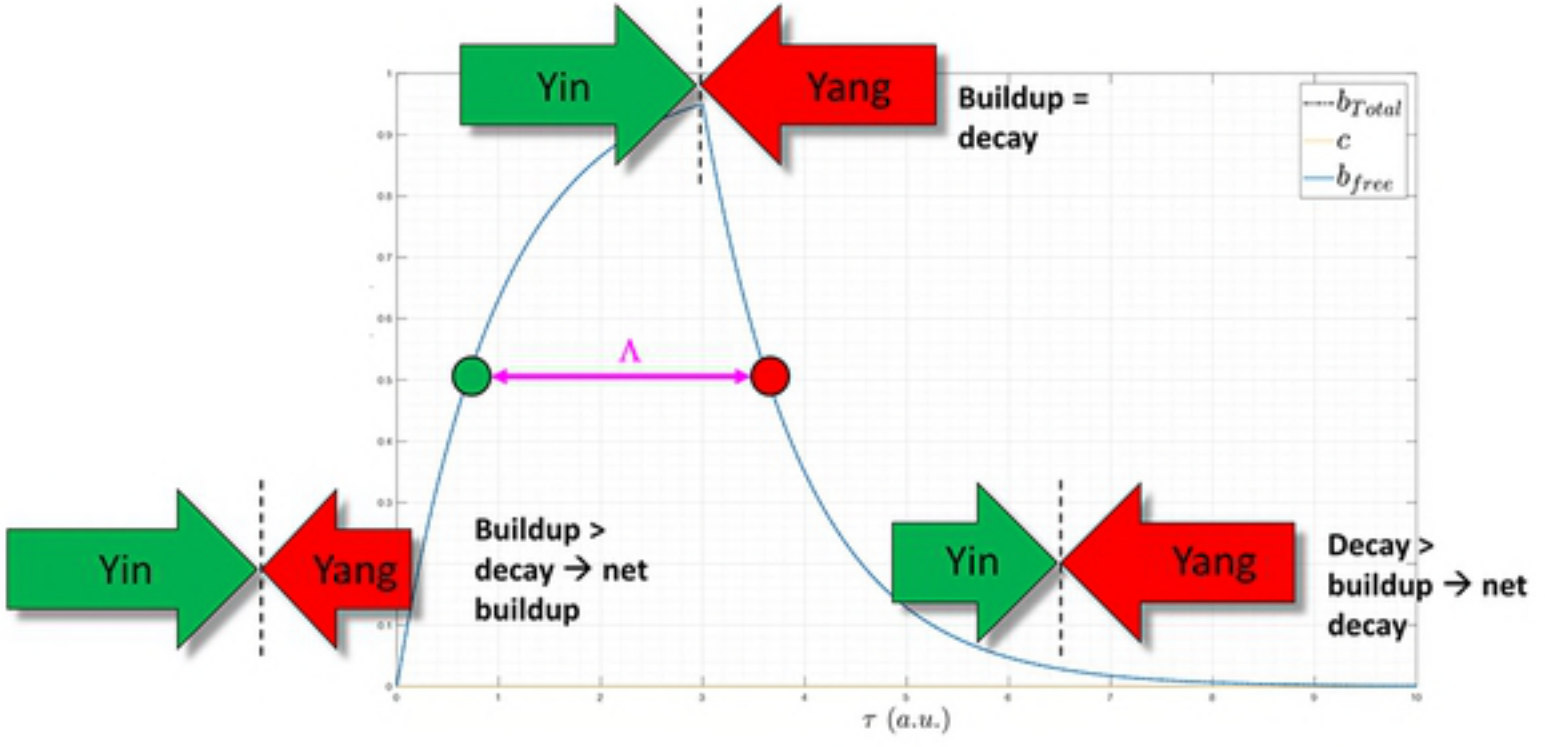
Yin
Yang
Buildup = decay
b_{Total}
c
b_{free}
Λ
Yin
Yang
Buildup > decay → net buildup
Yin
Yang
Decay > buildup → net decay
τ (a.u.)

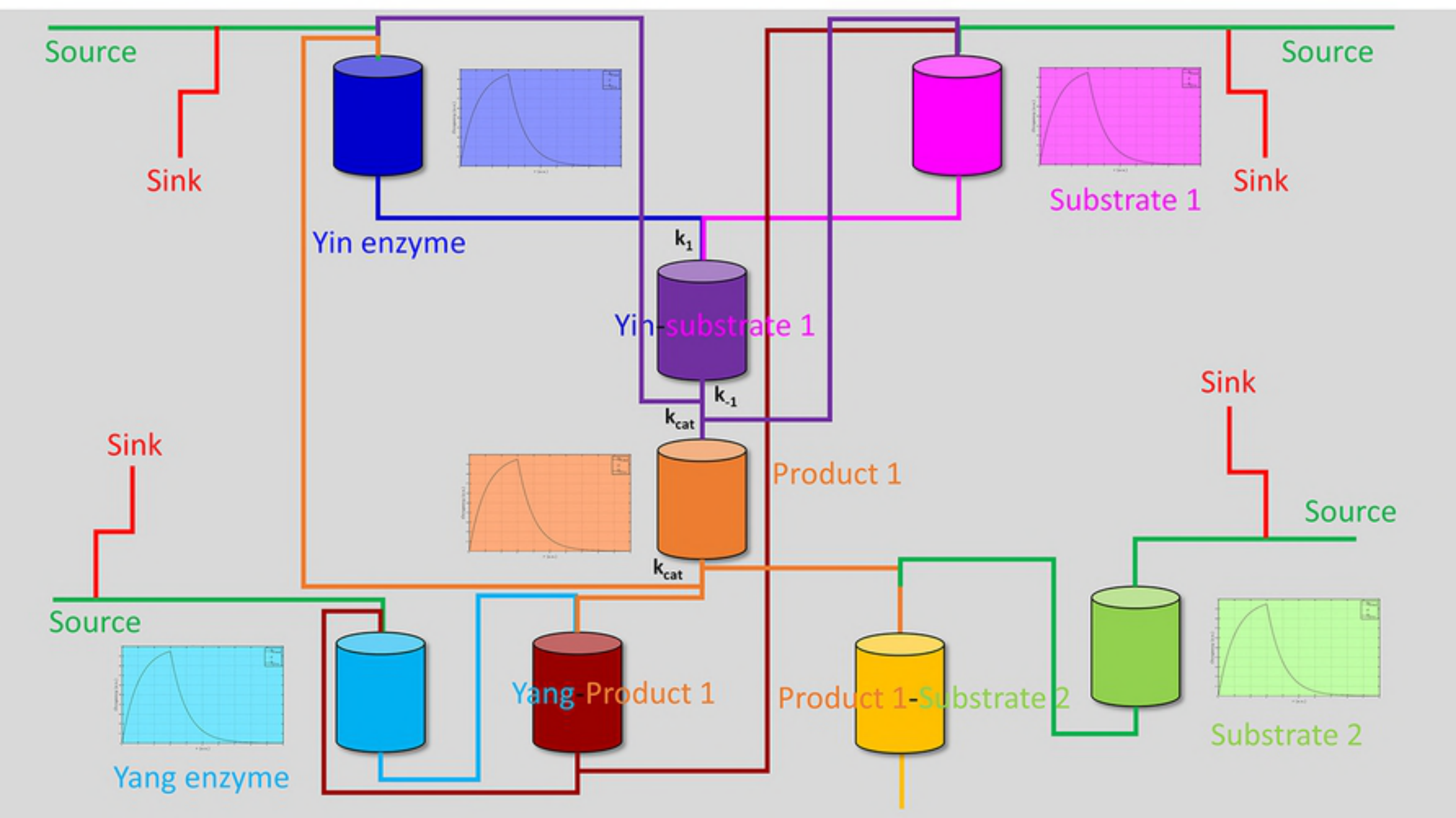
Source
Sink
Yin enzyme
Source
Sink
Substrate 1
k_1
Yin-substrate 1
k_{-1}
k_{cat}
Product 1
k_{cat}
Sink
Source
Sink
Source
Yang enzyme
Yang-Product 1
Product 1-Substrate 2
Substrate 2

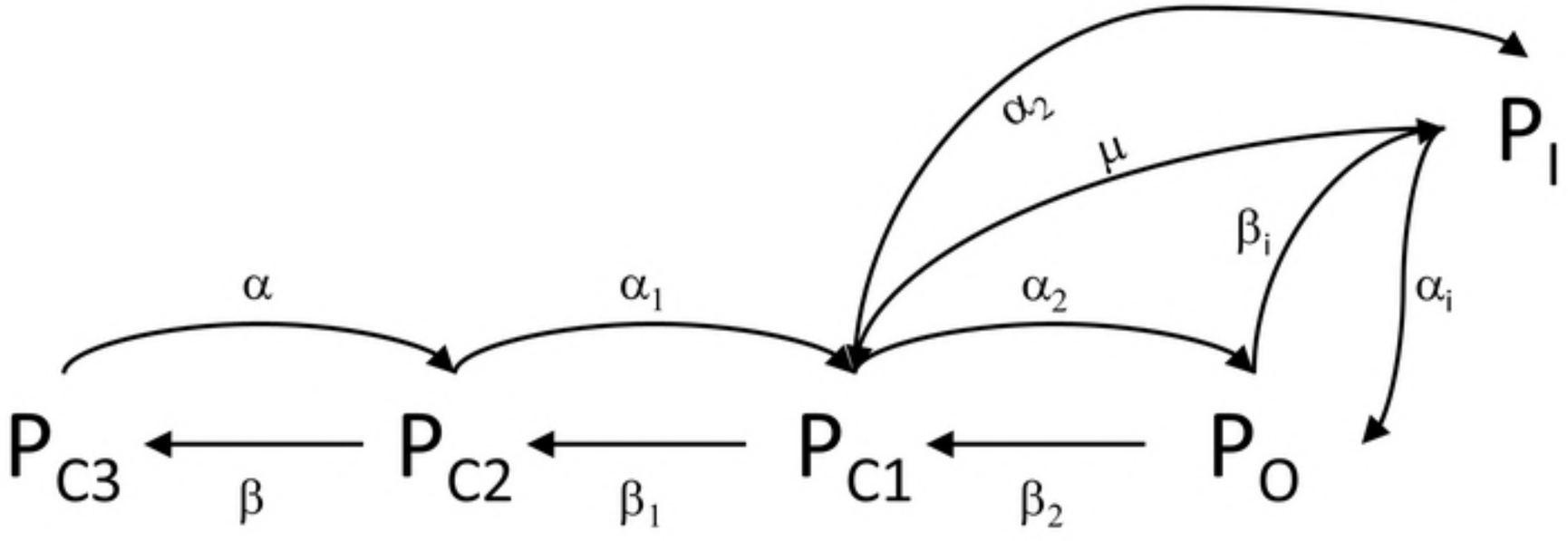
P_{C3}
P_{C2}
P_{C1}
P_O
P_I
α
α_1
α_2
α_2
α_i
μ
β_i
β
β_1
β_2

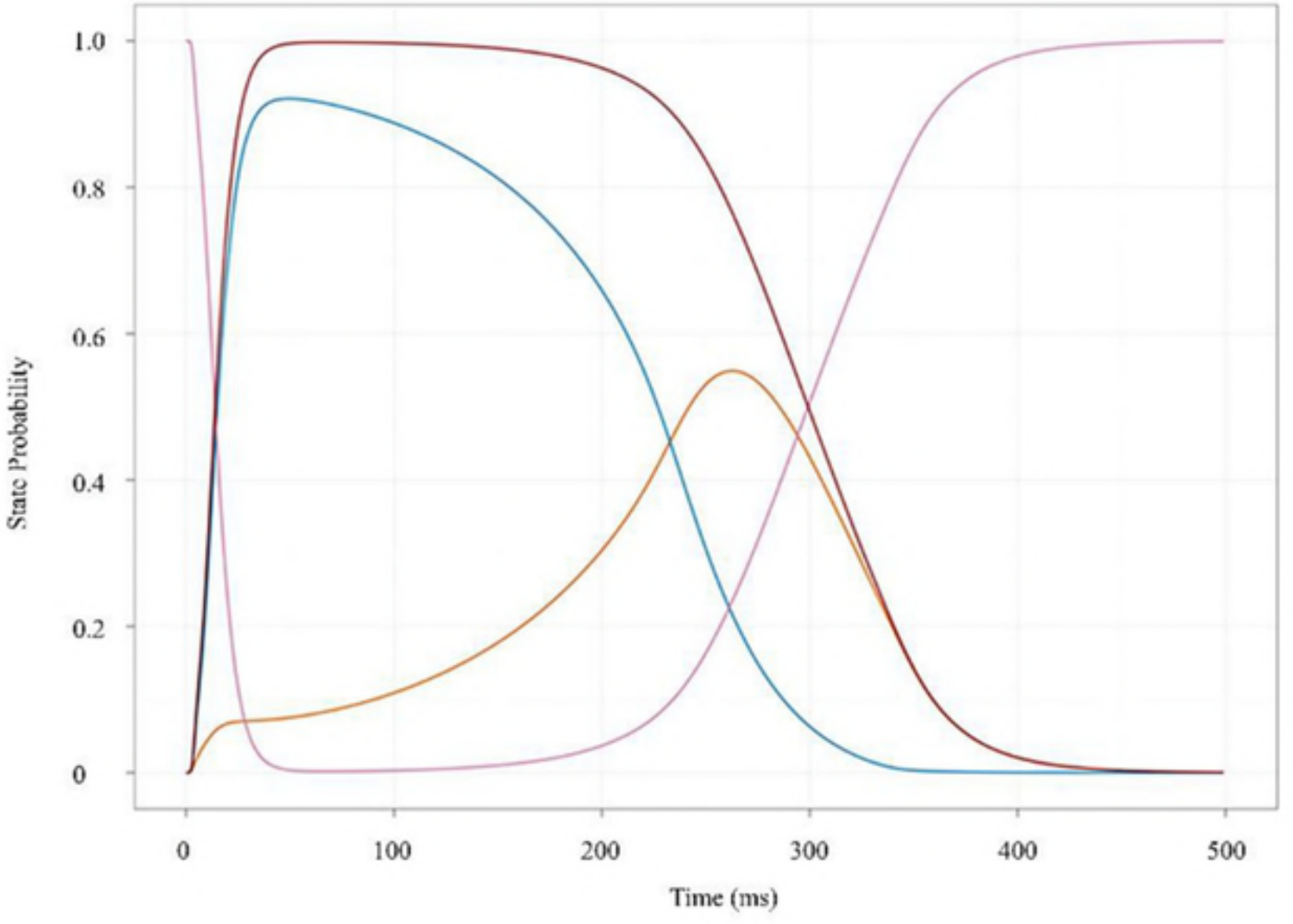
1.0
0.8
0.6
0.4
0.2
0
State Probability
0
100
200
300
400
500
Time (ms)